ISSN 0038-531X

Russian Original Vol. 59, No. 6, December, 1985

June, 1986

SATEAZ 59(6) 957-1054 (1985)

SOVIET ATOMIC ENERGY

АТОМНАЯ ЭНЕРГИЯ
(ATOMNAYA ÉNERGIYA)

TRANSLATED FROM RUSSIAN

c/b CONSULTANTS BUREAU, NEW YORK

SOVIET ATOMIC ENERGY

Soviet Atomic Energy is a translation of *Atomnaya Energiya*, a publication of the Academy of Sciences of the USSR.

An agreement with the Copyright Agency of the USSR (VAAP) makes available both advance copies of the Russian journal and original glossy photographs and artwork. This serves to decrease the necessary time lag between publication of the original and publication of the translation and helps to improve the quality of the latter. The translation began with the first issue of the Russian journal.

Soviet Atomic Energy is abstracted or indexed in *Chemical Abstracts, Chemical Titles, Pollution Abstracts, Science Research Abstracts, Parts A and B, Safety Science Abstracts Journal, Current Contents, Energy Research Abstracts,* and *Engineering Index.*

Consultants Bureau journals appear about six months after the publication of the original Russian issue. For bibliographic accuracy, the English issue published by Consultants Bureau carries the same number and date as the original Russian from which it was translated. For example, a Russian issue published in December will appear in a Consultants Bureau English translation about the following June, but the translation issue will carry the December date. When ordering any volume or particular issue of a Consultants Bureau journal, please specify the date and, where applicable, the volume and issue numbers of the original Russian. The material you will receive will be a translation of that Russian volume or issue.

Subscription (2 volumes per year)
Vols. 58 & 59: $645 (domestic); $715 (foreign)
Vols. 60 & 61: $695 (domestic); $770 (foreign)
Single Issue: $100
Single Article: $9.50

CONSULTANTS BUREAU, NEW YORK AND LONDON

c/b
233 Spring Street
New York, New York 10013

Published monthly. Second-class postage paid at Jamaica, New York 11431.

Mailed in the USA by Publications Expediting, Inc., 200 Meacham Avenue, Elmont, NY 11003.

POSTMASTER: Send address changes to *Soviet Atomic Energy,* Plenum Publishing Corporation, 233 Spring Street, New York, NY 10013.

SOVIET ATOMIC ENERGY

A translation of *Atomnaya Énergiya*

June, 1986

Volume 59, Number 6 December, 1985

CONTENTS

Engl./Russ.

CONTENTS

(continued)

Engl./Russ.

The Russian press date (podpisano k pechati) of this issue was 12/2/1985. Publication therefore did not occur prior to this date, but must be assumed to have taken place reasonably soon thereafter.

PHYSICOCHEMICAL FOUNDATIONS OF THE MODELING OF THE COMPOSITION OF THE WATER COOLANT IN A NUCLEAR POWER PLANT

V. M. Sedov, L. V. Puchkov,
V. G. Kritskii, and V. I. Zarembo

UDC 621.187:628.163.0015

The operational reliability and safety of modern power plants are largely determined by the water-chemical conditions. There now exist mathematical and physicochemical models which describe the interaction of the coolant with the structural materials and which take into account the corrosion of iron. The models of the deposits of corrosion products on equipment surfaces and the growth in the total radioactivity of the equipment take into account the fact that during mass transport the iron can be in the ionic, colloidal, and undissolved (oxide) forms. These forms exist in virtually the entire temperature interval of the coolant. Is is natural to expect that the mechanisms of deposition of these forms on surfaces are different. Reducing the inflow of iron into the active zone of boiling water reactors [1] has decreased the rate of growth of the total radioactivity of the equipment. This could be linked to the fact that the solubility of iron in the coolant also plays a determining role in mass transport of radioactive cobalt isotopes.

The diversity of the forms in which iron is present in the coolant poses the question of the necessity of taking these forms into account in models of corrosion, mass transport, and deposition. The possibility of developing such models is determined by the reliability and accuracy of the data, on which the calculations are based, on the equilibrium solubility of different forms of corrosion products as a function of the state parameters of the coolant, the presence of different impurities and corrective additives in the coolant, as well as dissolved gases.

The solution of these problems can be based on the methods of equilibrium thermodynamics, which enable determining the number of different chemical forms of components, their transformation with increasing temperature, pressure, concentration of correcting additives, or dissolved gases, on the basis of *a priori* representations of the chemical composition of the coolant, if the information required for the calculations on the thermodynamic functions is available. Methods have now been developed for calculating the equilibria in multicomponent heterogeneous systems, and with the help of fast computers such problems are now solved comparatively easily.

In this formulation the problem is one of obtaining reliable information on the standard values of the Gibbs energy of formation of ions and charged or neutral ionic associates in a water solution at high temperature and pressure. Two computational methods [2, 3] are now primarily used to solve this problem; of these, the most widely used is the Criss–Cobble "correspondence principle" [2], though in our opinion it has no advantages over Khodakovskii's method [3]. This is apparently explained by the fact that foreign investigators (and it is they who first began to use widely the methods of equilibrium thermodynamics in order to analyze the interaction of structural materials with the coolant) primarily use the correspondence principle. Algorithms and programs which utilize this method to calculate the Gibbs energy of different forms of dissolved components for T = 298-573°K now exist [4].

Nevertheless the results obtained thus far do not satisfy investigators. The reason for this lies in the fact that the above-indicated methods are limited to a definite temperature interval. The Criss–Cobble correspondence principle was proposed by them for temperatures $\leqslant$473°K; in addition, they specifically stipulate that they are not responsible for results obtained by extrapolation with the help of their method to higher temperatures. Almost all investigators who use the correspondence principle in their calculations forget this stipulation in practice. It should be noted that even the most highly active supporters of this method do not present calculations for T > 573°K, though such calculations are un-

Translated from Atomnaya Énergiya, Vol. 59, No. 6, pp. 395-398, December, 1985. Original article submitted November 16, 1984.

0038-531X/85/5906-0957$09.50

do of bivalent cations in a water solution at T = 523-573°K computed with the help of this method have a temperature coefficient whose sign is opposite to that obtained in experimental investigations. An altered variant of the correspondence principle for single-atom ions has been extended up to 573°K [6]. This method is, however, limited to definite chemical forms of the ions. Khodakovskii's method, which we proposed for T $\leqslant$ 473°K, does not have this restriction. A comparison of the predictions and the experimental data shows that this method can be used for singly charged ions at higher temperatures also (up to 573°K). However, the temperature extrapolation of the Gibbs energies with the use of this method must be done with great care and the results obtained must be critically interpreted. Thus in the calculation of the Gibbs energy of formation of $NaReO_4$ ions, which have a positive limiting partial molar heat capacity at 298°K, in the solution of a stoichiometric mixture, we shall obtain a temperature dependence which is precisely opposite to that obtained experimentally. This is valid for all stoichiometric mixtures of ions which have a positive or close to zero limiting partial heat capacity.

The indicated methods have the common and principal disadvantage that they cannot be used to calculate the Gibbs energy of formation of neutral ionic associates in solutions at high temperature, especially since as the temperature is increased the molecular component of the solubility in the overall concentration of the saturated solution increases [7]. For this reason, in the absence of experimental investigations of the dissociation constants of electroneutral associates, the solubility at high temperature cannot be calculated thermodynamically based only on the Criss–Cobble and Khodakovskii methods.

We propose a method for calculating the temperature and pressure dependences of the Gibbs energy of formation of ions in a water solution whose correctness is based on comparison with experimental results on 26 binary water–salt systems, obtained in our laboratory and taken from [8]. The method enables obtaining quantitative results for 298-873°K and pressures from equilibrium pressure up to 500 MPa with water densities >0.4 g/cm^3.

The equation for the calculation of the standard Gibbs energy of formation of an individual ion of any chemical form in solution at a temperature T and pressure p has the form

$$\Delta G^{0,\ T,\ p}_{f,\ aq} = \Delta G^{0,298,\ p_0}_{f,\ aq} + \int_{p_0}^{p} \bar{V}^0_{2i}\, dp - (T-298)\,\bar{S}^{0,298,\ p_0}_i + C_{p_r}[(T-298) - \tag{1}$$

$$-T\ln T/298] + n_i\{[G^{H_2O}_T - G^{H_2O}_{298} + S^{H_2O}_{298} \times$$

$$\times (T-298)]_{p_k+p} - [G^{H_2O}_T - G^{H_2O}_{298} + S^{H_2O}_{298}(T-298)]_p\} + \eta a_i (1/\varepsilon_{T,\ p} - 1/\varepsilon_{298,\ p}) + \eta a_i Y_{298,\ p}(T-298),$$

where $\Delta G^{0,298,p_0}_{f,aq}$ and $\bar{S}^{0,298,p_0}_i$ are the standard Gibbs energy of formation of the ion in the water solution and its absolute entropy at 298.15°K and 0.1013 MPa, respectively; $\bar{V}^0_{2i}$, absolute limiting partial molar volume of an ion in a water solution; C_{pg}, molar heat capacity of the ion in the perfect-gas state; n_i, corodination number of the ion; G^{H_2O} and S^{H_2O}, Gibbs energy and entropy of formation of water, respectively; ε, dielectric constant of water; $\eta = N_A e^2/8\pi\varepsilon_0$ (N_A is Avogadro's number; e is the electron charge; ε_0 is the dielectric constant); $a_i = z_i^2/r_i$ (z_i is the ion charge and r_i is the ion radius, within which the dielectric saturation of the solvent is admitted); $Y_{298,p} = 1/\varepsilon(\partial \ln \varepsilon/\partial T)$; p_k, some effective pressure, which has the same value for large groups of ions, determined by whether they are cations or anions, single-atom or many-atom ions, as well as by their charge.

Let the dissociation occur according to the scheme

$$cC \rightleftarrows aA + bB. \tag{2}$$

In this case, from the viewpoint of formal thermodynamics, the problem of the temperature and pressure extrapolation of the electrolytic dissociation constants of a dissolved charged ionic associate must be solved uniquely with the help of Eq. (1). For the dissociation constnats of a dissolved charged ionic associate must be solved uniquely with the help of Eq. (1). For the dissociation reaction $H_2PO_4^- \rightleftarrows H^+ + HPO_4^{2-}$ the predictions coincide practically completely with the experimental results [9] and the predictions of [10] (see Fig. 1). In the case of the dissociation $HCO_3^- \rightleftarrows H^+ + CO_3^{2-}$ the difference from the data in [10], obtained from an analysis of the experimental results of different authors, does not exceed several pK_{dis}. Based on the error in the data in [7, 10-12] the agreement of the results may be regarded as satisfactory.

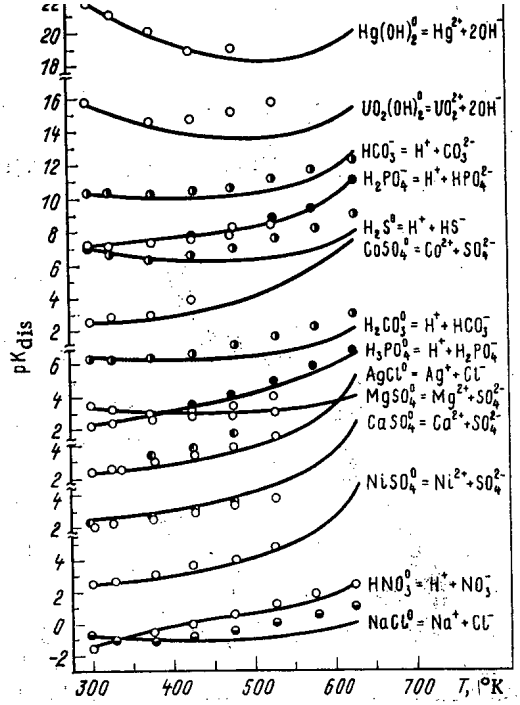

Fig. 1. Comparison of pK_{dis} for several ionic associates, obtained by a computational method, with the published data: ○ — experimental data [7]; ● — prediction [10], ◑ — data in [10] obtained based on an analysis of experimental data ◐ — [11]; ◒ — [12]; calculations of this work.

TABLE 1. Standard Values of the Gibbs Energy of Formation of the Ionic Associate $NaCl^0$ in a Water Solution at the Saturation Vapor Pressure of Pure Water, kJ/mole

Temp., °K							Source or method for obtaining the value
298	373	423	473	523	573	623	
388,02	394,38	400,13	406,62	413,22	418,54	417,41	[12]
388,02	393,1	396,8	400,8	405,1	409,4	414,1	Calc. with total dehydration
388,02	392,7	395,3	398,1	400,8	403,6	406,7	Calc. without dehydration

An important point in this case, from our viewpoint, is the assertion made in [13] that in the case of dissociation according to the scheme (2), when the ions A and B combine and form the charged ion C, the mechanism of uniform distribution of the total charge of the ions A and B over the sphere of the ion C is implausible. In the case of the formation of a neutral ionic associate, however, it admits the compensation of the charges of the A and B ions. The calculations presented show that the model determination of the dissociation constant of a charged ionic associate by the scheme (2) is possible precisely in accordance with the mechanism of uniform distribution of the total charge of the dissociation reaction products over the sphere of the starting ion.

The calculation of the dissociation constants of charged ions was in practice predetermined by the proof of the correctness of Eq. (1) [8], whereas in the case of the calculation of the Gibbs energy of formation of neutral ionic associates there arise three questions whose solution will determine the possibility of their quantitative modeling.

mental studies performed in the monographs [7, 11] as well as attempts to examine the question of the formation of ion pairs from the viewpoint of the electrostatic theory show that in the first approximation this polarization can be neglected, i.e., in the formation of a neutral molecule, more precisely, of a neutral ionic associate, the electric charge of its constituent ions is mutually compensated. This also follows logically from the conclusion drawn above regarding the uniform distribution of the total charge of the dissociation reaction products over the sphere of the starting ionic associate. Thus if it is assumed that Eq. (1) is the general equation for calculating the Gibbs energy of formation of both ions and ionic associates in a water solution, then in the case of the calculation of the Gibbs energy of formation of a neutral ionic associate the last terms of this equation, associated with the polarization hydration, vanish.

2. Does the specific hydration associated with the transfer of water molecules from the solvent into the coordination sphere of the ions, forming an ionic pair, remain when a neutral ionic associate forms, i.e., is the dehydration of ions accompanied by the formation of a neutral ionic asosciate? If so, then what is its significance?

3. What is the heat capacity C_p of the neutral asssociate?

The last two questions can be answered only by correct model calculations for extreme cases. For the base system for answering the last two questions we selected the system $NaCl-H_2O$, for which the Gibbs energy of formation of sodium and chlorine atoms as well as the dissociation constant of the molecule $NaCl^0$ are known in a wide temperature interval [12]. According to Eq. (1), from which the terms associated with polarization hydration were eliminated, we calculated the values of the Gibbs energy of formation of the neutral ionic associate NaCl with a saturation vapor pressure of the pure solvent for the case of total hydration and for the case when the coordination numbers of the sodium and chlorine ions are preserved by the ionic associate (see Table 1). These calculations presume that C_{pg} ($NaCl^0$) is equal to the maximum heat capacity of the NaCl molecule in the excited state of the perfect gas (9/2) R. When the last factor is replaced by (7/2) R – the minimum heat capacity of molecules in the unexcited state – we obtain a difference in the values of $\Delta G^0_{f,aq}, T, P_0(NaCl^0)$ not exceeding 1 kJ/mole at 623°K. Analysis of Table 1 shows that the predictions in both cases are more positive than the experimental values. The predictions obtained under the assumption of total dehydration, however, are closer to the experimental values. Their difference does not exceed 3.3 kJ/mole at 623°K. Thus for calculating the standard values of the Gibbs energy of formation of neutral associates in a water solution at the saturation vapor pressure of pure water the following particular case of Eq. (1) was obtained:

$$\Delta G^{0,\ T,\ p_0}_{f,\ aq} = \Delta G^{0,298,\ p_0}_{f,\ aq} - \bar{S}^{0,298,\ p_0}_{i}(T-298) + C_{p_g}[(T-298) - T\ln T/298]. \quad (3)$$

In the first approximation the problem of calculating the change in the Gibbs energy of the reactions of different transitions with the participation of dissolved components can be regarded as solved, of course, within the limits of error of present high-temperature investigations. But, unfortunately, the method requires a knowledge of the thermodynamic functions of the solution compoennts at 298.15°K and 0.1013 MPa, and this information is widely available only for simple ionic forms; it is limited primarily to the Gibbs energy for the charged ionic associates and there is virtually no information for neutral associates. The method of quantitative evaluation of the entropy at 298.15°K is limited to the chemical forms of the components of the solution, and quantities such as the partial volumes of the neutral ionic associates in a water solution are not available at all.

We did not attempt to build another model of hydration. The need for such a model followed from practical problems, primarily energetics. The purpose of such a model is to establish the quantitative composition of complicated water–salt systems at high temperature and pressure on the basis of *a priori* information about their composition. Using the required data at 298.15°K and 0.1013 MPa from [10, 13], the solubility of magnetite, goethite, amakinite, FeO, and $Fe(OH)_3$ in water for $T \leqslant 623$°K at the saturation vapor pressure of the pure solvent has now been calculated by the method of minimization of the Gibbs energy.

LITERATURE CITED

1. Y. Mishima, "Study on the influence of water chemistry on fuel cladding behavior of LWR in Japan," in: IAEA Specialist's Meeting, Leningrad, June 6-10, 1983 (1983), pp. 17-34.
2. C. Criss and J. Cobble, "The thermodynamic properties of high-temperature aqueous solutions. IV. Entropies of the ions up to 200° and the correspondence principle," J. Am. Chem. Soc., 86, 5385-5390 (1964).
3. I. L. Khodakovskii, "Thermodynamics of water solutions of electrolytes at high temperatures (entropy of ions in water solutions at high temperatures)," Geokhimiya, No. 1, 57-63 (1969).
4. C. Chen and K. Aral, "A computer program for constructing stability diagrams in aqueous solutions at elevated temperatures," Corrosion NACE, 38, No. 4, 183-190 (1982).
5. P. Tremaine and S. Goldman, "Calculation of Gibbs free energies of aqueous electrolytes to 350° from an electrostatic model for ionic hydration," J. Phys. Chem., 82, No. 21, 2317-2321 (1978).
6. U. Sen, "Study of electrolytic solution process using the scaled-particle theory. Part 3. Effects of thermal dilution on standard thermodynamic functions," J. Chem. Soc., Faraday Trans. I, 77, 2883-2899 (1981).
7. B. N. Ryzhenko, Thermodynamics of Equilibria in Hydrothermal Solutions [in Russian], Nauka, Moscow (1981).
8. V. I. Zarembo and L. V. Puchkov, "Standard values of the Gibbs energy of formation of ions and ionic associates in a water solution with high state parameters," Reviews on Thermophysical Properties of Materials/TFTs, No. 2 (46) (1984).
9. R. Mesmer and C. Baes, "Phosphoric acid dissociation equilibria in aqueous solution to 300°C," J. Solut. Chem., 3, No. 4, 307-322 (1974).
10. G. B. Naumov, B. N. Ryzhenko, and I. L. Khodakovskii, Handbook of Thermodynamic Quantities [in Russian], Atomizdat, Moscow (1971).
11. E. A. Mel'vin-Kh'yuz, Equilibrium and Kinetics of Reactions in Solutions [Russian translation], Khimiya, Moscow (1975).
12. H. Helgeson, D. Kirkham, and G. Flowers, "Theoretical prediction of the thermodynamic behaviour of aqueous electrolytes at high pressures and temepratures. IV," Am. J. Sci., 218, No. 10, 1249-1516 (1981).
13. V. S. Belyanin, "Study of thermodynamic properties of water iron compounds," Reviews on Thermophysical Properties of Materials/TFTs, No. 4 (36), 109-166 (1982).

PROBLEMS OF CHEMICAL-ANALYTICAL MONITORING IN NUCLEAR POWER

L. N. Moskvin

UDC 621.039

Further increase of the reliability and efficiency of the operation of nuclear power plants depends on the comprehensive solution of many problems, of which the problem of optimization and increase of the informativeness of chemicotechnological monitoring is gaining in importance. There is a clear rift between the level of scientific ideas and technical solutions on which nuclear power plants are based and the existing approach to the organization of chemical monitoring. Everyone understands the necessity of chemical monitoring, but many people do not regard it as a necessary element for ensuring normal operation of a nuclear power plant. The lack of standard requirements and a standard methodical base markedly lowers the reliability of the results of analyses, and behind this lies possible breakdowns of the water-chemical conditions.

How can this situation be explained? The consequences of deviations of water-chemical conditions from regulation standards are by no means manifested immediately. Apparent well-being at any given time creates the impression that the requirements of the chemical laws can be ignored with impunity. But there is also another reason for the disdainful attitude toward chemical monitoring. Chemical-technological monitoring at a nuclear power plant reduces to the determination of $\sim$20 water-quality indicators for the basic and auxiliary systems. Considering the number of existing points at which samples are extracted in each block of a nuclear power plant and the frequency with which the analyses are performed, it is not difficult to imagine the impressive number of the overall volume of data obtained. Thus the total number of analyses per month for one block of a nuclear power plant with RBMK-1000 approaches 15,000 [1]. In addition, as a rule, these are single measurements, whose error it is virtually impossible to estimate exactly. Moreover, regardless of how conscientious the chemists-analysts at the technological laboratories are, in the monotony of repeating values it is difficult to escape big blunders in the case of unforeseen deviations of the parameters in the water-chemical conditions. Under these conditions there is no hope of obtaining reliable information for each of the measurements, making sense of the observational results, and drawing correct conclusions. We arrive at a paradox. By increasing the number of parameters monitored and the number of points at which samples are extracted we strive to increase the information content of chemical monitoring, but we actually achieve the opposite result.

At the present time, when nuclear power has transformed from a unique source of energy to one of the most important elements of the power production in the country, it is essential to reexamine the concepts forming the basis for the implementation of chemical-analytical monitoring at nuclear power plants. At the first nuclear power plants the research and technological functions of analytical monitoring were balanced, and preference was often given to obtaining research information. For serially produced nuclear power plants research programs are a rare episode. It is evident that the main reason for this situation is hidden in the existing standards and requirements imposed on the chemical monitoring system at nuclear power plants. At the first stages of development of nuclear power the striving toward performing as much analysis as possible and over the entire technolgocial loop was justified, whereas at the present time, as experience in operating nuclear power plants in this country and abroad shows, the time has come to search for new approaches to the problem of analytical monitoring of the quality of water heat carriers.

The successful solution of the problem of analytical monitoring is often linked primarily with the instrumentation. But the number of methodical and instrumentation developments continues to increase, and the chemical-technological monitoring remains as before one of the laborious and unreliable elements in the overall chain of operational monitoring of nuclear power plants. Fundamental restructuring of the overall scheme of such monitoring is possible only based on automatic or, at least, automated means of chemical analysis.

Translated from Atomnaya Énergiya, Vol. 59, No. 6, pp. 398-401, December, 1985. Original article submitted November 16, 1984.

 0038-531X/85/5906-0962$09.50

But this is still a secondary question, one of the constituent parts of a program which must be implemented in order to achieve a qualitatively new level in the organization of an on-line, informative, and effective chemical-technological monitoring program.

At the present time there is no clear understanding of the problems of chemical-technological monitoring at nuclear power plants; these problems are formulated in terms of the evaluation of the corrosion state of the equipment and the presence of deposits in different sections of loops, primarily, in the active zone [2]. Is this true? The occurrence of corrosion processes is a regular consequence of the maintenance of water conditions. The establishment of strict relationships between the quality of the heat carrier and the rate of conversion is a scientific research problem. As in any chemical-technological process, in the chemical technology of a nuclear power plant the problem of monitoring reduces primarily to obtaining reliable analytical information about the regulated parameters. In addition, for nuclear power plants the consequences of optimal flow of chemical processes are not only the minimum rate of corrosion of structural materials, but also problems of safety, linked, for example, with the state of the systems for afterburning of the fulminating mixture for boiling water reactors.

These problems predetermine the approach to the solution of the main problem. Either the operating personnel are reponsible for solving the extremely complicated problem of evaluating and forecasting the corrosion environment, which at the present time can by no means always be solved by specialists in the area of corrosion of structural materials, or they are required only to obtain reliable information on the parameters of those processes to which they can react in real time. Here it is very important to understand the particular parameters of the process which the operating personnel can affect and which parameters are a consequence of technological failures or intraloop processes and cannot be controlled on-line. For example, some indicators of the quality of the water heat carrier (specific electrical conductivity, pH, concentration of sodium and chlorine ions, corrective additives for correcting the conditions) can be regulated by operating personnel when their values move outside the regulated zone, or technical meausres which prevent the values of the parameters from changing substantially in the heat carrier can be adopted. At the same time, some monitored indicators correspond to intraloop physicochemical processes which the operating personnel can affect only indirectly through the change in the parameters listed above. Thus two types of indicaotrs can be distinguished: regulatable and informative. This separation enables, by understanding the cause-effect links, simplifying and in some cases lowering the volume of monitoring based on the number of controllable indicators and points of sample extraction as well as on the frequency of on-line monitoring. For example, a significant fraction of the total labor involved in chemical analysis goes into determining the concentration of iron and copper. And it is precisely these indicators, as a rule, which are the least reliable, since the content of these elements is often at the limits of detection by suitable methods; in addition, the probability of errors owing to random impurities is maximum.

Today the formulation of the problem itself could be surprising: is it necessary to monitor iron and copper within the framework of technological monitoring? But let us consider what the purpose of these indicators is. Observing the high content of iron in water in the process of prestartup flushing, during the startup period or during the operation of the plant, the operating personnel wait until it drops, since they observe the deviations of the water conditions which led to this jump a long time ago on the basis of other parameters and took appropriate measures. In none of the possible situations does an indicator such as the concentration of iron require on-line interference in the technological process, i.e., this is a typical informative indicator. And since it is informative, it is possible and necessary to decrease the volume of monitoring of the iron concentration right down to complete elimination of this parameter as our depth of understanding of intraloop processes increases. The same can be said about copper.

A substantial reduction in the number of analyses performed can apparently be achieved by taking into account the internal interrelationship of the indicators of the quality of the water heat carrier and not only of it, but also of the cooling water. Why, for example, should the "hardness" of the vapor condensate be determined? The presence of leaks can be judged from indicators such as the concentration of sodium and chlorine ions. If, on the other hand, it is necessary to know the exact content of "hardness salts," then it is simpler to determine the ratio of the sodium and calcium concentrations in the cooling water,

which, as a rule, remains constant for reservoir coolant, and to determine the hardness by a computational method using the correlation coefficient found. At the present time it is difficult to give practical recommendations for taking into account the existing correlations in the nature of the changes of different parameters of the water heat carrier, since there are few studies of this question because of the inadequate reliability of the primary information, obtained, as a rule, with the use of simple-extractive methods of analysis, which are distinguished by low metrological characteristics.

Very often, especially when laboratory methods of analysis are discussed, the determination of the content of one or another component of the water solution is unreliable because the essence of the methods used are not understood or because of the fact that any method of determination, even the best method, is inherently uncertain and ignored. Several examples can be presented. At many nuclear power plants the nephelometric method with a lower limit of determination of ~25 μg/l is used to determine the concentration of chloride ions. Detailed studies [3] have shown, however, that in order to achieve the indicated limit a sample volume of not less than 400 ml is required, but even in this case the reliability of determination does not exceed 50%. Another example is associated with the determination of the specific electrical conductivity and the pH. Quite often these indicaotrs are determined by sample-extraction methods, forgetting that in this case contact with the atmosphere changes these indicators in an uncontrollable fashion because carbon dioxide dissolves in the samples extracted. The use of automatic instruments without proper maintenance also does not exclude the possibility of the appearance of large errors. These errors are most often caused by the inability to perform correctly the primary calibration of the apparatus. For example, in the method for calibrating the "pNa-meter" proposed in the technical documentation for this device, it appears that the residual content of sodium atoms in the reference water is taken into account, but it is not clear how this residual content is determined. Finally, a quite prevalent rough error is the use of only one determination as the result of the analysis. It is evident that it is either necessary to know the reproducibility and the accuracy of the analysis and give the results with the corresponding error or to perform a series of parallel measurements and to determine the average value. In this sense reduction of the volume of monitoring will enable meeting more strictly the metrological requirements in performance of laboratory analyses. The most important result of the reduction of the volume of chemical monitoring as a whole is the possibility of complex automation and, as a consequence, raising the relibility and validity of the results obtained.

The transition from manual sample-extracting methods of monitoring to automatic monitoring means not only continuous acquisition of data, but also the possibility of utilizing the data for forecasting and determining the reasons for deviations from fixed water conditions and for well-founded on-line interference in the technological process. Experience in operating automatic chlorine meters at nuclear power plants shows that the change in the concentration of chloride ions can be recorded earlier than the change in the electrical conductivity. This is linked to the fact that the specific conductivity is an integral indicator, to which the most highly mobile hydroxyl ions and activated protons make the main contribution. From here it follows that when selecting the means for monitoring it is primarily necessary to develop sensors which react selectively to definite impurities. There now exists an instrumental-methodical foundation for continuous monitoring of the most important parameters of the coolant in the flow under correction-free water conditions.

The changeover to automated chemical monitoring systems is inseparably linked with the introduction of automated systems for processing of the results of analysis. In addition, such systems must not only fix the entire set of data and compare the results according to the times and points at which samples are extracted, but it must also have the capability of forecasting the possible flow of the technological process, as well as providing information on the reasons for the breakdown of the water conditions.

This closes the logical chain. The improvement of the chemical technology of nuclear power plants opens up the possibility of reducing the volume of chemical monitoring. The minimum number of monitored parameters is an insurance for reliability of the results and opens up a real possibility for full automation of chemical monitoring. Automated means of chemical monitoring based on flow through sensors will maximize the effectiveness of analytical information on the technological process. From here follows the conclusion that the most important problems of chemical-analytical technological monitoring at nuclear power plants now lie at the boundary with technological problems and cannot be solved only by

chemists-analysts. It is difficult to expect significant progress in this question, if only the methods and means of chemical monitoring are improved.

LITERATURE CITED

1. É. P. Kazakova, V. A. Mamet, and V. F. Tyapkov, Nuclear Power Plants [in Russian], No. 2 (1979), pp. 180-183.
2. O. I. Martynova, L. M. Zhivilova, and N. P. Subbotina, Chemical Monitoring of the Water Conditions in Nuclear Power Plants [in Russian], Atomizdat, Moscow (1980).
3. Yu. M. Kostrikin, Teploénergetika, No. 1, 52-54 (1976).

REMOVAL OF CORROSION PRODUCTS FROM THE STEEL SURFACE IN THE AQUEOUS COOLANT OF NUCLEAR POWER PLANTS

V. G. Kritskii, A. S. Korolev,
I. G. Berezina, and M. V. Sof'in

UDC 621.039.553.36

Corrosion of the materials of the low-pressure preheater tubes and casings, piping, and other elements of the condensate supply channel of NPP does not usually affect their operational reliability and life. However, during operation, a part of the products passes into water, and is subsequently transported to the reactor and enters the primary circuit. In boiling water reactors, the corrosion products settle mainly on the surface of the fuel elements. They can cause damage to the fuel elements and, after activation, they are distributed along the circuit surfaces and significantly increase the total level of the coolant activity and the radiation dose from the system. A knowledge of the conditions under which there is an increased removal of the corrosion products helps one to considerably decrease entry of the corrosion products into the primary circuit of the reactor.

This paper deals with the investigation on the effect of different factors on the transfer of the corrosion products of steels into the aqueous medium. The kinetics of corrosion and removal of the corrosion products was studied on the specimens tested under the conditions of the condensate supply channel of a NPP having RBMK reactors and under static conditions. The indicator-specimens were placed in the deaerator tanks, deaerator column (in the decontaminated condensate stream), and in the mechanical filtration unit of supply water. The specimens were withdrawn after testing for 3200, 5000, and 9000 h. The quality of water of the condensate supply channel met the specification OST 95-743–79. In one experiment, we monitored the oxygen content in the decontaminated condensate, and under static conditions – the content of the oxidizing agent H_2O_2 in water. The treatment of the specimens before and after testing, and the calculations of the corrosion rate and the rate of removal of the corrosion products were carried out according to the procedure described elsewhere [1] (Table 1).

The magnitudes of corrosion and removal of the corrosion products in the supply water are described by the so-called "sigmoidal" curves (Fig. 1). The initial incubation period is particularly noticeable in the case of the Kh18N10T steel. In the case where the quantity of the corrosion products retained in the specimens exceeded the quantity calculated on the basis of their weight loss after removing the films, we considered that the precipitation processes of the corrosion products from water took place.

In the conventional method of evaluating the magnitude of removal of the corrosion products [1, 2], the degree of transfer of the corrosion products into water has been established using the ratio of the specific weight of the product entering water and the specific weight of all the corrosion products of the steel formed under the given conditions as the criterion. It was found that the removal of the corrosion products varies smoothly (continuously) with time and depends on the chromium content in the alloy. Such a trend of the curves is less informative. In the computed models, the tabulated values of the percentage removal for each grade of steel (under different conditions) are simply assigned.

Translated from Atomnaya Énergiya, Vol. 59, No. 6, pp. 401-403, December, 1985. Original article submitted November 16, 1984.

0038-531X/85/5906-0965$09.50

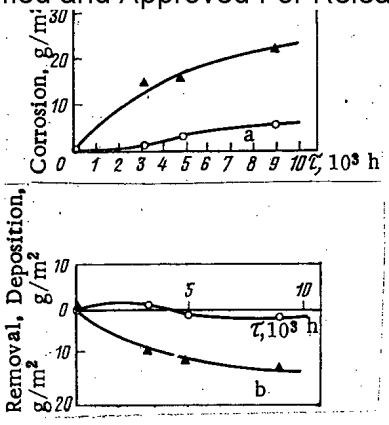

Fig. 1

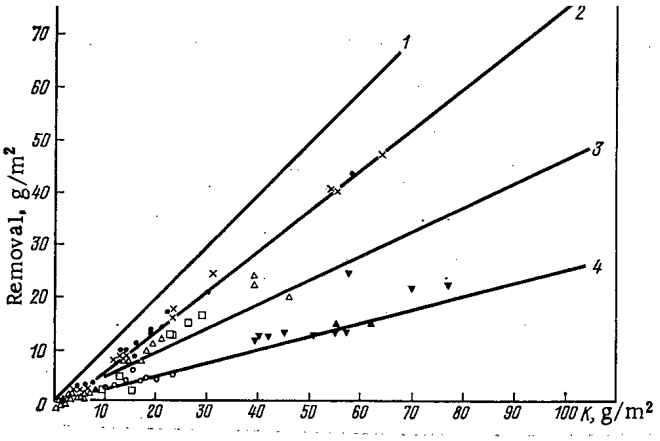

Fig. 2

Fig. 1. Corrosion (a), and deposition and removal of the corrosion products (b) in the supply water: ▲) steel 20; ⊙) steel Kh18N10T.

Fig. 2. Relationship between the magnitudes of corrosion and the removal of corrosion products observed in the tests in two water-chemical (hydrochemical) regimes: 1, 3) A = 1; 0.5; 2) oxygen-free water; 4) water with oxygen (40-300 μg/kg); •) supply water (test duration: 4750 h, June 1983); Δ) deaerator No. 51 (tank) (3262 h, June 1982); ×) deaerator No. 61 (tank) (3240 h, June 1982); □) deaerator No. 21 (tank) (8950 h, December 1981); ▲) multiple forced-circulation loop (8030 h, December 1981); ○) deaerator No. 61 (column) (3240 h, June 1982); ▼) deaerator No. 51 (column) (3262 h, June 1982).

TABLE 1. Chemical Composition of the Experimental Steels

Melt number	Weight content of the elements, %							
	C	Si	Mn	Cr	Cu	Ni	P	S
8	0,08	0,37	0,40	21,7	—	—	—	—
9	0,08	0,29	0,37	13,0	0,25	—	—	—
16	0,08	0,17	0,26	4,8	1,05	0,66	—	—
17	0,08	0,21	0,26	9,0	—	2,1	—	—
68	0,10	0,3	0,6	0,03	—	—	0,010	0,021
70	0,14	0,3	0,6	1,50	—	—	0,011	0,020
305	0,11	0,46	0,52	0,065	0,24	0,1	—	—
307	0,08	0,38	0,52	0,19	0,67	0,38	—	—
3	0,03	0,37	0,36	16,0	—	—	—	—
4	0,03	0,41	0,44	24,2	—	—	—	—
Kh18N10T	Standard composition							
73	0,3	0,3	0,6	2,6	—	—	0,010	0,021
AS-9	Standard composition							
205	0,03	0,29	0,23	11,6	—	—	—	—
22R	0,26	0,32	0,77	0,18	—	0,05	0,017	0,029

There is a complete change in the pattern when the data of the corrosion tests are plotted in different coordinates: the absolute values of corrosion on the x axis, g/m^2, and the removal (deposition) of the corrosion products recalculated with respect to the metal content in the corrosion products on the y axis. For a series of specimens, the relationship between corrosion and removal (which, in turn, are nonlinear functions of time and the degree of alloying) can be described by the following linear equation (Fig. 2)

$$B = A(K - K_0), \quad (1)$$

where B is the removal within the test duration, g/m^2; K is the corrosion within this period, g/m^2; K_0 is a constant that may be interpreted as the weight of the metal contained in the minimum protective layer under the conditions of testing, g/m^2; and A is a constant that depends on the type of water-chemical (hydrochemical) regime.

Equation (1) shows that the film thickness $\Delta\zeta$ can be found out from the equations $\Delta\zeta = K - B$; $\Delta\zeta = K - AK + AK_0$. If $AK_0 = \Delta\zeta_0$ – the initial thickness of the protective film – then $\Delta\zeta - \Delta\zeta_0 = K(1 - A)$. This experimentally established fact was verified on the published data for steels in all the water-chemical regimes that are of interest in the nuclear power engineering. In this case, the following values were established for the constant A: $A \approx 1$ (for the primary circuit of the PWR reactors); $A \approx 0.5$ (for the primary circuits of the BWR and RBMK reactors); $A \approx 0.66$ (for deaerated supply water having pH ≈ 7); and $A \leqslant 0.5$, usually ~ 0.25 [for the decontaminated condensate with pH ≈ 7 and with dosing of oxidizing agents (air, O_2, or H_2O_2)].

The steels having different chromium contents usually have the same value of A in a given water-chemical regime; on the other hand, the change in the magnitude of removal with time is a phenomenon apparently related to the duration required for the formation of the initial protective oxide film (see Fig. 2). In the general case, the topochemical reaction of the formation (growth) of the protective surface layer takes place at first, and is followed by a transition to the diffusion-controlled (through the already formed layer) kinetics.

The growth rate of the oxide layer is usually described by the following differential equation [3]

$$\frac{\partial \Delta\zeta}{\partial\tau} = \frac{K_p}{2}\Delta\zeta^{-1}, \tag{2}$$

where $\Delta\zeta$ is the layer thickness; and K_p is the parabolic-growth constant. If we assume that the removal of the corrosion products is accomplished independent of $\Delta\zeta$ and time (erosive wash-off), the resulting rate can be written as

$$\frac{\partial \Delta\zeta}{\partial\tau} = \frac{K_p}{2}\Delta\zeta^{-1} - C, \tag{3}$$

where C is the constant of the erosion process. In case the removal of the corrosion products is due to the redistribution of the incoming ions from the metal between the oxide film and the solution, the growth rate of the film is given by

$$\frac{\partial \Delta\zeta}{\partial\tau} = \frac{K_p}{2}[\Delta\zeta(1-A)]^{-1}, \tag{4}$$

where A is the constant of removal as obtained from Eq. (1). Integration of the Eqs. (2)-(4) gives

$$\tau = \frac{1}{K_p}\Delta\zeta^2 + \text{const}; \tag{5}$$

$$\tau = \frac{1}{K_p}[\Delta\zeta^2 - \Delta\zeta_0^2] + \frac{4}{3}\left(\frac{C}{K^2}\right)[\Delta\zeta^3 - \Delta\zeta_0^3] + \ldots; \tag{6}$$

$$\tau = \frac{1}{K_p}[(1-A)\Delta\zeta + \Delta\zeta_0]^2, \tag{7}$$

respectively, where $\Delta\zeta_0$ is the initial thickness of the film at $\tau = 0$. At C = 0 and A = 0, Eqs. (6) and (7) transform into Eq. (5).

Using the coordinates $\Delta\zeta = f\left(\frac{\tau}{\Delta\zeta}\right)$ and computer analysis of the results, the values of all the constants entering Eqs. (5)-(7) are generally obtained. However, in this case, one requires the value of the coefficient A obtained when determining the magntiude of the removal (transfer) of the corrosion products into water. Therefore, it is recommended that one must not only record the corrosion (metal) losses, but also study the film. This is particularly important in view of the fact that in neutral media (according to the results of numerous experimental investigations) there is a correlation between the quantity of the material settled in the external 'loose' (porous) layer and that settled in the dense film. The complex approach adopted to determine the redistribution of the metal between the oxide layer and the coolant during the corrosion process of the metal shows that this process is not accidental and that it depends on the properties of the coolant.

LITERATURE CITED

1. V. M. Nikitin, A. M. Gvozd', and T. Ya. Karpova, "Regularities in the transition of the corrosion products of steels into the aqueous media," Teploénergetika, No. 8, 44-48 (1981).
2. I. K. Morozova, A. I. Gromova, V. V. Gerasimov, et al., Removal and Deposition of the Corrosion Products of the Reactor Materials [in Russian], Atomizdat (1975), p. 280.
3. K. Hauffe, Reactions in Solids and on Their Surfaces [Russian translation], Part II, Izd. Inostr. Lit., Moscow (1963).

CALCULATION OF THE MAGNITUDES OF DEPOSITION AND CONCENTRATION OF CORROSION PRODUCTS IN BOILING WATER REACTORS

O. T. Konovalova, M. I. Ryabov, L. N. Karakhan'yan, and T. I. Kosheleva

UDC 621.039.548.5

In order to establish the characteristics of the water (aqueous) regime and the means of maintaining it, it is necessary to determine the concentration of the corrosion products in the multiple forced-circulation loop (MFCL) of a boiling water channel reactor. The quantity of corrosion products of iron (c.p.i) entering the coolant from the i-th segment of the loop (circuit) per unit time can be expressed as

$$B_i = K_i p_i S_i \tau^{-0.5}, \quad (1)$$

where $K_i\tau^{-0.5}$ is the corrosion rate, g/(m²·h); p_i, fraction of the corrosion products entering the coolant; S_i, surface area of the segment of the loop, m²; and τ, time, h. The total quantity of the corrosion products entering MFCL is given by

$$B = 0.5 \sum_1^n B_i = 0.5 \left(\sum_1^n K_i p_i S_i\right) \tau^{-0.5}. \quad (2)$$

The coefficient 0.5 takes into account the degree of decontamination from the corrosion products during the condensate purification treatment.

During decontamination of the loop, G_1 gram corrosion products are removed per hour: $G_1 = 0.5PC$, where 0.5 represents the degree of decontamination; P is the coolant consumption for decontaminating the loop, kg/h; and C is the concentration of the corrosion products, g/kg.

Steam carries away $G_2 = K_1NC$ corrosion products, where K_1 is the coefficient of distribution of the corrosion products between water and steam; and N is the productivity of steam, kg/h.

On the surface of the heat liberating elements one observes deposition (settling) of the corrosion products amounting to $G_3 = 0.5tK_2C$, where 0.5 is the coefficient of nonuniformity of deposition along the length of the fuel element; S_t is the total surface area of the fuel elements, m²; and K_2 is the coefficient of deposition of the corrosion products in the area of boundary (wall) layer boiling. The balance equation of the corrosion products assumes the following form:

$$0.5 \left(\sum_1^n K_i p_i S_i\right) \tau^{-0.5} = (0.5P + K_1 N + 0.5 S_t K_2) C. \quad (3)$$

In the case of a boiling water channel reactor, the equation has the following form

$$\lg C = -3.6 - 0.5 \lg \tau. \quad (4)$$

We experimentally obtained the following time dependence of the concentration of the corrosion products

$$\lg C = -(3-4) - 0.5 \lg \tau. \quad (5)$$

Translated from Atomnaya Énergiya, Vol. 59, No. 6, pp. 403-405, December, 1985. Original article submitted November 16, 1984.

 0038-531X/85/5906-0968$09.50

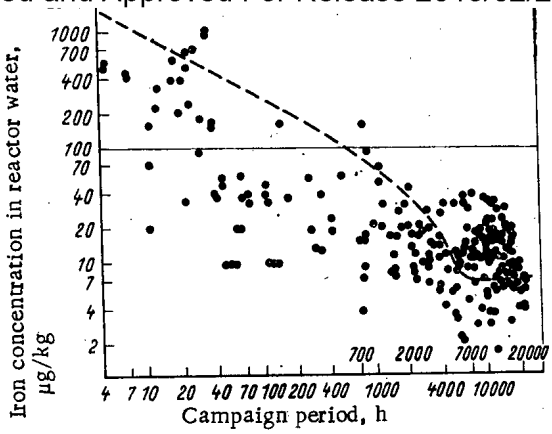

Fig. 1

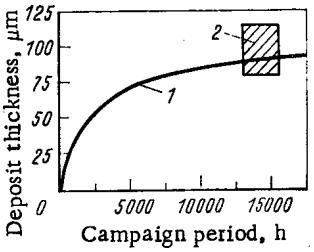

Fig. 2

Fig. 1. Calculated (---) and experimental (•) values of the iron concentration in the MFCL of a boiling water reactor [2].

Fig. 2. Calculated (1) and experimental (2) values of the deposits on the fuel elements of the boiling water reactor [3].

Along with the aforementioned method of calculating the concentration of c.p.i in reactor water, there was a parallel development of another method of calculating the mass transfer and the maximum deposition of c.p.i based on the theory of formation of deposits (precipitates) [1] according to which in the general case, the deposition mechanisms of c.p.i are described by different mathematical relationships in the regions of single phase stream with convective heat exchange, boundary layer and developed bubbly boiling, and in the zone of cyclic flow regime of the steam–water mixture. The c.p.i can exist in reactor water in two forms: dissolved and undissolved. Both forms of c.p.i. precipitate on the fuel elements, but the mechanisms of their deposition are different. The quantitative relationship between the concentrations of the dissolved and the undissolved c.p.i depends on the temperature and the water (aqueous) regime.

According to the stated method, the time dependent concentration of c.p.i is found out based on the balance between the entrance and the removal of c.p.i. into the reactor water:

$$C = \left(C_p + \frac{B - S_t \bar{g}_p - NK_1 C_p}{S_t \bar{K}_t^* \rho + S\bar{K}^* \rho}\right) \Big/ \left(1 + \frac{\varkappa P + N\varepsilon_k}{S_t \bar{K}_t^* \rho + S\bar{K}^* \rho}\right), \qquad (6)$$

where C_p is the concentration of the dissolved c.p.i, g/kg; S, area of the unheated surfaces of MFCL, m^2; $\bar{g}_p$, average deposition rate of the dissolved c.p.i on the fuel elements according to the crystallization mechanism, $g/(m^2 \cdot h)$; $\bar{K}_t^*$ and $\bar{K}^*$, average deposition coefficients of the particles of c.p.i on the fuel elements and on the unheated surfaces, m/h; ρ, coolant density, kg/m^3; ε_k, coefficient of dropwise removal; and $\varkappa$, coefficient of effectiveness (efficiency) of the decontamination system.

Using the known concentration of c.p.i in MFCL, one can find out the values of deposits on the fuel elements and on the unheated surfaces, and extraction of iron by the decontamination system. For example, the quantity of deposits on a local fuel element segment G (g/m^2) is given by:

$$G = g_p \tau + \int_0^\tau K_1 (C - C_p) \rho \, d\tau = g_p \tau + \frac{K_t^* \rho \{0.5 B_0 \sqrt{\tau} - \tau [C_p (\varkappa P + N\varepsilon_k + NK_1) + S_T \bar{g}_p]\}}{S_t \bar{K}_t^* \rho + S\bar{K}^* \rho + \varkappa P + N\varepsilon_k}, \qquad (7)$$

where the first term takes the deposition of the dissolved c.p.i into account and the second term (integral) accounts for the deposition of the particles of c.p.i; g_p is the local growth rate of the deposits of dissolved c.p.i on the fuel elements, $g/(m^2 \cdot h)$; K_t^* is the local coefficient of deposition of the particles of c.p.i on the fuel elements, m/h; and $B_0 = \Sigma K_i \rho_i S_i$. All the parameters entering Eqs. (6) and (7) can be determined quantitatively using the previously published relationships [1].

Figure 1 shows a comparison of the calculated and the experimental values of the iron concentration in the MFCL of a boiling water reactor.

During the intial period of campaign (during which one observed the maximum growth of deposits), the calculated values of the iron concentration lie close to the upper limit of the experimental values. After operating the reactor for 5000 h, the level of the experimental values of the iron concentration sometimes exceeds the level of the calculated values. Apparently, this fact is related to the periodic erosion (wash off) of the deposits because of the transient periods and other circumstances.

Figure 2 shows a comparison of the calculated and the experimental values of the deposits on fuel elements of the boiling water reactor. After operating for 2 years and acid washing, the thickness of the deposits in the zone of the boundary layer boiling reaches a level of 100 μm; the calculated curve also indicates this level. For the purpose of calculations, the density of the deposits was taken as 2 g/cm^3.

In the experiments, we recorded the local deposition of c.p.i under the spacer grids (SG) in the fuel elements assemblies of the boiling water reactors which exceeds the deposition on the adjacent regions of the fuel elements by 1.3-5 times. In this case, as one approaches the exit end of the assembly (i.e., with increasing flow rate of the steam–water mixture), there is a relative growth (increase) of the deposits under the grids.

The effect of SG may be explained in the following way. They hydraulically act on the coolant flow such that it partially deviates from the axis and streams directed towards the fuel elements develop in it. During this process, all the particles of c.p.i moving in such a stream reach the fuel elements surface overcoming the boundary layers of water due to inertia. The growth rate of the deposits under the action of such a stream g_{SG}, g/(m^2·h), is given by

$$g_{SG} = 3600 C_w W \rho \xi, \tag{8}$$

where C_w is the concentration of the particles of c.p.i in water, g/kg; W, local flow rate, m/sec; $\xi = \exp(-E/RT)$, probability of adherence of the particles of c.p.i to the wall; and E, activation energy of the surface dehydration process of the particles of c.p.i, kJ/kg.

According to Gerasimov [1], $\xi \approx 10^{-4}$. The speed (flow rate) of the coolant washing the assembly increases along its height from 2 up to 20 m/sec. The local coefficients of the deposition process of the particles of c.p.i (K^*_{SG}, m/h) on the fuel elements under the influence of SG are equal to $K^*_{SG} = 3600 W\xi = 3600\ (2\text{-}20)10^{-4} \approx 0.5\text{-}10$.

The local coefficients of deposition on the fuel elements under the influence of the other processes examined earlier [1] are equal to $K^*_t = 0.2\text{-}15$ m/h. As one approaches the upper end of the assembly, K^*_t values decrease because of the reduced thermal flux.

Thus, SG can make the coolant stream deviate towards the wall, and, thereby, cause additional growth of the deposits that is comparable to the effect of other factors. This relative contribution of the effect of SG on the deposition process must increase with increasing flow rate; this agrees with the experimental data. In order to avoid increased deposition under SG, it is necessary to decrease the total concentration of iron in reactor water.

LITERATURE CITED

1. V. V. Garasimov, Corrosion of Reactor Material [in Russian], Atomizdat, Moscow (1980), pp. 163-181.
2. A. I. Gromova and V. P. Sentyurev, "USSR–UK Seminar on the water-chemical regimes and the structural materials of boiling water channel reactors," At. Énerg., 45, No. 1, 77 (1978).
3. I. A. Varovin, A. P. Eperin, M. P. Umanets, and V. G. Shcherbina, "A decade-long experience on the operation of the Leningrad NPP," ibid., 55, No. 6, 349 (1983).

FORMATION OF DEPOSITS ON THE SURFACE OF THE FUEL ELEMENTS OF RBMK-1000

I. A. Varovin, S. A. Nikiforov,
A. P. Eperin, Yu. N. Aniskin,
V. G. Kritskii, and Yu. A. Khitrov

UDC 621.039.553.36

At the present time, it is considered that the phenomenon of particle binding on the surface of the fuel elements directly leads to the formation of the structures of constant density. Here, the particle binding stage is visualized as the crystallization of the dissolved substance (form) and dehydration of the dispersed particles (d.p.) on the surface [1]. The following observations (that are useful for ensuring reliable operation of the fuel elements) reflect this concept: safe operation of the fuel elements is determined only by the effect of the total thickness of the deposit (precipitate) layer; the coefficient of thermal conductivity of the deposits remains constant.

There is yet another possible theoretical interpretation for the phenomenon of d.p. deposition. Their binding is a consequence of the initial formation and continuous densification of the low-density structures. In this case, the coefficient of thermal conductivity of the deposits becomes a variable that depends on the rate of formation of the layer of the more porous (loose) structure and its transformation into a more dense structure and, also, on the d.p. concentration in water and the operational duration of the power system. Under these conditions, safe operation of the fuel elements may not be determined by the total thickness of the deposit layer, but it may depend on the porous (loose) portion of this layer that has the maximum thermal resistance.

The published values of the average coefficients of thermal conductivity of the deposit layer vary over a wide range: 8.6-0.015 kcal/(m·h·deg) [2, 3]. It is difficult to explain such a large discrepancy of the experimental data if the formation of the constant-density deposits occurs directly. At the same time, it is natural if we note that the average coefficient of thermal conductivity of the deposits is a function of the relationship between the layer thickness and the duration of existence of the deposits. In view of this, the concept of variable density of the deposit layer is fairly admissible. A special study is required for answering the question: which of the two aforementioned hypotheses reflects the physical essence of the processes occuring under the actual conditions?

EVOLUTION OF VARIABLE-DENSITY STRUCTURES — A ROUTE FOR THE FORMATION OF DEPOSITS

Separation (precipitation) of the deposits from the solutions containing d.p. is often a result of the formation of the periodic colloidal structures (p.c.s.) which is an intermediate stage of the formation of dense deposits during the evolution process of the electrophoretic deposits of d.p. At the present time, it has been shown [4] that the polarizing interaction of the particles and the possibility of their subsequent aggregation must be taken into acocunt when studying the evolution processes of the electrophoretic deposits. The dominating effect of the polarizing interaction during the formation of p.c.s. offers a possibility for the separation of dense coatings owing to comparatively easy sliding of the particles and their aggregates (chains) relative to each other.

The hydroxides entering the composition of the dispersed products have a significant polarizing dipole moment [4]. Electric fields form in the boundary liquid layer also. These fields form due to the corrosion processes and thermal flux. Heat transfer through the boundary layer requires temperature gradients inducing thermal diffusional processes as well as diffusion of the dissolved form of the barely soluble compounds whose solubility decreases with temperature variations.

Translated from Atomnaya Énergiya, Vol. 59, No. 6, pp. 405-409, December, 1985. Original article submitted November 16, 1984.

0038-531X/85/5906-0971$09.50

The formation of the electrical fields is related to the differences in the ionic mobility during the diffusion and thermal diffusion processes and, to the tendency of the solution to remain electrically neutral. This internal electric field accelerates the slower ions and decelerates the faster ones. In a binary electrolyte solution it ensures identical ion transfer rate during the diffusion and thermal diffusion process. The electric potential difference appearing in the liquid is one of the components of the diffusion and thermal diffusion potentials that can be measured using electrochemical methods [5, 6].

The existence of the electric field in water and the dipole moments in d.p. is a sufficient condition for the formation of the layer of the variable-density deposits as a result of the formation of p.c.s. They form in the liquid boundary layers of the power systems. Now, the question is: how significant is the effect of this field on the structure evolution of the deposits? The answer to this question requires determination of the boundary-layer electric field intensity, and also, the intrinsic and polarizing dipole moments of the particles. At the present time, direct measurement of the component of the diffusion and thermal diffusion potentials (having the physical meaning of an internal electric field in the electrolyte solution) remains an unsolved experimental problem [6]. In certain cases, it may be evaluated theoretically; for example, it is possible to calculate the electric fields developing in dilute solutions under the influence of the diffusional processes. In the isothermal liquid layer, calculating the electric field intensity of the dilute solutions is complicated because of the absence of the data on the coefficients of thermal diffusion of ions. In view of this, it is difficult to give a theoretical evidence for the possibility of deposit formation of a result of the development of p.c.s.

At the same time, there are experimental data which can be interpreted as a confirmation of the suggestion that in certain cases, the process of deposit formation on the heat transferring surfaces occurs precisely in this way. In fact, when the heat flux decreases significantly, reversal of the corrosion products is often observed [2, 7]. A change in the heat flux causes a change in the electric field intensity in the heat-transferring liquid layer and a corresponding change in the polarizing interaction forces. Bond weakening within p.c.s. results in the hydrodynamic separation of certain d.p.

However, these experimental data can be interpreted differently: the reversal of the corrosion products under reduced thermal flux is a consequence of the increased solubility of magnetite with decreasing temperature [2] and, therefore, the observed experimental fact must not be considered as a direct proof for the formation of the deposits through p.c.s.

EXPERIMENTAL CONFIRMATION OF THE DEPOSIT FORMATION THROUGH THE STAGE OF THE PERIODIC COLLOIDAL STRUCTURE EVOLUTION

A theoretical examination of the process of deposit formation on the heat transferring surfaces shows that at the present time, there are, in principle, two approaches available for understanding this aspect.

1. The deposit formation process consists of two stages: supply (admission) and binding (pinning). The relationship between them is realized only through the d.p. concentration. The binding stage is related to their dehydration.

2. During the formation of deposits, there is an intermediate stage of p.c.s. evolution between the stages of dehydration and supply. The relationship between the supply and the formation of p.c.s. may be accomplished through the d.p. concentration as well as through the driving force of these processes.

The driving force of the process of d.p. transfer through the liquid boundary layer and the formation of p.c.s. is the electric field developing in this layer in the presence of temperature gradients. Based on an analysis of the theoretical and experimental dependences of the rate of deposit formation, one must not draw unequivocal conclusions regarding the route of deposit formation: directly through the dehydration stage or through a prior stage of p.c.s. formation. An answer to this question was obtained from an analysis of the temperature variation in the fuel element jackets in the region of the surface boiling zone of the thermometric fuel assemblies (FA).

The deposits accumulating in the fuel elements form an additional thermal resistance between the fuel element jacket and the main flow of water, and therefore, under constant thermal flux density, the formtion of deposits is invariably related to the temperature increase in the fuel elements.

The structures developed by the dehydrated particles and p.c.s. significantly differ from the standpoint of thermal conductivity. Dehydrated d.p. form porous structures that are close to the crystalline structures (magnetite type) and whose thermal conductivity is virtually determined by thermal conductivity of magnetite taking its porosity into account. The density of these structures (here again, taking the porosity into account) is approximately a few grams per cubic centimeter. Their thermal conductivity depends on the heat transfer zone in which they form. In the region of surface boiling, the thermal conductivity of these deposits is considerably higher than that observed in the zone of convective heat transfer and well-developed boiling [2]. According to these data, the effective thermal conductivity of the iron oxide deposits in the surface boiling zone amounts to 8.6 kcal/(m·h·deg).

The p.c.s. have a low density because of considerable separation of d.p. from each other. Their thermal conductivity may be taken as virtually equal to that of water 0.5 kcal/(m·h·deg). During heat transfer, the appearance of a p.c.s. layer is equivalent to thickening of the lamellar layer. Thus, in the region of surface boiling, the deposits forming directly through the stage of dehydration and through the intermediate stage of the p.c.s. evolution can differently affect the temperature in the fuel element jackets.

The rate of formation of the deposits is governed by the rate of entrance (arrival) of the corrosion products. The rate of out-flow of the corrosion products of the main materials of the NPP circuits decreases with time according to the law: $\tau^{-0.5}$, where τ is the operational time of the system. If the process of deposit formation occurs only through the dehydration stage, the jacket temperature at a point located in the region of the surface boiling zone under a given channel capacity (power) must increase linearly according to $T_p + b\tau^{0.5}$, where T_p is the temperature at the point after the channel is set to the normal capacity; and $b\tau^{0.5}$ is the temperature change during operation.

If the process of deposit formation takes place through the intermediate stage of p.c.s. evolution, the thickness of the intermediate layer of p.c.s. depends on the d.p. supply and dehydration rates. Depending on the ratio of these rates at the point located in the region of possible existence of the surface boiling zone, a different nature of temperature variation must be observed in the fuel element jackets when the channel is working at a constant capacity.

If the dehydration rate is substantially higher than the d.p. supply rate, the temperature of the fuel element jackets increases as in the absence of the stage of p.c.s. formation, i.e., as a function of the form $T_p + b\tau^{0.5}$.

If the rate of p.c.s. formation is slightly higher than the dehydration rate, the temperature of the fuel element jackets increases somewhat slower than that given by the function $T_p + b\tau^{0.5}$ because of the reduced thickness of the p.c.s. layer as a result of the decreased d.p. concentration in water with time.

If the rate of p.c.s. formation is much higher than the dehydration rate and the thermal conductivity of the hydrated deposits is much higher than that of the p.c.s. layer, then the temeprature of the fuel element jackets will be maximum at the initial operational period of the system during which the concentration is maximum, and it may decrease with time as the system continues to operate, i.e., $T = f(\tau, \delta_{p.c.s.})$.

Figure 1 shows that the maximum temperature of the internal jacket of the fuel elements decreases with time. This effect may be interpreted as a consequence of decreased capacity (power) of the fuel assemblies because of fuel depletion and reduction in the thermal resistance of the deposit layer. Using Fick's law, we can write

$$\frac{\Delta T_2}{\Delta T_1} = \alpha_T = \frac{q_2\delta_2\lambda_1}{p_1\delta_1\lambda_2} = \frac{N_2\delta_2\lambda_1}{N_1\delta_1\lambda_2}, \quad (1)$$

where q is the thermal flux density; δ is the thickness of the deposit layer; λ is the coefficient of thermal conductivity; and N is the thermal capacity of the channel. When the deposit layer forms at a rate that decreases in proportion to the square of time and the coefficient of thermal conductivity remains constant, Eq. (1) has the following form:

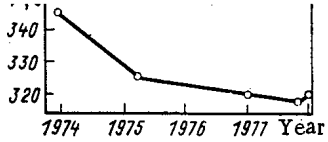

Fig. 1. Maximum temperature of the fuel element jacket of the thermometric cassette in the zone of surface boiling (cell 45-54, 1974 and 1977).

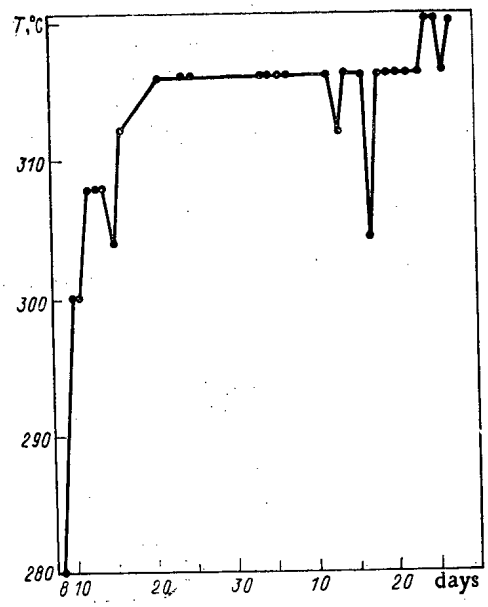

Fig. 2. Temperature increase in the fuel element jacket of the thermometric cassette when setting the unit to the nominal capacity within 3 days (August, September, 1978).

$$\alpha_T = \frac{N_2\tau_2^{0.5}}{N_1\tau_1^{0.5}}.$$

The maximum temperature of the fuel element jackets was recorded in 1974 approximately after 6 months operation of the apparatus. The fuel assembly (FA) was taken out in September, 1977, i.e., after operating for 39 months. During this period, the power of FA decreased by less than 2 times. For this case, from Eq. (2) we obtain $\alpha_T > 1$, i.e., the temperature of the fuel element jackets (if the thermal resistance of the deposits remains constant) must increase with increasing operational period of the system. Thus, the decrease in the temperature of the fuel element jackets with the growth of deposits indicates that if the deposits are not partially removed during operation, the thermal resistance of the layer is not a constant and the main contribution to it comes not from the dense layer of the hydrated corrosion products, but from the layer of colloids forming p.c.s. whose thickness decreases as a result of the reduction in the concentration of the corrosion products in water of the power systems with time.

However, if the colloid layer forms a significant thermal resistance during the steady-state operation of the system, then we expect that its formation can be observed even after a prolonged shutdown. In this case, the temperature of the fuel element jacket at the point located in the region of the surface boiling zone changes differently depending on the manner in which the deposits form. If the process of deposit formation does not occur directly through the dehydration stage, then, with increasing power of the system, the temperature of the fuel element jacket is determined not only by the time required for setting the system

to its capacity, but also by the time of formation of a boundary p.c.s. layer on which the rate of entrance of d.p. is equal to their dehydration rate.

Figure 2 shows that the increase in the jacket temperature continued with some deviations even after the system attained its nominal capacity on 11th August; the temperature was stablized only on 20th August. The temperature of the internal jacket of the fuel element remained constant up to 10th September after which we observed its deviation from the steady value. All the observed deviations are related to the changes in the channel power and the coolant consumption through the channel during the reactor monitoring process.

Thus, the experimentally observed nature of the temperature variation in the fuel element jackets is in support of the theoretical argument that the deposit layer formation occurs through the stage of p.c.s. evolution. In view of the fact that in the surface boiling zone the main thermal resistance is offered by the p.c.s. layer and not by the dehydrated layer, this conclusion is extremely important from the standpoint of ensuring reliable operation of the fuel elements having zirconium jackets in the boiling water reactors. The location of the surface boiling zone in the reactor, the medium and the maximum values of the thermal loads on the fuel elements, the permissible concentrations of the corrosion products in reactor water, and the amplitude and the frequency of vibrations (fluctuations) in the surface boiling zone (when they are programmed in advance) must be chosen on the basis of not only the total thickness of the deposits, but also the thermal resistance of the layer of colloids.

The significant effect of p.c.s. on the temperature of the fuel element jacket and the fairly rapid response of this layer to the changes in the surface conditions permit one to consider the temperature control of the jackets as an important part of the operative control of the effectiveness of the measures taken for setting the water-chemical regime and the start-up and the operational regimes of the system for improving the quality of water in the multiple forced circulation loop (MFCL).

From the aforementioned facts it follows that:

during the formation of deposits on the fuel elements in the surface boiling zone, the main thermal resistance can be offered by the layer of the hydrated colloidal-forms with the p.c.s. formed during the first few days after putting the system into operation;

the permissible total thickness of the dense localized deposits that is regarded at the present time as the unique condition for ensuring reliable operation of the fuel elements is not an adequate criterion;

the temperature control of the fuel element jackets is an important part of the operative control of the effectiveness of the measures taken for setting the water-chemical regime and the start-up and the operational regimes of the system for improving the quality of water in MFCL.

LITERATURE CITED

1. V. V. Gerasimov, Corrosion of Reactor Materials [in Russian], Atomizdat, Moscow (1980).
2. I. K. Morozova, A. I. Gromova, and V. V. Gerasimov, Removal and Deposition of the Corrosion Products of Reactor Materials [in Russian], Atomizdat, Moscow (1975).
3. A. G. Rassokhin, L. P. Kabanov, S. A. Tevlin, and V. A. Tersin, "Thermal conductivity of iron oxide deposits," Teploenergetika, No. 9, 12-15 (1973).
4. I. F. Efremov, Periodic Colloidal Structures [in Russian], Khimiya, Leningrad (1970).
5. J. Neumen, Electrochemical Systems [Russian translation], Mir, Moscow (1977), p. 464.
6. R. Haase, Thermodynamics of Irreversible Processes, Addison-Wesley (1968).
7. V. P. Brusakov, V. M. Sedov, K. D. Rogov, et al., "Regularities in the behavior of the corrosion products in the NPP circuits," in: Interinstitute Reports of the Lensovet LTI (1979).

REASONS FOR AND AGAINST THE OXYGEN DOSAGE IN CONDENSATE FEED CIRCUITS OF NUCLEAR POWER PLANTS WITH RBMK-1000 REACTORS

V. V. Gerasimov, A. I. Gromova,
V. N. Baranov, and Yu. V. Makarenkov

UDC 621.039.553.36:620.193.47.7

During operation (1973-1984) of nuclear power plants (NPP) with RBMK-1000 reactors, not a single failure was observed of controlled circulation loops (CCL) in 10 units, resulting from the corrosive action of the coolant. So far at the Leningradskaya, Kurskaya, Chernobyl'skaya, and Smolenskaya HPPs no underproduction of electric power has happened due to the damage caused by corrosion in the CCL or by large deposits of corrosion products leading to the failure of fuel elements [1].

Reliable operation of the CCL equipment during a long period is a convincing proof of the correct combination of the structural materials and reactor features, water chemistry (operating conditions), and the corrosion protection means chosen. Therefore, the improvement in the water regime is advisable when its advantages can be clearly substantiated for the units and when the reliability of the loop equipment will not be impaired with its introduction. As was shown in [2], the introduction of the oxygen regime in units of steam power plants lead to the decrease in deposits on heat-transfer surfaces. No deposits causing fuel-element damage were observed at NPPs with RBMK-1000 reactors [1], and the matter has not been raised of a need to reduce them. The advantage of the water chemistry is that it provides, as we believe, the possibility to decrease the deposit formation along the circuit, affecting the radiation conditions in the CCL. We will therefore consider the reduction in corrosion products radioactivity in the CCL, the γ radiation of which determines the radiation conditions in the buildings and around the pieces of equipment in this loop [3], for the improvement of the radiation conditions at the NPP leads in the long run to a reduction in maintenance costs.

In accordance with design and experimental investigations of the radiation conditions in the buildings and near the equipment of the main process loop and the radiation state of this loop [3-6], for a substantial, e.g. 10-fold, decrease in the dosage rate near the CCL equipment, the contents of the corrosion products of design materials in the coolant (iron oxides, cobalt oxides, etc.) should also be decreased 10-fold.

In NPP units with boiling water reactors, two variants of water chemistry are employed: a neutral regime without correction and a correction regime with oxidant additives. As oxidant, use is made of hydrogen peroxide (the Second Unit of the Beloyarskaya NPP; NPP(s) in FRG) and gaseous oxygen (VK-50 [7, 12-14], NPPs in Sweden and Japan). The choice of water chemistry for an NPP is dictated, as a rule, by the above factors and specific features of plants. At the moment, in view of the circumstances mentioned, the advisability of the introduction of the oxidant in the feed circuit of an NPP with the RBMK-1000 reactor is not considered to be clearly proven.

The purpose of this paper is to evaluate, on the basis of the Soviet and foreign experience of operation of NPPs with boiling-water reactors and oxidant feed-up, both the advantages of this regime when employed in the NPP with RBMK-1000 reactor and possible complications which its introduction creates for the main structural materials in the active zone and CCL (where the repair work is most difficult).

It can be said *a priori*, that the oxidant introduction in the condensate circuit will not change the water chemistry indices of the CCL. The dosage of the oxidant in the feed circuit will increase the oxygen concentration in the CCL, along with other factors, due to water radiolysis, which can, in turn, decrease the reliability of operation of channels and lines made of 08Kh18N10T steel. Oxygen dosage into the condensate feeding circuit (CFC) of the VK-50 reactor caused its concentration in the reactor water to increase from 180 to 250 μg/kg [7]. This method, therefore, deserves careful study.

Translated from Atomnaya Énergiya, Vol. 59, No. 6, pp. 409-413, December, 1985. Original article submitted April 5, 1985.

 0038-531X/85/5906-0976$09.50

It is known that the introduction of the oxidation regime in the heat power industry caused unexpected failures at steam power plants (SPP) [8-11]: corrosion-erosion damage of high-pressure heater (HPH) steam attemperator tubes on the heating steam side, damage of the internal partitions of the HPH hot well and heating steam condensate pipeline, failure of the convective HPH coils made of Kh18N12T steel in the overheat zone, and clogging of the turbine flow section with deposits.

The observed reduction in the iron ([Fe]) concentration in the reactor water from 22 to 10 μg/kg during the VK-50 service is connected with the oxygen introduction in the feed circuit [7, 12-14]. The change in the [Fe] in the reactor water during the whole period of operation of the plant shows that the [Fe] decrease was observed at various times and that no additional measures were taken. Thus, with no correction regime employed, in 1966-1977 the [Fe] content in the rector water decreased from 75 to 22 μg/kg. The general pattern established for the [Fe] content in the reactor water, which decreased during various periods of plant operation, can most probably be explained by kinetic factors rather than just oxygen dosage (see Fig. 1).

In the VK-50 reactor 33% of the total area is accounted for by pearlitic steel parts, and 14% by austenitic stainless steel. In the RBMK reactors the total area of parts made of pearlitic steels does not exceed 5% of the total area of parts made of structural materials, and in the CFC where the passivation of stainless steel is possible the total area of the stainless steel parts is 1.2% and 50%. The remaining sections of parts made from structural materials are already operating in oxygen-containing media (up to 7 μg/kg). If the oxygen dosage has not changed the established pattern with regard to the iron balance in water in the VK-50 reactor, the chance of this happening will be even less in the RBMK-1000 reactor where the oxygen introduced can passivate only 1.2% of the total area. The results of the first stage of the oxygen dosage in the condensate circuit of the RBMK-1000 reactor (the Third Unit of the Chernobyl'skaya NPP) have confirmed the forecasts made: neither positive nor negative effect has been observed.

It should be noted that the [Fe] content in the reactor water of the VK-50 reactor, after 17 years of service including about four years of operation in oxygen regime (10 μg/kg) is higher than the [Fe] content in the reactor water of the First Unit of the RBMK-1000 reactor after nine years of operation at the Leningradskaya NPP (2-7 μg/kg); this can be explained, probably, by the ratio of the areas of pearlitic steel parts.

Consider the possible change in the [Fe] content in the feed water of the RBMK-1000 reactor with the oxygen dosage, by making several assumption, for simplicity. It is known that various authors gave various evaluations of the effect of the oxidant introduction in water; they pointed out both negative and positive effects on the corrosion velocity in pearlitic steel, the estimated effect being 5-10-fold.

Assumption One. It is assumed that the oxygen introduction in the CFC of the NPP with the RBMK-1000 reactor leads to the maximum, i.e. about 10-fold decrease in the pearlitic steel corrosion.

Assumption Two. The interaction of the metal with water and the oxidant contained in it will take part not at the already oxidized (as usual) surface but with the unoxidized surface, the expected effect being maximum. Assume the amount of corrosion product removed with water being equal for pearlitic steel to 50% of the corrosion rate value.

Assumption Three. The general corrosion rate of chromium-nickel austenitic steel in water virtually does not change with the change in the oxidant concentration from 0.02 to 0.2 μg/kg, therefore, assume the steel corrosion rate to be equal to the corrosion rate under the regime without correction. The amount of the corrosion product removed we assume to be equal to 10% of the corosion rate for the both cases (water with and without the oxidant).

The areas of parts made of pearlitic steel: the feed circuit, 1500 m^2; the condensate circuit, 1300 m^2; deaerators, 700 m^2, the rest of the surfaces of parts made of pearlitic class steel are already in contact with oxygen-containing steam flows. The total area of parts made of austenitic steel in the CFC is 1800 m^2.

Consider two possible variants of the oxidant dosage: its introduction both ahead of and after the deaerator, and ahead of the deaerator only. In both variants deaerator tanks (700 m^2) are not subjected to passivation. To evaluate the change in the iron carry-

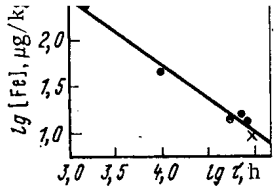

Fig. 1. Iron concentration in the reactor water, VK-50 [7, 12-14]: •) operation in the regime without correction; ×) operation with the oxygen dosage in the CFC (about 200 μg/kg).

TABLE 1. Evaluation of Iron Carryover to the Coolant [15, 16]

t, °C	Pearlitic steels		Stainless steels	
	corrosion rate	corrosion products carryover	corrosion rate	corrosion products carryover
280	$0,7\ \tau^{-0,5}$	$0,35\ \tau^{-0,5}$	$0,14\ \tau^{-0,5}$	$0,014\ \tau^{-0,5}$
160	$0,5\ \tau^{-0,5}$	$0,25\ \tau^{-0,5}$	$0,01\ \tau^{-0,5}$	$0,001\ \tau^{-0,5}$
40	$0,016\ \tau^{-0,5}$	$0,008\ \tau^{-0,5}$	—	—

TABLE 2. Corrosion Products Carryover from Part Surfaces in the CFC of the NPP with the RBMK Reactors

Section	Steel	Surface area, m^2	Carryover rate (g/h), regime	
			neutral	oxygen
Pipelines, condensate circuit to deaerator	carbon	900	7,2	0,72
		400	100	10
Pipeline systems of LPH (low-pressure heater), deaerator heads	austenitic	18000	18	18
Deaerators (tanks)	carbon	700	175	175
Pipelines of SSS (superheated steam section), the heating steam side	austenitic	22000	22	22
Feed circuit	carbon	1500	375	37,5
			697,2	263,2

over to the coolant, we will use the following known data [15, 16] tested during operation of units (see Table 1). Possible variations in the iron carryover to water in the CFC of the NPP with the RBMK-1000 reactors are listed in Table 2.

In accordance with optimistic evaluations, when the oxygen dosage is being carried out according to the first variant, with the account taken of the corrosion products formed in the CCL ($485\tau^{-0.5}$), the total amount of the corrosion products entering the CFC ($651.1\tau^{-0.5}$), and the coefficient of condensate purification equal to 0.5, the amount of the corrosion products will be $(651.6 + 485 + 263.2)\tau^{-0.5} = 1400\tau^{-0.5}$, while its observed value in the water regime without correction is $1800\tau^{-0.5}$. Thus, the decrease in the amount of the corrosion products entering the reactor will be $\leqslant$20% of the total amount of the corrosion products. If the oxidant dosage is carried out ahead of the deaerator only, the maximum possible positive effect will drop to 5%. This means that the dose rate near the CCL equipment will decrease by 20% at best, and may decrease just by 5%. With the account taken of the total error in the dose rate measurement, this positive effect, i.e. the decrease in the dose rate caused by the oxygen, can go unnoticed.

The decrease in the coolant radioactivity and corrosion in the condensate circuit is being reached at the Japanese reactors by combining the following measures [17]: increased condensate purification, use of 'dry' and 'wet' conservation during prolonged and short shutdowns, installation of additional filters ahead of condensate purification filters to

TABLE 3. Cases of Corrosion Damage of Parts Made of 304 Stainless Steel in the First Loop of BWR Reactors

NPP	Unit	Nature of Damage	Damage Cause	Literature Cited
Oyster Creek	Standpipes, branch pipes, flanges, plated housing areas	ICC* in gaps	Residual stresses. High oxygen concn. in water (3 ml/liter) and high iron oxide concn.	[19, 20]
	Plated housing areas	CSC†	—	[21]
Tarapur	Housing branch pipes, standpipe end-pieces, plated housing areas	CSC and ICC in gaps	Sensitization in the manufacture. High oxygen concn. in water (3 ml/liter) and high halogens concn.	[16-19, 22]
Elk River	Sprinkling branch pipes, steam branch pipes	ICC near welded joints	Stress localization, oxygen concn. 3 mg/liter	[19, 23]
Big Rock Point	Fuel-element jackets	CSC	High oxygen concn. in the reactor water	[19, 23]
Vallesitos	Ditto	ICC and CSC	Oxygen concn., stresses, radiation	[19]
Humboldt Bay	Ditto	IC SC (intercrystalline stress cracking)	Ditto	[18, 19, 23]

*Intercrystalline corrosion.
†Corrosion stress cracking.

Declassified and Approved For Release 2013/02/20 : CIA-RDP10-02196R000300070006-9

trap nonsoluble corrosion products, use in heating systems of austenitic steel with lower cobalt content, and introduction of oxygen in the CFC.

From this is follows that to decrease the amount of the corrosion products entering the reactor it is necessary to provide the oxygen dosage in the feed circuit; the latter will, in turn, cause the radiolysis increase in the CCL water, a further increase in the oxygen concentration in the reactor water [7], and, therefore, the increase in the corrosion rate of zirconium alloys and will increase the probability of the development of corrosion cracking in parts made of 08Kh18N10T steel. The above factors can lead to a decrease in the service reliability of the reactor basic equipment.

It is appropriate to remind about failures of the basic equipment at the SPP [8-11] and NPP [18-23] observed during operation with the oxygen dosage (see Table 3). Obvious advantages of the employment of the oxygen regime in the NCC with RBMK-1000 reactors (as compared with the regime without correction) are substantially decreased because of this damage of equipment. Corrosion damage of equipment, technological problems, unavoidable materials substitutes due to the oxidant use, increased deposit formation in the turbine, use of various (in various units) oxidants (oxygen, hydrogen peroxide, air, etc.), indicate that no optimal water regime with the oxygen dosage is known today that can be used on the SPP, even though it has been reported [27] that a weak alkali water regime (pH 8-8.5 NH_4OH) with the oxygen dosage of up to 200 μg/kg can be considered today a rational regime for the CFC of SPP power units.

At foreign NPPs with BWR reactors corrosion damage of the main equipment has been recorded systematically. In 1975-1980 the number of intercrystalline corrosion cracking cases at NPPs all over the world increased from 64 to 213 [18-23]. More recent data [19, 23, 24] confirm a continuous increase in the number of cases of corrosion cracking in pipes of BWR reactors (see Table 3). At Swedish NPPs operating in the oxygen water regime cases were observed of intercrystalline corrosion cracking of stainless steel [25] which made it necessary to turn to the old water regime without correction. To lower the steel sensitivity to corrosion cracking, hydrogen is introduced in the circuit [25, 26].

In the existing nuclear reactors restriction of the oxygen concentration in the coolant proved to be an efficient measure. Recorded cases of corrosion damage in reactors with increased oxygen concentration in the coolant confirm the fact that the oxygen regime has not been mastered yet and give us concern about the oxygen dosage in the CFC in the NPP with the RBMK-1000 reactors.

The increase in the oxygen concentration in the CCL (caused by the radiolysis increase), provided the oxygen dosage in the feed circuit is employed, will make the operation of equipment made of stainless steel more complicated. It is known [28] that corrosion cracking of 0Kh18N10T steel is fixed in case of concentration of chloride-ions at steel surfaces and is intensified with the increase in the oxygen concentration in the medium.

Particular attention should be given to increasing the oxygen concentration in the CCL water as regards the operation of technological channels made of zirconium alloy with 2.5% Nb, based on 30-yr reactor service life. Corrosion of such an alloy increases 4-fold in 3500 h if the oxygen concentration in water is increased from 0.3-0.6 to 12-17 mg/kg under radiation conditions [29].

The advantages and possible complications encountered when the oxygen dosage is used in the CFC of NPP with the RBMK-1000 reactors can be formulated as follows:

the oxygen dosage in the condensate circuit (200 μg/kg) can reduce the [Fe] content in the CCL by 5% at best, as compared with the value now defined;

the oxygen dosage in the condensate and feed circuits can reduce the [Fe] content in the reactor water by about 20%. At the same time, the corrosion rate of the base metal of technological channels will increase, and corrosion of welded seams and adjoining zones will increase with the inevitable decrease in the channel service life. The increase in the oxygen concentration in the reactor water will increase the risk of the development of corrosion cracking in type 0Kh18N10T steel in the most stressed sections of the CCL. The above advantages of the oxygen dosage in the feed circuit by no means warrant the worsening of operating conditions for stainless steel and zirconium alloy (with 2.5% Nb) causing the decrease in their serivce life in the CCL.

Therefore, the oxygen dosage in the condensate circuit only can be considered admissible for the NPP with RBMK-1000 reactors.

LITERATURE CITED

1. I. A. Varovin, A. P. Eperin, M. P. Umanets, and V. G. Shcherbina, "Ten-year experience of operating the Leningrad NPP," At. Énerg., 55, No. 6, 349 (1983).
2. M. E. Shitsman, Yu. I. Timofeev, L. S. Midler, et al., "27,000 h of the NRG operation without serivce acid washing," Énergetik, No. 12, 4 (1978).
3. Yu. A. Egorov and I. Ya. Emel'yanov, "The state and problems of studying the radiation safety at the NPP in connection with further development of nuclear power," in: Radiation Safety and Protection at the NPP [in Russian], Énergoizdat, 7, Mosocw (1982), p. 5.
4. Yu. A. Egorov, A. A. Noskov, V. P. Sklyarov, et al., "The study and use of the TRAKT-1 model for calculation of the corrosion products activity in the technological circuit of the NPP with a channel-type reactor," ibid., Atomizdat, 5, Moscow (1981), p. 5.
5. V. S. Grechishkin, Yu. A. Egorov, G. N. Krasnozhen, et al., "Radiation Conditions at the Chernobyl'skaya NPP in the Initial Operation Period," ibid., Énergoizdat, 7, Moscow (1982), p. 92.
6. N. I. Bogdanov, A. V. Borunova, Yu. A. Egorov, et al., "Corrosion Products in the CCL (Controlled Circulation Loop) of the NPP with the RBMK Reactor," ibid., Énergoizdat, 8, Moscow (1984), p. 22.
7. E. P. Anan'ev, A. B. Andreeva, I. S. Dubrovskii, et al., "Efficiency of using the neutral-oxygen water chemistry regime in operating the NPP boiling shell-type reactor," At. Énerg., 52, No. 1, 10-14 (1982).
8. N. I. Gruzdev, Z. V. Deeva, B. É. Shkol'nikova, et al., "Possibility of the development of brittle fractures in the heat boiler surface in the neutral-oxidizing regime," Teploénergetika, No. 7, 8 (1983).
9. V. I. Gorin, "Some results of operating power units at supercritical pressure in neutral-oxidizing water regime," ibid., p. 2.
10. N. A. Lyashevich, "Operation reliability of heat surfaces of power units in the water regime with the oxidant dosage," ibid., p. 11.
11. G. P. Sutotskii, G. V. Vasilenko, Yu. V. Zenkevich, et al., "Water chemistry regimes of SCP (supercritical pressure) units," in: Water Treatment and Water Chemistry and Corrosion of the SPP and NPP [in Russian], TsKTI (Tsentr. NIiPKkotloturbinnyi Inst.), 158, Leningrad (1978), p. 20.
12. A. I. Zabelin, A. B. Andreeva, Yu. V. Chechetkin, et al., "Corrosion and Activation in the Circuit of the NPP with a Boiling Reactor in Neutral Water Chemistry Regime without Correction," Preprint 364 [in Russian], NIIAR-5, Dimitrovgrad (1979), pp. 1-14.
13. A. I. Zabelin, A. B. Andreeva, V. M. Eshcherkin, et al., "Use of carbon steel in the water chemistry regime without correction of the NPP VK-50," At. Énerg., 49, No. 4, 229-232 (1980).
14. A. I. Zabelin, "Study of Water Chemistry Regimes of the NPP VK-50," Preprint 538 [in Russian], NIIAR-23, Dimitrovgrad (1982).
15. V. V. Gerasimov, Steel Corrosion in Neutral Water Media [in Russian], Metallurgiya, Moscow (1981).
16. V. V. Gerasimov, Corrosion of Reactor Materials [in Russian], Atomizdat, Moscow (1981).
17. J. Mushima, "Water chemistry in the Japanese light water reactors," in: Proc. IAEA Specialists Meetings on Influence of Power Reactor Water Chemsitry on Fuel Cladding Reliability. Italy, Pisa, 12-16 Oct. 1981. Vienna: IAEA, 1982, p. 230.
18. J. Danko and K. Stahlkopf, "An overview of boiling water reactor pipe cracking," J. Pressure Vessels and Piping, No. 9, 401-419 (1981).
19. C. Cheng, "Intergranular stress-assisted corrosion cracking of austenitic alloys in water-cooled nuclear reactors," J. Nucl. Mater., 57, No. 11, (1975).
20. W. Casto, "Recent occurrences at nuclear reactors and their causes," Nucl. Safety, 15, No. 4, 466-477 (1974).
21. W. Casto, "Recent occurrences at nuclear reactors and their causes," ibid., No. 6, 742-750.
22. "Pipe cracking in boiling water reactors," Nuclear Regulatory Commission report, Nucl. Safety, 17, No. 4, 475 (1976).
23. D. Locke, "Review of experience with water reactor fuels 1968-1973," Nucl. Eng. Design, 33, No. 2, 94 (1975).

24. M. Taylor, "Boiling water reactor stress corrosion cracking of piping-utility industry research program," ibid., 69, No. 2, 223-227 (1982).
25. "Hydrogen stops growing cracks in BWRs," Nucl. Eng. Int., 25, No. 295, 6 (1980).
26. G. M. Kalinin, "Intercrystalline corrosion cracking and methods of recovering NPP pipelines," At. Tekh. Rubezhom, No. 1, 17-20 (1985).
27. O. I. Martynova, "Further development of oxidizing water chemistry regime at power units with direct-flow channels in Western Europe," Énergokhozyaistvo Rubezhom, No. 3, 8-13 (1982).
28. "Structure materials corrosion under operation regimes of the first loop of the NPP with boiling reactors. Stainless, and pearlitic steels and zirconium alloys," in: Proc. of the Jubilee Conf. on the Occasion of the 20th Anniversary of Nuclear Power Engineering [in Russian], Obninsk, June 25-27 (1974), p. 201.
29. A. S. Zaimovskii, A. V. Nikulina, and N. G. Reshetnikov, Zirconium Alloys in Nuclear Power Engineering [in Russian], Énergoizdat, Moscow (1981).

STUDY AND SELECTION OF NEW EXTRACTANTS FOR ACTINIDE EXTRACTION

A. M. Rozen, A. S. Nikiforov,
Z. I. Nikolotova, and N. A. Kartesheva

UDC 66.061.5:546.7

Previous studies [1-12] have established rules linking the extractive ability of monodentate organic compounds with their structure (electronegativity of the substituents X, electron density at the reaction center q, alkalinity pK_a, et al.). It was found that the extractive ability increases with q on the functional atom of the extractant (and correspondingly with pK) and decreases when the electronegativity of the substituents increases, since $|q| = a'' - b''\Sigma X$ (Fig. 1),

$$\lg K = A - B\Sigma X = a' + b' |q| = a + bpK_a. \quad (1)$$

It was also established that the length of the hydrocarbon chain has virtually no effect on extraction: curves with a weak maximum when the number of carbon atoms $N_C = 8$, are observed (Fig. 2).

In a different series of studies the extractive ability of bidentate compounds [12-20] and crown esters [21] was studied.

The rules found enable controlling the extractive ability. They were used in subsequent studies and in the selection of extractants (mono-, bi-, and polydentate) for extracting actinides.

Monodentate Extractants

We posed the problem of improving the extraction system based on TBP, widely used all over the world for regenerating spent nuclear fuel. The extractive properties of TBP are practically optimal, but physically they are not entirely satisfactory: the solubility in the water phase is too high, the solvates of quadrivalent actinides are poorly compatible with the hydrocarbon diluents (a secondary organic phase already forms at moderate concentrations of thorium and plutonium nitrates [22, 23]). Efforts to improve this system were made both in the USSR [24-27] and in the USA [28]. We posed the problem of improving the physical properties of the extractant, while preserving the extractive ability based on TBP. The latter condition, as follows from theoretical considerations [1-12], requires preserving in molecules of neutral phosphoorganic extractants (NPOE) the same values of the electronegativity of the substituents as in TBP, i.e., the use of compounds of the same class — trialkylphosphates, since a change in the chemical nature of the substituent gives rise to a significant change in the electronegativity and, as a consequence, in the extractive ability (see Eq. (1)). The physicochemical properties can be improved by optimizing the hydrocarbon chain: reducing the solubility of esters in water by lengthening the chain and improving the compatibility of the solvates with long-chain hydrocarbon diluents by

Translated from Atomnaya Énergiya, Vol. 59, No. 6, pp. 413-421, December, 1985. Original article submitted March 25, 1985.

 0038-531X/85/5906-0982$09.50

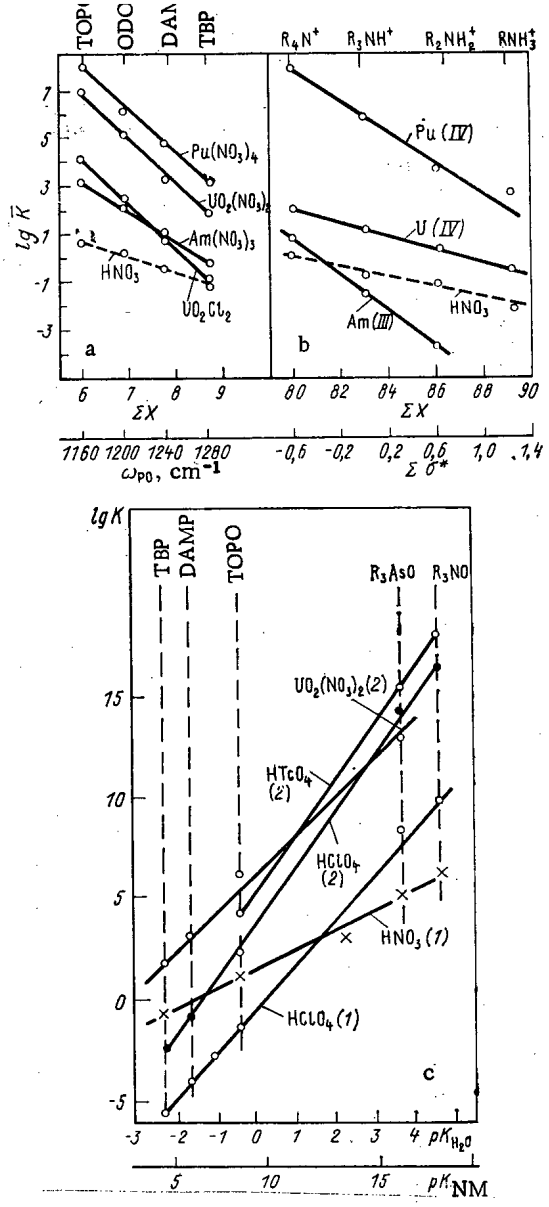

Fig. 1. Dependence of the extractive ability of organic compounds relative to the actinides and acids on the structural properties of the extractants: a) neutral phosphoorganic compounds (the series TBP-TOPO); b) amines (series of primary, secondary, and ternary amines, quaternary ammonium bases); c) series of neutral organic compounds TBP (tributyl phosphate)–DAMF (diisoamylmethyl phosphonate)–TOPO (trioctyl phosphine oxide)–TOASO (trioctyl arsenoxide)–TOAO (trioctyl amine oxide); the numbers in parentheses indicate the number of molecules of the organic ligand in the complex; ωPO is the frequency of the stretching vibrations of the PO group; ΣX is the sum of the electronegativities of the substituent groups (X_R = 2.0; X_{RO} = 2.9; X_H = 2.3); $\Sigma\sigma^*$ is the sum of the Taft constants for the substituent groups; pK_{H_2O} and pK_{NM} are the alkalinity of the organic compounds referred to water and nitromethane.

increasing the length of the hydrocarbon chain of esters and using isostructures. As indicated above, these structural changes have virtually no effect on the extractive ability. The theoretical forecast was confirmed experimentally [27]. Because of the difficulties of flushing the acidic impurities (products of hydrolysis and radiohydrolysis) in the case when the length of the hydrocarbon chain is increased, trialkylphosphates with ΣnC = 15-18 [24-27], both symmetrical [$(i\text{-}C_nH_{2n+1}O)_3PO$, where n is equal to 5 or 6] and heteroradical (for example, diisobutylisooctyl phosphate, ΣnC = 16), were recommended.

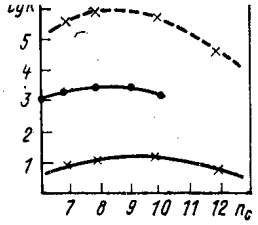

Fig. 2. Dependence of the extraction constants of uranyl and plutonium nitrates (---) on the length of the hydrocarbon chain of the extractant: ×) amines; •) phosphonates.

We note that in the USA triisoamyl phosphate (Σn_C = 15), trihexyl phosphate (Σn_C = 18), and triisooctyl phosphate (Σn_C = 24) were recommended. A successful check of the latter in hot chambers was reported in [28]. A report of the effective flushing of long-chain acidic products of hydrolysis, i.e., D2GFK, by the usual methods is puzzling.

Bidentate Extractants

The second practical problem is the selection of effective extractants for extracting transplutonium elements and lanthanides from the discarded solutions of radiochemical technology. As pointed out previously [15, 20], because of the so-called effect of anomalous aryl strengthening (AAS), tetraaryl methylene disphosphonine dioxides have the highest estractive ability relative to trivalent actinides and lanthanides, permitting their extraction from solutions with any acidity without preparation. However, they are poorly compatible with hydrocarbon diluents; compatibility can be improved by introducing alkyl radicals into the benzene cores, stabilization (for example, with tributyl phosphate [15, 29]), as well as changing over to mixed aryl-alkyl dioxides, which makes the synthesis more complicated.

In recent years interest has appeared in bidentate compounds with the groups P = O and C = O – dialkyldialkyl carbamoyl methylene phosphonate and phosphine oxides, which are undoubtedly easier to synthesize than dioxides, and their compatibility with hydrocarbon diluents is appreciably higher [29-34]. It is therefore desirable to study the change in the extractive ability in a wider range of bidentate phosphoorganic compounds (from diphosphine dioxides to carbamoyl phosphine oxides and phosphonates), to discuss the controversial questions of the coordination of actinides accompanying the use of carbamoyl compounds, as well as to establish whether or not the AAS effect exists in these systems (according to [32] it does not exist and according to [33] it does exist). Of course, since the effect was observed during extraction of nonsymmetrical diphosphine dioxides, one would expect that it also exists in the case of carbamoyl phosphine oxides.

Effect of Anomalous Aryl Strengthening. As is evident from Eq. (1), the introduction of electronegative substituents into the molecule of the extractant decreases the donor ability of the functional atom (on our case oxygen) and lowers the alkalinity and extractive ability. The only breakdown of this rule was observed in extraction by dibentate phosphoorganic compounds – diphsophine dioxides $R'_2P(O)CH_2(O)PR''_2$. When electronegative groups such as RO (X = 2.4), $Cl(CH_2)_2$ (X = 2.36) were introduced, the rules (1) were obeyed. when the alkyl substituents (X = 2) were replaced with more electronegative phenyl groups (X_{Ph} = 2.36) the alkalinity, as expected, decreased; judging from the changes in the infrared spectra (increase in the frequency of the stretching vibrations of the group P = O) and in the extraction of HNO_3 (characterized by monodentate coordination), the charge on the oxygen and its donor and the extractive ability decreased. The extraction of trivalent actinides and lanthanides nevertheless increased substantially (Figs. 3a, b, c) [13, 14]. Since the same effect was also observed when other aryl substituents were introduced, it was called AAS. It was found that it remains when the nitrate medium is replaced by HCl, H_2SO_4 and is especially large in a $HClO_4$ medium.

It turned out, however, that the effect vanishes when the aryl substituent is separated from the phosphorus by the CH_2 group, which interferes with the conjugation (for example, when the phenyl is replaced by benzene), and when the bridge is lengthened – when the

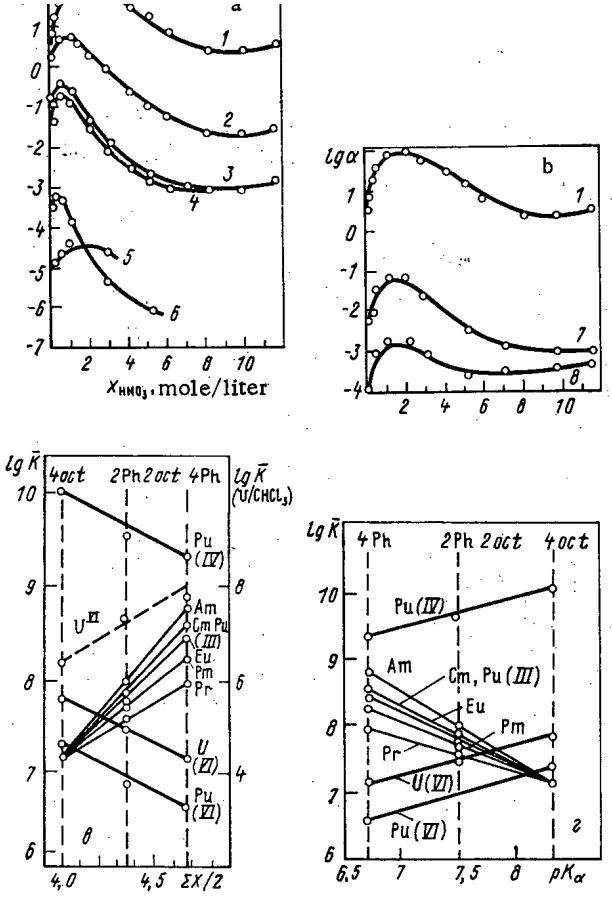

Fig. 3. AAS effect for complexes accompanying extraction of trivalent actinides and lanthanides by diphosphine dioxides (0.01 mole/liter solutions in dichloroethane): a) distribution factors [1) $(C_6H_5)_2P(O)CH_2(O)P(C_6H_5)_2$ (or 4 Ph); 2) $(C_6H_5)_2P(O)CH_2OP(C_8H_{17})$ (or 2 Ph 2 oct); 3) $(C_8H_{17})_2P(O)CH_2OP(C_8H_{17})_2$ (or 4 oct); 4) $(C_4H_9)_2P(O)CH_2(O)P(C_4H_9)_2$ (or 4 But); 5) TOPO (0.2 mole/l); 6) TOPO (0.2 mole/l)]; b) effect of the length of the alkyl bridge [1) 4 Ph; 7) $(C_6H_5)_2P(O)(CH_2)_2(O)P(C_6H_5)_2$; 8) $(C_6H_5)_2P(O)(CH_2)_3(O)P(C_6H_5)$]; c, d) dependence of the extraction constants on the electronegativity sum ΣX and alkalinity pK_a (—— dichloroethane diluent, ---- chloroform diluent).

methylene bridge is replaced by an ethylene or propylene bridge (Fig. 3d). The replacement of the ethylene bridge by a vinylene bridge CH=CH restored the effect. Calorimetric measurements show that the effect has a bonding nature (the enthalpy of extraction of europium by tetraphenyl dioxide $Ph_2P(O)CH_2(O)PPh_2$ was equal to 11.6 kcal/mole, as compared with 8.8 kcal/mole for tetraoctyl dioxide). All these facts can be explained by assuming that complexing is accompanied by delocalization of the electron density from the aryl groups into the central cycle of the complex and, possibly, aromatization of the six-term or, in the case of dioxides with the vinylene bridge (CH = CH), even the seven-term cycle formed. The latter proposition is supported by the high mobility of the protons in the methylene bridge in the complex observed in [19]. They become capable of isotropic exchange with chloroform (while the proteins of the ligand bridge are not capable of exchange).

Study of the Extractive Ability of Bidentate Phosphoorgenic Compounds. We studied the following compounds: carbamoyl methylene phosphonates $(i\text{-}C_8H_{17}O)_2P(O)CH_2C(O)N(C_2H_5)_2$ [or $(i\text{-octO})_2/Et_2$], $(i\text{-}C_5H_{11}O)_2P(O)CH_2C(O)N(C_4H_9)_2$ [or $(i\text{-amyl O})_2/But_2$], phosphine oxides

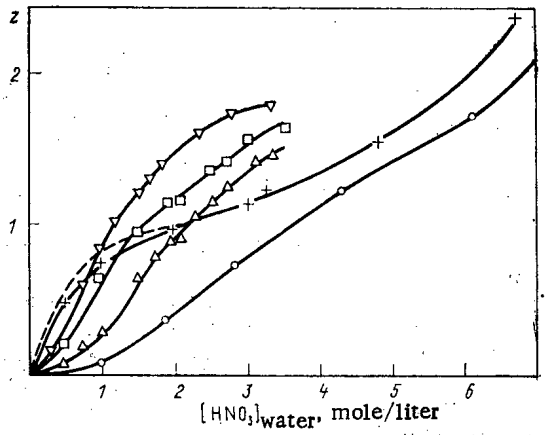

Fig. 4

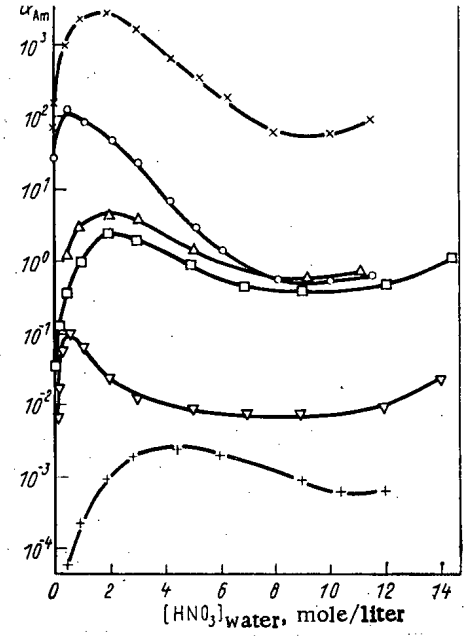

Fig. 5

Fig. 4. Extraction isotherms of HNO_3 extracted by bidentate phosphoorganic compounds (the diluent is dichloroethane): $z = y_H/L_0$, ▽) 4 oct; □) 4 Ph; +) oct_2/But_2; ○) amyl O_2/But_2; ---) TOPO.

Fig. 5. Effect of the structure of bidentate phosphoroorganic compounds on their extraction ability (0.05 mole/liter solutions in dichloroethane); ×) 4 Ph; ○) 2 Ph 2 oct; Δ) Tol_2/But_2; □) Ph_2/But_2; ▽) oct_2/But_2; +) (i-amyl $O)_2/But_2$.

$(C_8H_{17})_2P(O)CH_2C(O)N(C_4H_9)_2$ (or oct_2/But_2), $(C_6H_5)_2P(O)CH_2C(O)N(C_4H_9)_2$ (or Ph_2/But_2), $(C_6H_4CH_3)_2P(O)CH_2C(O)N(C_4H_9)_2$ (or Tol_2/But_2), dioxides $(C_6H_5)_2P(O)CH_2P(O)(C_8H_{17})_2$ (or 2 Ph 2 oct) and $(C_6H_5)_2P(O)CH_2P(O)C_6H_5)_2$ (or 4 Ph).

We extracted traces of americium and other actinides from nitrate media, when the concentration of "free" extractant (L), which must be known in order to describe the equilibrium, was determined by the extraction of HNO_3, which we studied up to concentrations of 13 mole/liter (Fig. 4). The quantity $z = [HNO_3]_{org}/L_0$, where L_0 is the starting concentration of the ligand (extractant), characterizes the number of HNO_3 molecules per ligand molecule. As is evident from Fig. 4, the value of z for carbamoyl phosphonates approaches 4 (and there is no saturation), i.e., the complexes $(HNO_3)_i(H_2O)_hL$, where $i \geqslant 4$, form. Assuming that HNO_3 molecules attach directly to both reaction centers ($h_1 = h_2 = 0$), that subsequent molecules attach through water, and that $h_3 = 1$, $h_4 = 2$, we conclude that the complexes $HNO_3 \cdot L$, $(HNO_3)_2 \cdot L$, $(HNO_3)_3(H_2O) \cdot L$ and $(HNO_3)_4(H_2O) \cdot L$ form. From the law of mass action we find their concentrations y_i in the organic phase:

$$y_1 = K_1 aL; \quad y_{1/2} = K_{1/2}a^2L; \quad y_{1/3} = K_{1/3}a^3a_{H_2O}L; \quad y_{1/4} = K_{1/4}a^4a_{H_2O}L, \tag{2}$$

where the activity of the acids $a = [HNO_3]^2_{water}\gamma^2_{\pm}$ ($\gamma_{\pm}$ is the activity coefficient; a_{H_2O} is the activity of water). The total concentration of acid in the organic phase is given by

$$y_H = y_1 + 2y_{1/2} + 3y_{1/3} + 4y_{1/4} + \ldots, \tag{3}$$

while the concentration of the free ligand is given by

$$L = L_0/(1 + K_1a + K_{1/2}a^2 + K_{1/3}a^3a_{H_2O} + K_{1/4}a^4a^2_{H_2O} + \ldots). \tag{4}$$

The least-squares determinations of the extraction constants are presented in Table 1, and the extraction isotherms, calculated from Eqs. (2)-(4) and these values of the constants, are presented in Fig. 4 (solid lines). The predicted values are in good agreement with the experimental values.

TABLE 1. Extraction Constants of Nitric Acid and Americium Extracted by Carbamoyl Phosphoryl Compounds

Compound	Diluent	HNO_3				Am	
		K_1	$K_{1/2}$	$K_{1/3}$	$K_{1/4}$	K_2	K_3
$(i\text{-octO})_2/Et_3$	$C_2H_4Cl_2$	0,25	$2{,}6\cdot10^{-3}$	$2{,}1\cdot10^{-6}$	$1{,}0\cdot10^{-13}$	$5{,}0\cdot10^{2}$	$5.0\cdot10^{2}$
$(i\text{-amylO})_2/But_2$	$C_2H_4Cl_2$	0,23	$1{,}1\cdot10^{-3}$	$2{,}2\cdot10^{-5}$	$3{,}2\cdot10^{-9}$	—	$1{,}8\cdot10^{3}$
oct_2/But_2	$C_2H_4Cl_2$	7,2	0,15	$1{,}0\cdot10^{-4}$	$1{,}4\cdot10^{-7}$	$2{,}5\cdot10^{5}$	$1{,}2\cdot10^{7}$
Ph_2/But_2	$C_2H_4Cl_2$	0,89	$1{,}3\cdot10^{-2}$	$8{,}8\cdot10^{-5}$	$1{,}6\cdot10^{-8}$	$3{,}8\cdot10^{3}$	$2{,}5\cdot10^{7}$
Ph_2/But_2	$CHCl_3$	0,16	$5{,}6\cdot10^{-4}$	$2{,}1\cdot10^{-6}$	$1{,}0\cdot10^{-9}$	$1{,}5\cdot10^{2}$	$1{,}3\cdot10^{4}$
Tol_2/But_2	$C_2H_4Cl_2$	1,7	$4{,}8\cdot10^{-2}$	$2{,}0\cdot10^{-4}$	$1{,}0\cdot10^{-7}$	$1{,}0\cdot10^{6}$	$2{,}0\cdot10^{7}$
Tol_2/But_2	$CHCl_3$	0,23	$1{,}3\cdot10^{-3}$	$5{,}0\cdot10^{-6}$	$1{,}0\cdot10^{-11}$	$1{,}0\cdot10^{3}$	$1{,}0\cdot10^{2}$
2Ph 2oct	$C_2H_4Cl_2$	2,4	0,33	—	—	$1{,}4\cdot10^{8}$	$1{,}3\cdot10^{2}$
2Ph 2oct	$CHCl_3$	0,62	$1{,}4\cdot10^{-2}$	$2{,}4\cdot10^{-5}$	$1{,}0\cdot10^{-7}$	57	$1{,}3\cdot10^{7}$
4Ph	$C_2H_4Cl_2$	0,85	$7{,}0\cdot10^{-2}$	—	—	$7{,}0\cdot10^{8}$	$8{,}0\cdot10^{10}$
4Ph	$CHCl_3$	0,14	$4{,}0\cdot10^{-3}$	$2{,}8\cdot10^{-6}$	$8{,}4\cdot10^{-9}$	$8{,}0\cdot10^{5}$	$1{,}6\cdot10^{8}$

The dependence of the distribution ratios of americium α_{Am} on the acidity of the water phase (x_H) is shown in Figs. 5-8. In the experiments we used solutions of dioxides with a concentration of 0.01 mole/liter, phosphine oxides with a concentration of 0.05 mole/liter, and phosphonates with a concentration of 0.5 mole/liter. In Figs. 5-8 the data are scaled to the concentration 0.05 mole/liter, in the case of dichloroethane as the diluent (apparent solvation number equal to two) we multiplied the data for dioxides by $5^2 = 25$, we divided the data for phosphonates by 10^2, and for dilution with chloroform ($q = 3$) we multiplied the data for dioxides by $5^3 = 125$. The curves in the figures just as those obtained in [13, 14], have a maximum, characteristic for extraction of metals by the solvation mechanism [in the form $Am(NO_3)_3L_q$] and is determined by the combination of the salting out and displacing action of HNO_3 [35]. The subsequent minimum and growth of α_{Am} are linked with the changeover to extraction by the acid complexes $H_pAm(NO_3)_{3+p}L_q$ (probably $p \geqslant 3$), when α_{Am} becomes proportional to $[H^+]$ with a high power of $3 + 2p$. By the equilibrium shift method (dilution) it was found that the apparent solvation number of americium is equal to 2.3 (dichloroethane is the diluent) and 3 (chloroform), i.e., di- and trisolvates are formed. Correspondingly,

$$\alpha_{Am} = \alpha_2^{Am} + \alpha_3^{Am} = (\overline{K}_{2Am}L^2 + \overline{K}_{3Am}L^3)\,[NO_3]^3\,\gamma_{\pm}^4. \qquad (5)$$

The values of the formation constants of di- and trisolvates K_2 and K_3, found from the data in Figs. 5-8 by the least-squares method using Eq. (14), are presented in Table 1.

From the data in Figs. 5-8 and Table 1 we can draw the following conclusions:

– extraction decreases in the series 4Ph > 2Ph 2oct > Tol_2/But_2 > Ph_2/But_2 > oct_2/But_2 > $(i\text{-amyl O})_2/But_2$ $(i\text{-oct O})_2/Et_2$, independently of the nature of the diluent;

– the changeover from diphosphine dioxides to carbamoyl phosphine oxides lowers the extraction of americium approximately by 3-3.5 orders of magnitude. We note that when one of the groups P = O was replaced by S = O, a drop by only a factor of 500 was observed [36], so that the replacement of the P = O group by C = O group lowers the extraction more strongly than the replacement of P = O by S = O. This is linked to the weaker extractive ability of the group C = O (the amides $RC(O)NR_2$ extract americium at the level of phosphonates). Nevertheless the extractive ability of carbamoyl phosphine oxides remains very high ($\overline{K}_{3Am} \approx 10^6$ instead of 10^3 for the usual phosphine oxide);

– the AAS effect is observed in the extraction of americium by carbamoyl methylene phosphine oxides just as for diphosphine dioxides (the series 4Ph – 2Ph 2oct – 4oct; see Figs. 3 and 5): Ph_2/But_2 extracts more strongly than oct_2/But_2 (in this respect Ph_2/But_2 is the analog of the dioxide 2Ph 2oct). Thus the results of [33] are valid, while the data on [29] were not confirmed;

– extraction is appreciably increased by replacing phenyl substituents with tolyl substituents (see Figs. 5 and 6), which indicates that the AAS effect remains and that the alkyl radical introduces an additional electronic effect;

– it is evident that the repalcement of alkyl substituents by more electronegative alkoxy groups, i.e., the changeover from phosphine oxides to phosphonates lowers the extraction constant by approximately a factor of 10^3. This result is trivial, and is in

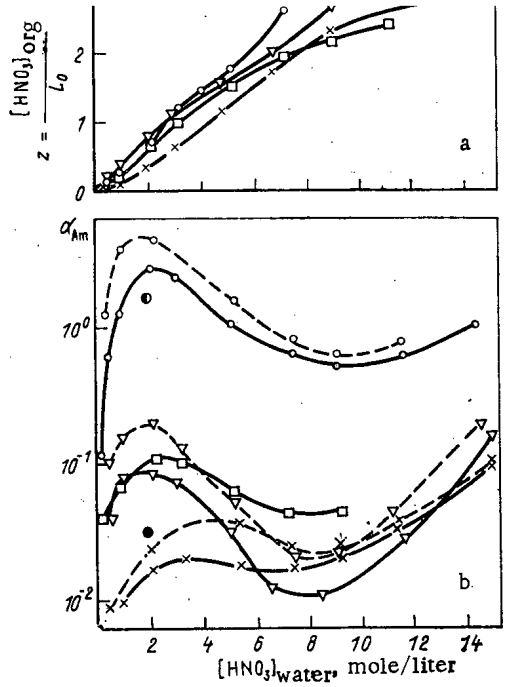

Fig. 6. Effects of diluents on the extraction of HNO_3 (a) (0.1 mole/liter of the ligand) and Am (b) (0.05 mole/liter of the ligand) by carbamoyl phosphine oxides Ph_2/But_2 (——) and Tol_2/But_2 (---): ○) dichloroethane; ▽) C_6H_6; □) CCl_4; ×) $CHCl_3$; •) Ph_2/But_2 in isoamyl alcohol; ◐) Ph_2/But_2 in C_6H_6 + 1 mole/liter TBP.

agreement with the previously obtained data for monoentate compounds [1-12] and for diphosphine dioxides as well as with the results of [32]; and,

– it was found that for carbamoyl compounds extraction increases in the series Am < U < Pu.

We shall now discuss the questions of coordination. It was previously established [13-20] that HNO_3 coordinates to diphosphine dioxides in a monodentate manner and to actinides in a bidentate manner. In the case of carbamoyl phosphine oxides the nature of the coordination is undoubtedly the same: the preservation of the AAS effect indicates bidentate coordination of the actinides (to the phosphoryl and carbonyl oxygen atoms of phosphine oxide). In [31] and elsewhere, however, an attempt was made to prove that for extraction with carbomoyl phosphonates the coordination is monodentate, as in the case of the usual monodentate phosphonates $(RO)_2RPO$, while the role of the second center reduces to creating barriers to the extraction of HNO_3 ("buffer action"). Because of this, a smaller fraction of the extractant is bound by the acid and the distribution ratios of americium increase. As additional proof, it was pointed out that in the extraction of americium from $LiNO_3$ solutions in the absence of HNO_3 the difference between its extraction by bidentate carbamoyl phosphonates and the usual phosphonates decreased significantly. These arguments, however, are incorrect, because they ignore the fact that the $CH_2C(O)NR_2$ extracted less HNO_3 than the monodentate analog $R_2P(O)CH_2(O)PR_2$; the extraction increased with the length of the alkylene bridge, i.e., as the influence of the second center was weakened. And, without the coordination by the center C = O, in the lithium system americium would be extracted less strongly by carbamoyl phosphonates than by monodentate phosphonates. In reality, the opposite situation occurs. Thus the data in [31] prove not the point of view of the authors, but rather the presence of bidentate coordination.

Effect of Diluents. As is evident from Figs. 5-8, the nature of the diluents has an unusually strong effect on the extraction of actinides by bidentate phosphoorganic compounds, expecially diphosphine dioxides and diaryldialkyl carbamoyl phosphine oxides. The distribu-

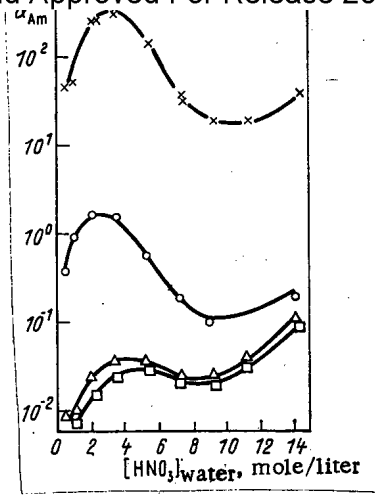

Fig. 7

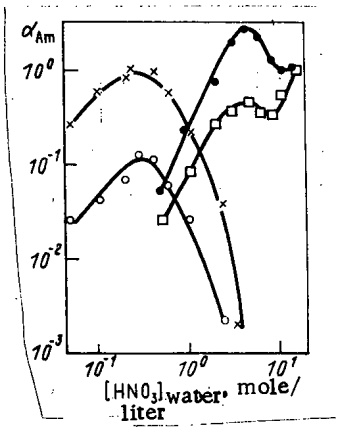

Fig. 8

Fig. 7. Effect of the structure of bidentate phosphoroorganic compounds on their extractive ability (0.05 mole/liter solutions in chloroform): ×) 4Ph; ○) 2Ph2oct; Δ) Tol_2/But_2; □) Ph_2/But_2.

Fig. 8. Effect of diluents on the extraction of americium by TOPO and carbomoyl methyl phosphonates (i-amyl O)$_2$/But_2; ×) 0.1 mole/liter TOPO – dichloroethane; ○) 0.1 mole/liter TOPO – C_6H_6; •) (i-amyl O)$_2$/But_2 – dichloroethane; □) (i-amyl O)$_2$/But_2 – C_6H_6.

tion ratios accompanying the use of dichloroethane and benzene differ by approximately a factor of 200. In the meantime, in the extraction of HNO_3 (i.e., with monodentate coordination), the effect of the diluent is small (see Fig. 6). An exception is chloroform, which forms H bonds with the oxygen in ligands.

The strong effect of the diluent on the extraction of actinides is explained by the apppearance of an interaction between the diluent and complexes with bidentate coordination. The mechanism of this interaction is still not understood.

It is evident from Figs. 5 and 6 that aryl carbamoyl phosphine oxides have definite advantages, and especially ditolyl dibutyl carbamoyl methylene phosphine oxides Tol_2/But_2, whose extractive ability is increased by the AAS effect and the electronic effect of the methyl radical. In addition, the introduction of hydrocarbon radicals and a benzene core in accordance with the recommendations of [15, 37] lowers the compatibility with hydrocarbon diluents, solubilization of TBP gives an additional effect [15, 29] (for example, when 1 mole/liter TBP is introduced, 0.5 mole/liter of the ligand solution can be used). Compounds of this class are of definite practical interest and can be recommended for technological studies.

Extraction by Polydentate Extractants (Crown Esters)

The use of stereo specific macrocyclical extractants can help to solve the problem of selectivity, since this is precisely the way this problem is solved in nature (for example, heme transfers only iron). Until recently the extractive properties of crown esters were studied predominantly for alkali and alkaline-earth metals. The significant selectivity of these extractants was noted. For example, crown esters of the type 18-crown-6 (the first number is the number of atoms in the cycle and the second number is the number of oxygen atoms) selectively extract potassium and strontium; 15-crown-5 selectively extract sodium; crown-4 selectively extract lithium [38]. These results were explained by the structural correspondence between the ion sizes and the dimensions of the cavity in the macrocycle.

Extraction of actinides was first studied by B. N. Laskorin et al. [39]. It was noted that quadrivalent actinides, forming disolvates, are extracted strongly while hexavalent actinides (monosolvates) are extracted weakly; the values of the extraction constants were

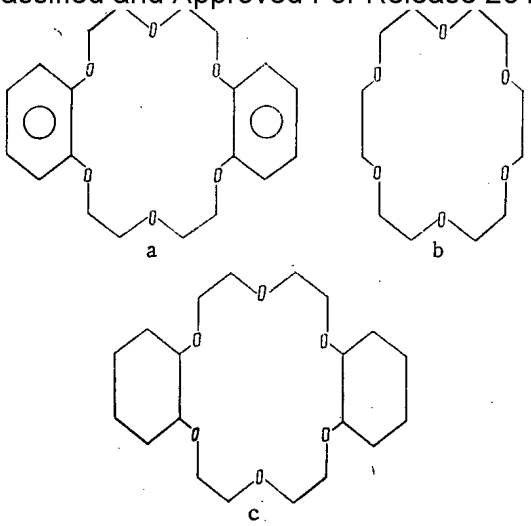

Fig 9

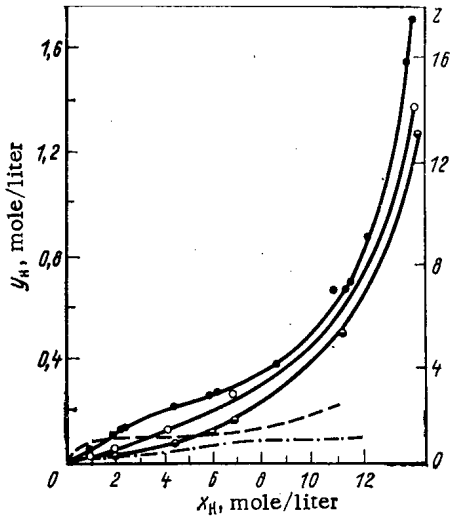

Fig. 10

Fig. 9. Structure of dibenzo-18-crown-6 (a), 18-crown-6 (b), and dicyclohexyl-18-crown-6 (c).

Fig. 10. Extraction isotherms for HNO_3 extracted by 0.1 mole/liter solutions of crown esters in dichloroethane: •) dicyclohexyl-18-crown-6, ○) 18-crown-6; ◒) dibenzo-18-crown-6; ---) TOFO, -·-) TBP; $z = [HNO_3)_{org}/[L]_{start}$; $x_H = [HNO_3]_{water}$; $y_H = [HNO_3]_{org}$.

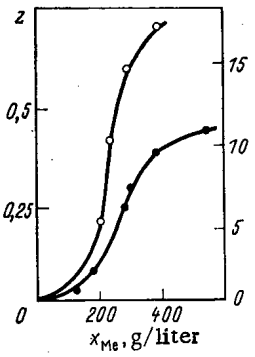

Fig. 11

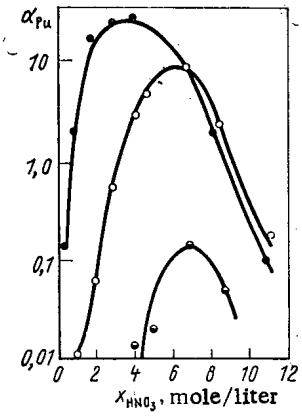

Fig. 12

Fig. 11. Extraction isotherms for Th(•) and U (○) extracted by dicyclohexyl-18-crown-6: $y_{Me} = [Me]_{org}$.

Fig. 12. Dependence of the distribution factors of Pu (IV) on the HNO_3 concentration of 0.1 mole/liter during extraction by solutions of crown esters in dichloroethane: •) dicyclohexyl-18-crown-6; ○) 18-crown-6; ◒) dibenzo-18-crown-6.

presented. In our studies [21] data are presented on the distribution of nitric acid and thorium, uranyl, and plutonium nitrates in the extraction by several esters, predominantly dibenzo-18-crown-6, 18-crown-6, and dicyclohexyl-18-crown-6 (Fig. 9). The chemical nature was discussed and the quantitative characteristics of the extractive equilibria were found. The very strong extraction of HNO_3, exceeding the extraction observed with the use of a strong extractant such as TOPO, was most unexpected (Fig. 10). The mechanism of the extraction is not completely understood. In [21] we proposed to form the complexes $(HNO_3)_iH_2O_{hi}L$ according to the type of damped chain polymerization with the group H_3O^+ in the cavity and the groups NO_3^- and H_3O^+ or HNO_3 alternating in the perpendicular direction. But NMR studies did not prove the coordination of two water molecules to each oxygen of the crown ester.

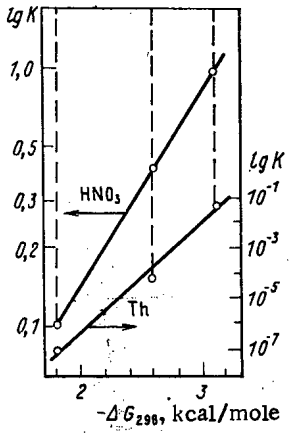

Fig. 13. Dependence of the extraction constants of HNO_3 and Th on the alkalinity of the crown esters: 1) dicyclohexyl-18-crown-6; 2) 18-crown-6; 3) dibenzo-18-crown-6; ΔG_{298}) Gibbs energy of interaction of the extractant with phenol [40].

The extraction isotherms of thorium are not entirely the usual isotherms (Fig. 11). However, the observed dependence of the distribution ratios of plutonium on the acidity (curves with a maximum in Fig. 12) is characteristic for extraction with neutral compounds [35]: the acid first acts as a salting out agent and then as a competitor, binding the ligand.

The previously established (for neutral organic compounds) dependence of the extractive ability on the electronegativity of the substituents and on the alkalinity of the esters was also observed: when electron-donor cyclohexyl substituents are introduced the extraction decreases (dibenzo-18-crown-6) (see Figs. 10-12). The correlation with the alkalinity is approximately linear (Fig. 13), though deviations from linearity are possible owing to "favorable" conformations. This indicates that both spatial factors and to a significant extent electronic factors play a role in extraction by crown esters, which can be explained by the significant contribution of acceptor–donor interaction. We recall that alkali and alkaline-earth elements interact with crown esters predominantly electrostatically. Actinides, on the other hand, exhibit distinct acceptor properties, which is what gives rise to the increase in the role of this interaction, and attenuates the role of structural correspondence.

We shall now study the question of the application of crown esters for extraction and separation of actinides. The strong extraction of plutonium and weak extraction of uranium enables in principle the use of crown esters for separation of these elements. This is hardly desirable, however, because amine salts – which are incomparably cheaper and more accessible extractants – have an analogous, though weaker, property.

Crown esters of the 18-6 type cannot, unfortunately, be used for both extraction and separation of trivalent actinides and lanthanides – the alkalinity and extractive ability of these extractants are inadequate. For example, in extracting americium with a 0.5 mole/liter solution of DTsG-18-crown-6 in dichloroethane and the introduction of a salting out agent [2 mole/liter $Al(NO_3)_3$], a distribution factor of only 0.05 was achieved.

The extractive ability of esters of the dibenzo-18-crown-6 type, containing the phosphoryl group P = O, was also checked. It turned out to be very low (approximately at the level of the corresponding phosphonate), i.e., the combined (P = O and crown-ester) coordination did not arise.

It is desirable to develop macrocyclical extractants, whose spatial characteristics and alkalinity are adapted to the extraction and fine separation of trivalent actinides and lanthanides.

Thus definite progress has been achieved in investigations and selection of new extractants for extracting actinides. However, although a series of mono- and bidentate compounds can be recommended for practical applications, macrocyclical extractants for extraction and separation of trivalent actinides require additional development.

LITERATURE CITED

1. A. M. Rozen and Z. I. Nikolotova, "Dependence of the extractive ability of organic compounds on their structure and electronegativity of substituent groups," Zh. Neorg. Khim., 9, No. 7, 1725-1743 (1964).
2. A. M. Rozen and N. A. Konstantinova, "Dependence of the extractive and reactive abilities of organic compounds on their structure," Dokl. Akad. Nauk SSSR, 167, No. 1, 132-135 (1966).
3. A. M. Rozen, "Problems of physical chemistry of extraction," Radiokhimiya, 10, No. 3, 272-309 (1968).
4. A. M. Rozen, Z. I. Nikolotova, A. A. Vashman, et al., "Dependence of the extractive ability on the structure of the extractant," in: Chemistry of Extraction Processes [in Russian], Nauka, Moscow (1972), pp. 41-45.
5. A. M. Rozen, Z. I. Nikolotova, and N. A. Kartasheva, "Mechanism of extraction with organic oxides P_3XO and bases P_4XNO_3 in the series N–P–As," Dokl. Akad. Nauk SSSR, 209, No. 6, 1369-1372 (1973).
6. A. M. Rozen, Z. I. Nikolotova, and N. A. Kartasheva, "Some rules for extraction of actinide elements," Radiokhimiya, 16, No. 5, 686-695 (1974).
7. A. M. Rozen, "Control of the extractive abiltiy of organic compounds," in: Hydrometallurgy [in Russian], Nauka, Moscow (1976), pp. 194-198.
8. A. M. Rozen and D. A. Denisov, "Approximate quantum-chemical justification of the equations of extractive ability (Hammet–Taft method of electronegativities)," Radiokhimiya, 18, No. 6, 921-923 (1976).
9. A. M. Rozen, Z. I. Nikolotova, and N. A. Kartasheva, "Effect of extractant structure on extractive ability," Zh. Neorg. Khim., 24, No. 6, 1642-1651 (1979).
10. A. M. Rozen and A. S. Skotnikov, "Effect of the structure of compounds in the series $(RO)_3PO - R_3PO - R_3AsO - P_3NO$ on the extraction and nature of complexification with $HReO_4$ and $HTcO_4$," Dokl. Akad. Nauk SSSR, 259, No. 4, 869 (1981).
11. A. M. Rozen, Z. I. Nikolotova, N. A. Kartasheva, et al., "Effect of the structure of organic compounds on their extractive ability," Radiokhimiya, 25, No. 5, 603-608 (1983).
12. A. M. Rozen, "Dependence of the extractive ability on the structure of the extractant and separation of the contributions of solvation and hydration to the equilibrium constant," in: Extraction Chemistry [in Russian], Nauka, Novosibirsk (1984), pp. 68-95.
13. A. M. Rozen, Z. I. Nikolotova, N. A. Kartasheva, et al., "Extraction of americium by diphosphonic dioxides," Radiokhimiya, 17, No. 2, 237-243 (1975).
14. A. M. Rozen, Z. I. Nikolotova, N. A. Kartasheva, et al., "Anomalous dependence of the strength of americium (III) complexes and other Me (III) complexes iwth diphosphonic dioxides on their structure," Dokl. Akad. Nauk SSSR, 222, No. 5, 1151-1154 (1975).
15. A. M. Rozen, Z. I. Nikolotova, N. A. Kartasheva, et al., "Diphosphonic dioxides – unique extractants for extraction of actinides," in: Abstracts of Reports at the 2nd All-Union Conference on the Chemistry of Transplutonium Elements, Dezisy Dokladov, Dimitrovgrad (1983), p. 10.
16. A. M. Rozen, Z. I. Nikolotova, and N. A. Kartasheva, "Anomalous aryl strengthening of complexes in extraction of americium and europium by alkaline diphosphonic dioxides from perchloric media," Radiokhimiya, 20, No. 5, 725-734 (1978).
17. A. M. Rozen, Z. A. Berkman, L. É. Bertina, et al., "Extraction of nitric acid by alkaline diphosphonic dioxides," Radiokhimiya, 18, No. 4, 493-501 (1976).
18. A. M. Rozen, Z. I. Nikolotova, N. A. Kartasheva, et al., "Extraction of americium by vinylene diphosphonic dioxides," Radiokhimiya, 18, No. 6, 846-847 (1976).
19. A. M. Rozen, V. V. Akhachinskii, N. A. Kartasheva, et al., "Reasons for the anomalous aryl strengthening of actinide and lanthanide (III) complexes with diphosphonic dioxides," Dokl. Akad. Nauk SSSR, 263, No. 4, 938-942 (1982).
20. A. M. Rozen, Z. I. Nikolotova, and N. A. Kartasheva, "Diphosphonic dioxides as extractants for actinide elements (in connection with the problem of anomalous aryl strengthening of complexes)," in: Research in the Reprocessing of Irradiated Fuel [in Russian], Atomic Energy Commission of Czechoslovakia, Vol. 2, Prague (1977), pp. 22-29.

21. A. M. Rozen, Z. I. Nikolotova, N. A. Kartasheva, et al., "Extraction of actinides and nitric acid by crown esters," Dokl. Akad. Nauk SSSR, 263, No. 5, 1165-1169 (1982).
22. A. Rozen, "Problems in the physical chemistry of solvent extraction," in: Solvent Extraction, Proceedings of the International Conference, North-Holland, Amsterdam (1967), pp. 195-235.
23. A. Mills and W. Logan, "Third phase formation between some actinide nitrates and 20% tri-n-butylphosphate odourless kerosene," ibid., pp. 322-326.
24. A. M. Rozen, A. S. Nikiforov, V. S. Shmidt, et al., "Method for extracting actinides," Inventor's Certificate No. 841140, Byull. Izobr., No. 14, 319 (1982).
25. A. S. Nikiforov, V. S. Shmidt, and A. M. Rozen, "Choice of organic solvent for extraction processes in regeneration of spent nuclear fuel," in: Abstracts of Reports at the 13th Mendeleev Conference, Nauka, Moscow (1981), p. 182.
26. A. S. Nikiforov, V. S. Shmidt, A. M. Rozen, et al., "Physicochemical foundations for the selection of organic solvent for extraction processes in regeneration of spent nuclear fuel," Radiokhimiya, 24, No. 5, 631-636 (1982).
27. A. M. Rozen, V. S. Shmidt, Z. I. Nikolotova, et al., "Physicochemical foundations for the optimization of the structure of the extractant for regeneration of spent nuclear fuel," Dokl. Akad. Nauk SSSR, 274, No. 5, 1139-1144 (1984); At. Énerg., 58, No. 1, 38-43 (1985).
28. D. Crouse, W. Arnold, and F. Hurst, "Consolidated fuel reprocessing program alternate extractants to tributylphosphate for reactor fuel reprocessing," in: Proc. ISEC-83, Denver (1983), pp. 90-91.
29. E. Horwitz, H. Diamond, D. Kalina, et al., "Octyl(phenyl)-N, N-diisobutylcarbamoylmethylphospfine oxide as an extractant for actinides from nitric acid waste," ibid., pp. 451-452.
30. W. Schulz and L. McIsaac, "Removal of actinides from nuclear fuel reprocessing waste solutions with bidentate organophosphorus extractants," Transplutonium-1975, North-Holland, Amsterdam (1976), pp. 433-477; Proc. ISEC-77, Vol. 2, Toronto, pp. 619-629.
31. E. Horwitz, A. Muscatello, D. Kalina, et al., "The extraction of selected transplutonium (III) and lanthanide (III) ions by dihexyl-N, N-diethylcarbamoylmethylphosphonate from aqueous nitrate media," Separ. Sci. Technol., 16, No. 4, 417-437 (1981).
32. D. Kalina, E. Horwitz, L. Kaplan, et al., "The extraction of Am (III) and Fe (III) by selected dihexyl-N, N-dialnylcarbamoylmethyl – phosphonates–phosphinates – and phosphine oxides from nitrate media," ibid., No. 9, 1127-1145.
33. T. Ya. Medved', M. K. Chmutova, N. P. Nesterova, et al., "Dialkyl (diaryl)[dialkylcarbamoylmethyl]phosphonic oxides," Izv. Akad. Nauk SSSR, Ser. Khim., No. 9, 2121-2127 (1981).
34. M. K. Chmutova, N. P. Neserova, N. E. Kochetkova, et al., "Extraction and concentration of transplutonium elements from nitrate media by diphenyl[dialkylcarbamoylmethyl]phosphinic oxides," Radiokhimiya, 24, No. 1, 31-37 (1982).
35. A. M. Rozen, "Thermodynamics of extraction equilibria of uranyl nitrate," At. Énerg., 2, No. 5, 445-458 (1957); in: Extraction [in Russian], No. 1, Atomizdat, Moscow pp. 6-87.
36. A. M. Rozen, Z. I. Nikolotova, N. A. Kartasheva, et al., "Complexification of americium, curium, and lanthanides with organic dioxides and the problem of anomalous aryl strengthening of the complexes," Radiokhimiya, 19, No. 5, 709-719 (1977).
37. A. M. Rozen, Z. I. Nikolotova, and N. A. Kartasheva, "Method for extracting and concentrating actinides and lanthanides," Inventor's Certificate No. 601971, Byull. Izobr., No. 35, 2571 (1979).
38. A. V. Bogatskii, N. G. Luk'yanenko, V. A. Shapkin, et al., "Extraction of picrates of alkali and alkaline-earch metals with macrocyclical esters," Zh. Org. Khim., 16, No. 10, 2057-2059 (1980).
39. V. V. Yakshin, E. A. Filippov, V. A. Belov, et al., "Coronas in extraction of uranium and actinides from nitrate solutions," Dokl. Akad. Nauk SSSR, 241, No. 1, 159-162 (1978).
40. V. V. Yakshin, V. M. Abaskin, and B. N. Laskorin, "Electron-donor properties of macrocyclical polyesters," Dokl. Akad. Nauk SSSR, 244, No. 1, 157 (1979).

MATHEMATICAL MODEL OF THE TEMPERATURE FIELD AROUND A BOREHOLE WITH RADIOACTIVE WASTES AND ITS EXPERIMENTAL VERIFICATION IN FIELD CONDITIONS

E. G. Drozhko, V. I. Karpov,
A. S. Stepanov, I. I. Kryukov,
V. F. Savel'ev, V. V. Kulichenko,
V. A. Bel'tyukov, and A. A. Konstantinovich

UDC 621.036

Radioactive wastes must be reliably isolated from the environment. At present, the most widespread method is storage in geological formations [1-4]. In the burial of wastes with a high level of energy liberation, the reliability of their isolation is largely determined by the thermal effects on the rock of the geological mass. As a result of these effects, temperature stress arises in the rock and may exceed the limiting permissible value under certain conditions. This may lead ultimately to loss of structural integrity of the store. In connection with this, the examination of burial options demands careful analysis of nonsteady temperature fields in the rock mass around the waste site. For most versions of burial, this analysis is only possible by means of finite-difference calculation schemes, for various reasons. In waste burial in mine galleries, the use of a finite-difference scheme is due to the dense lattice of boreholes with wastes, the dependence of the thermophysical parameters of the rock on the temperature, and the disrupted structure of the rock mass at the time of mine construction. However, with a simple burial scheme (for example, storage of the wastes in a system of deep boreholes [5]), the accuracy of analytical solutions of the heat-conduction equations may be sufficient for practical purposes. The use of deep boreholes allows high values of thermal load per unit area of the field and efficiency of the mine workings to be attained. The boreholes may be sunk at a distance excluding their mutual thermal influence, at least in the period of formation of maximum rock temperature.

The temperature field in a rock mass from a single borehole with radioactive waste may be estimated using the model of a linear source. The equation for a source of limited size perpendicular to an isothermal surface of a semiinfinite mass with thermal power varying according to the law of radioactive decay may be obtained by the instantaneous-source method

$$\begin{cases} t(r, z, \tau) = t_0 + \\ + \dfrac{Q}{8\pi Lk} l^{-\lambda\tau} \int\limits_0^\tau \dfrac{l^{\lambda\tau' - \frac{r^2}{4a\tau'}}}{\tau'} \psi(z, \tau')\, d\tau \\ \psi(z, \tau) = \operatorname{erf} \dfrac{(z-l)^{\beta_1}}{2\sqrt{a\tau}} + \operatorname{erf} \dfrac{(z+l)^{\beta_2}}{2\sqrt{a\tau}} - \\ - \operatorname{erf} \dfrac{(z+l+L)^{\beta_3}}{2\sqrt{a\tau}} - \operatorname{erf} \dfrac{(z-l-L)^{\beta_4}}{2\sqrt{a\tau}}, \end{cases} \tag{1}$$

where t(r, z, τ) is the rock temperature at the point with coordinates (r, z) at time τ; t_0, surface temperature of the rock; k, a, thermal conductivity and thermal diffusivity of the rock; Q, initial thermal power of the source; λ, radioactive decay constant; L, length of the heat source; l, depth of the source.

Using the relation [6]

$$\int\limits_0^\infty \frac{l-y}{y} \operatorname{erf}(\beta\sqrt{y})\, dy = 2 \operatorname{arsh} \beta, \tag{2}$$

Eq. (1) for a source of constant power (λ = 0) may be written in the form

Translated from Atomnaya Énergiya, Vol. 59, No. 6, pp. 422-425, December, 1985. Original article submitted October 30, 1984; revision submitted April 24, 1985.

 0038-531X/85/5906-0994$09.50

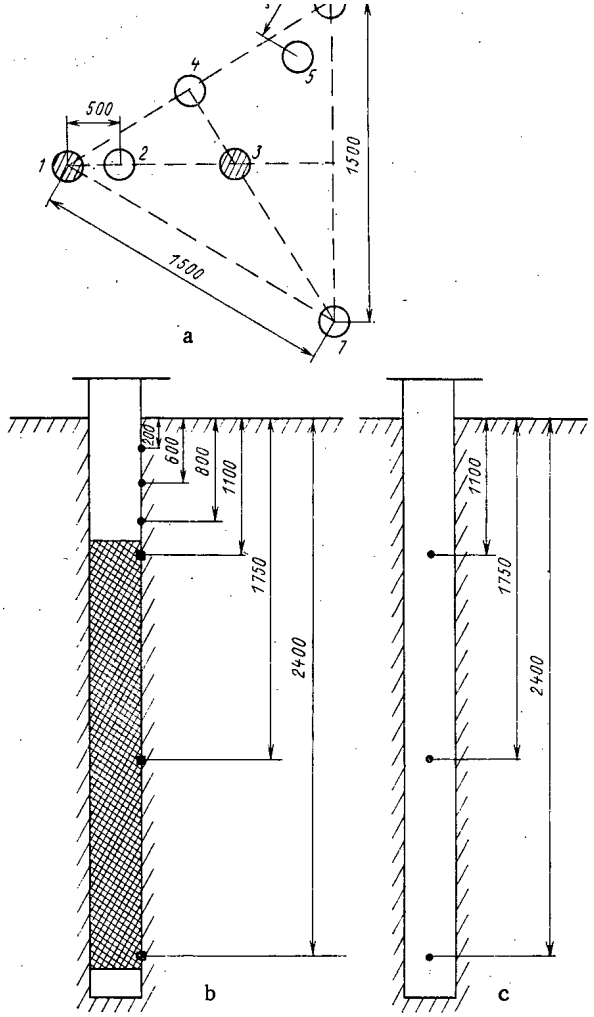

Fig. 1. Distribution of boreholes 1-7 (a) and of temperature sensors in boreholes 1 (b) and 2, 4-7 (c): the filled squares correspond to thermocouples and the filled circles to resistance thermometers.

$$\begin{cases} t(r, z, \tau) = T(r, z) - \dfrac{Q}{8\pi Lk} \displaystyle\int_{\tau}^{\infty} \frac{l^{-\frac{r^2}{4a\tau'}}}{\tau'} \psi(z, \tau')\, d\tau' \\ T(r, z) = \dfrac{Q}{4\pi Lk} \left(\operatorname{arsh} \dfrac{\beta_1}{2r} + \operatorname{arsh} \dfrac{\beta_2}{2r} - \right. \\ \left. - \operatorname{arsh} \dfrac{\beta_3}{2r} - \operatorname{arsh} \dfrac{\beta_4}{2r} \right), \end{cases} \tag{3}$$

where β_i are the coordinate indices of the given point.

Using the function T(r, z), the steady temperature field around a linear heat source is described. It has previously been used to estimate the temperature conditions of radioactive-waste burial [7]. At a great thermal-source length and considerable depth the equation for a nonsteady problem must be used.

The possibility of using Eq. (1) to estimate the temperature conditions of waste burial in a system of deep boreholes has been experimentally investigated in field conditions. For experimental verification, seven boreholes were sunk in loam (Fig. 1). In boreholes 1 and 3, electric heaters of diameter 85 nm and length 1.5 m connected to an ac grid of

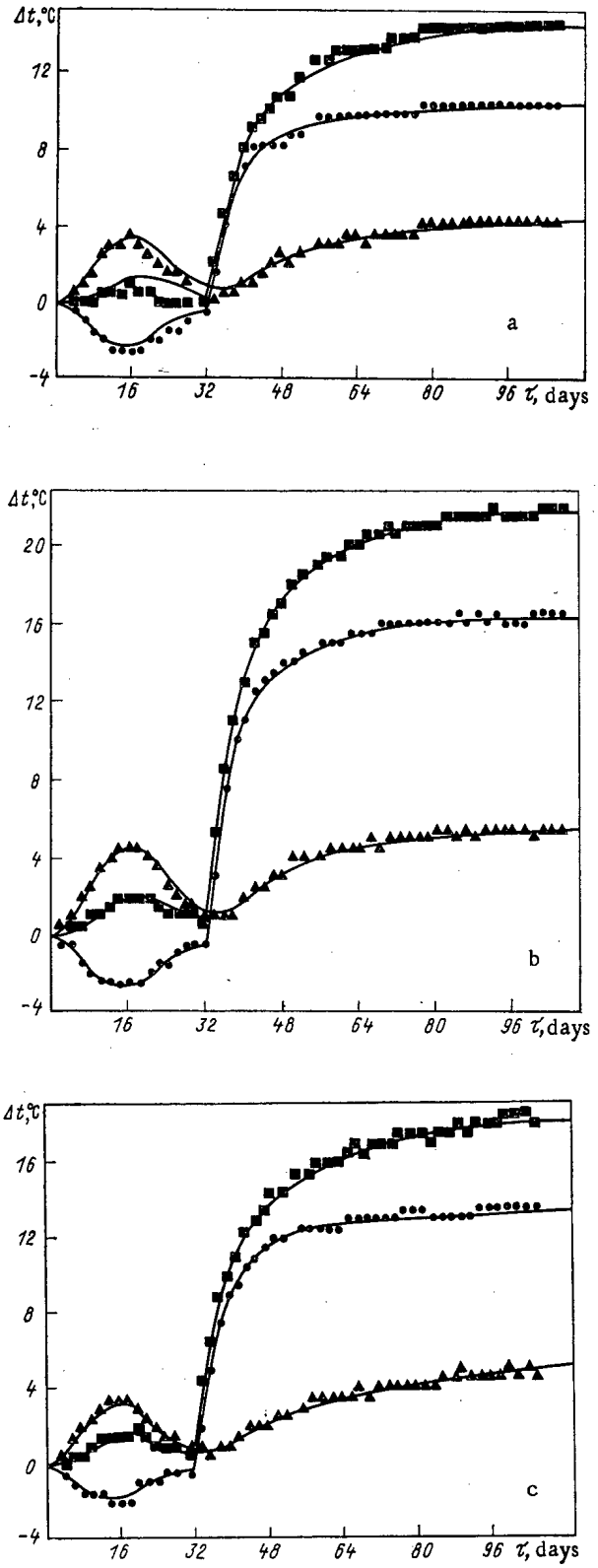

Fig. 2. Dependence of the temperature difference on the time for upper (a), middle (b), and lower (c) points of the resistance-thermometer battery in the boreholes: continuous curves correspond to calculation and points to experiment.

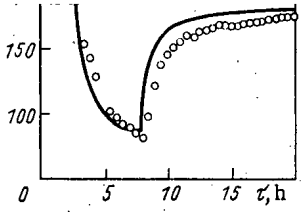

Fig. 3

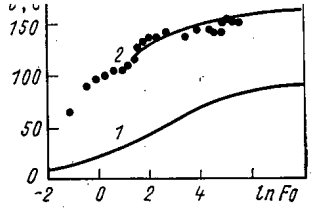

Fig. 4

Fig. 3. Surface temperature of borehole (1) and heater (2); the curve corresponds to calculation and the points to experiment.

Fig. 4. Surface temeprature of heater with brief disconnection of the electrical supply ($\tau < 20$ h): curves correspond to calculation and points to experiment.

potential 220 V were installed. After installing a bank of resistance thermometers, the boreholes were filled with the earth removed when they were dug. The thermometer readings were recorded by secondary instruments.

The basic aim of the work is to determine the influence of the heating-element dimensions and its depth on the conditions of nonsteady-field formation in the loam, in conditions of constant heater power, which is the simplest to investigate in field conditions. In addition, with a more complex dependence of the heat liberation, additional errors appear, associated with the need to maintain it accurately over time.

In the first stage, a heater of 400 W in borehole 3 was switched on, and operated for 14 days. The readings of the resistance thermometers on switching off the heaters were measured for a further 17 days after this, which offered the possibility of making measurements during the stepwise change in heater power. Subsequently, the heater in borehole 1 was switched on, and ran for more than three months until a steady temperature distribution was established in the soil.

The resistance-thermometer readings are analyzed using Eq. (3). To eliminate the influence of daily and seasonal variations in soil temperature, the difference in the readings of sensors positioned at the same level in any two boreholes are considered. The thermal conductivity and thermal diffusivity of the soil in natural conditions before the measurements was not determined. To estimate these parameters, the readings of the resistance thermometers in boreholes 2 and 6 at the level of the central cross section of the heating element are used. The thermal conductivity is estimated from the expression for a steady distribution [7], which gives 1.71 ± 0.27 W/m·K [8]. The thermal diffusivity of the soil is determined on the basis of Eq. (2) for a nonsteady temperature distribution in the soil. A theoretical dependence of the dimensionless temperature difference Θ_{26} on $Fo_2 = a\tau/r_2^2$ is obtained here

$$\Theta_{26} = [t_2(r_2, z_0, \tau) - t_6(r_6, z_0, \tau)]\frac{8\pi Lk}{Q}, \qquad (4)$$

where $t_i(r_i, z_0, \tau)$ is the soil temperature at the point (r_i, z); i is the borehole number.

On the basis of the resistance-temperature readings and in accordance with the preliminarily determined thermal conductivity, Θ_{26} is calculated, and then from the graphical dependence Fo_2 is determined for a fixed time. According to the estimate, the thermal diffusivity is $(0.46 \pm 0.09)\cdot 10^{-6}$ m^2/sec. The differences in readings of the other resistance thermometers at the same level are calculated for the resulting values of the soil thermal conductivity and thermal diffusivity (Fig. 2).

Analysis of the results of surface-temperature measurements for the heating elements shows that when $a\tau/r_0^2 \gg 1$, where r_0 is the borehole radius, Eq. (3) may be used to estimate the surface temperature of the borehole. At the same time, the temperature difference between the borehole and heater surfaces may be determined on the basis of the relations of steady heat transfer (Fig. 3). The wall temperature of the borehole is calculated from (1) and the temperature difference in the air gap between the heater and the borehole wall from the relation for the radiant heat transfer for the given emissivity of 0.7.

Initially, when $(z - \ell)/(2\sqrt{a\tau}) > 3$, the surface temperature of the heater may be calculated from the model of an electric cable of infinite length [9]. In Fig. 4, the results of measuring the readings of the central thermocouple of heater 1 on brief disconnection are shown together with the results of calculation on the basis of the electric cable model.

Field measurements show that the given model of a linear source is completely satisfactory in describing the formation of a nonsteady temperature field around a cylindrical heat source sunk vertically into a mass beginning at times satisfying the condition $a\tau/r^2 \gg 1$. With radioactive-waste burial in a deep borehole, this condition is satisfied for 1-2 months after loading. The energy liberation in the waste determined before burial by the radionuclides ^{90}Sr and ^{137}Cs is practically unchanged in this period. The initial period in which the linear-source model is inapplicable for temperature-field calculation in a rock mass is short and does not influence the conditions of maximum temperature formation in the rock determining its limiting thermostress state. If the thermal load on the rock is chosen so that the temperature variations in the thermophysical parameters of the rock are within the limits of accuracy of their determination for the rock as a whole, in this case the model of the linear source may be used to analyze the schemes of waste burial with sufficient accuracy for practical purposes, for example, in waste burial in rock at thermal loads of up to 300-400 W/m of borehole length.

LITERATURE CITED

1. A. S. Nikiforov, V. V. Kulichenko, and M. I. Zhikharev, Safe Storage of Liquid Waste from Atomic Power Plants and Radiochemical Production [in Russian], Énergoatomizdat, Moscow (1984).
2. I. I. Kryukov, V. V. Kulichenko, and Yu. P. Martynov, "Conditions of burial of high-activity solidified waste," in: Research in Spent-Fuel Reprocessing [in Russian], Vol. 2, COMECON, Prague (1972), p. 34.
3. N. N. Verigin, Yu. P. Marynov, and I. I. Kryukov, "Nonsteady temperature fields in soil burial of high-activity solid wastes," in: Research into the Safe Storage of Liquid, Solid, and Gaseous Radioactive Wastes and Deactivation of Contaminated Surfaces [in Russian], Atomizdat, Moscow (1978), pp. 129-131.
4. V. V. Kulichko, N. V. Krylova, and I. I. Kryukov, "Properties of highly active wastes determining their behavior on burial in geological formations," in: Underground Disposal of Radioactive Waste, IAEA, Vienna (1980), pp. 201-207.
5. T. Ringwood, "Safety and depth for nucler disposal," New Sci., 88, No. 1229 (1980).
6. N. N. Verigin, et al., Hydrodynamic and Physicochemical Properties of Rock [in Russian], Nedra, Moscow (1980), p. 66.
7. N. N. Verigin, V. V. Kulichenko, Yu. P. Martynov, and I. I. Kryukov, "Self-heating in the underground burial of solid radioactive wastes," in: Underground Disposal of Radioactive Waste, IAEA, Vienna (1967).
8. A. F. Chudnovskii, Thermophysical Characteristics of Disperse Materials [in Russian], Gos. Izd. Fiz.-Mat. Lit., Moscow (1962), pp. 430, 431, 434.
9. H. S. Carslow and J. C. Jaeger, Conduction of Heat in Solids, Oxford University Press, New York (1959).

PASSAGE OF PRIMARY PROTONS THROUGH A SHIELD WITH A RANDOM DISTRIBUTION OF THE MATERIAL

V. G. Mitrikas, V. M. Sakharov, and V. G. Semenov

UDC 539.125.42

When the radiation conditions inside spacecraft are calculated, one usually employs the assumption that the spacecraft can be modeled by a few sectors with a constant thickness of the material in each of the sectors [1] and that the proton dose is the superposition of the doses developing behind infinite plane layers of a homogeneous material the thickness of which is equal to the thickness of the material in the sectors.

The basis of this approach to the calculation of the absorbed proton dose inside a spacecraft has been considered in a large number of papers [1]. But there exists practically no information on the influence of the inhomogeneities of the material due to the design and the equipment of the spacecraft on the development of the dose. We consider in the present work the results of investigations in which the development of the doses in the equipment was studied, with the equipment being characterized by a randomly inhomogeneous distribution of the material. The investigations were made for the case of normal incidence of monoenergetic protons on the equipment.

The calculation of the primary proton spectra in the bulk of the equipment is based on the assumption that the equipment can be described by a random function in analytic form. The types of functions have been theoretically explained in [2]. We consider for the sake of simplicity functions of the Rayleigh type in which the probability of the material thickness x (g/cm^2) is represented for the geometric dimensions z (cm) in the following form:

$$P_z(x) = \frac{x-\gamma_z}{\eta_z^2} \exp\left[-\frac{(x-\gamma_z)^2}{2\eta_z^2}\right], \quad (1)$$

where γ_z denotes the average value of the thickness; η_z denotes the dispersion of the distribution; and the subscript z indicates a parametric dependence. With the range-energy relation for protons, $R = a \ln(1 + bE^{\alpha})$, where a, b, and α denote the constants depending upon the material of the equipment [3]; the material thickness x through which the radiation passes can be expressed as

$$x = a \ln[(1+bE_0^{\alpha})/(1+bE^{\alpha})],$$

where E_0 and E denote the energy of the protons incident upon the layer and behind the layer of thickness x, respectively. Since x is a random quantity which can be characterized by the distribution function of Eq. (1), the density of the proton distribution over the energy is

$$P_z(E) = \frac{x(E, E_0)-\gamma_z}{\eta_z^2} \exp\left\{-\frac{[x(E, E_0)-\gamma_z]^2}{2\eta_z^2}\right\} \frac{ab\alpha E^{\alpha-1}}{1+bE^{\alpha}} \quad (2)$$

behind the layer z.

When we derived Eq. (2), we used the well-known form of expressing the probability density of the distribution of a random quantity through another random quantity related to the first one by a dependence in the form of a function.

In real blocks of equipment, the range of possible thickness values on which the probability density is defined has its lower limit given by the x_{min} value (e.g., the sum of the thicknesses of the mounting plates) and its upper limit given by x_{max}. The normalization coefficient for $P_z(E)$ has the form

$$A^{-1} = \exp\left[-\frac{(\gamma_z-x_{min})^2}{2\eta_z^2}\right] - \exp\left[-\frac{(x_{max}-\gamma_z)^2}{2\eta_z^2}\right]. \quad (3)$$

Translated from Atomnaya Énergiya, Vol. 59, No. 6, pp. 425-428, December, 1985. Original article submitted April 26, 1984.

0038-531X/85/5906-0999$09.50

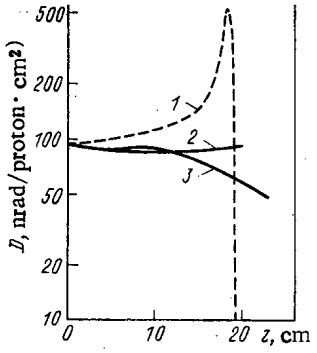

Fig. 1

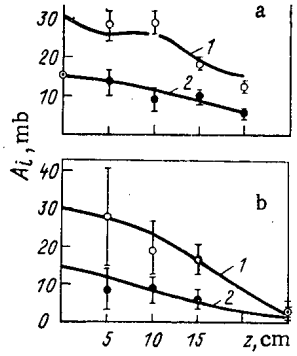

Fig. 2

Fig. 1. Specific absorbed proton dose D in a solid medium and in blocks of equipment with a thickness distribution in dependence upon the depth in the case of a Rayleigh distribution law: 1) solid medium ($\rho = 0.53 \cdot 10^3$ kg/m^3); 2) block 2; 3) block 1; ——) calculation.

Fig. 2. Activation integral A_i of the threshold detectors over the depth of block a) 1 and b) 2 of the equipment: 1) ^{19}F (p, pn) ^{18}F; 2) ^{27}Al (p, 3n) ^{24}Na; ○, ●) experiment; ——) calculation.

Equation (2) accounts for the proton losses only by ionization. The approach suggested by the authors of [4] was used to take into account the attenuation of the proton flux by nuclear interactions. The probability of a proton passing without nuclear interactions over a path on which its energy changes from E_0 to E as a consequence of ionization losses is given by the equation

$$k = \exp\left[-\int_{E}^{E_0} \frac{\mu(E')}{dE'/dx}\, dE'\right]$$

or, according to [4],

$$k = \sum_{i=1}^{n} C_i \exp(-\mu_{i\text{eff}}\, x). \tag{4}$$

In the general case, the proton spectrum in the depth z of a block of equipment is given by the product of Eqs. (2), (3), and (4):

$$\frac{dN}{dE}(z, E_0) = \frac{x(E, E_0) - \gamma_z}{\eta_z^2} \exp\left\{-\frac{[x(E - E_0) - \gamma_z^2]}{2\eta_z^2}\right\} \frac{ab\alpha E^{\alpha-1}}{1 + bE^{\alpha}} A \sum_{i-1}^{n} C_i \exp[-\mu_{\text{eff}}\, x(E, E_0)]. \tag{5}$$

Having obtained in this fashion the proton spectrum, we can more readily calculate the required functional relationship either in the form of the absorbed dose

$$D(z, E_0) = 1.6 \cdot 10^{-8} \int \frac{dN}{dE} \frac{dE}{dx}\, dE,$$

where $\frac{dE}{dx}$ denotes the ionization losses, or in the form of the activation integral

$$A_i(z, E_0) = \int \frac{dN}{dE} \sigma_i(E)\, dE, \tag{6}$$

where $\sigma_i(E)$ denotes the cross section for the activation of the i-th element by protons.

Figure 1 depicts the results of a calculation of the depth distribution of the absorbed dose of protons with E_0 = 100 MeV in solid aluminum and in randomly inhomogeneous media for distribution functions $P_z(x)$ of the type of Eq. (1) with the parameters $\gamma(z) = \bar{\rho}_z - 1.91\sigma_z$, $\eta^2(z) = 2.27\sigma_z^2$; the values of the parameters were determined from the results of gamma thickness measurements on blocks of equipment [2].

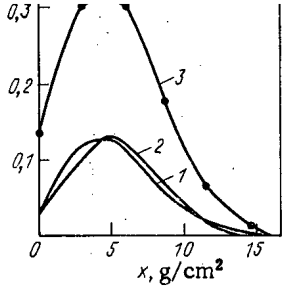

Fig. 3

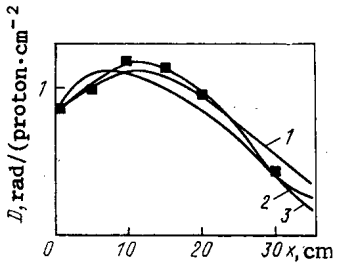

Fig. 4

Fig. 3. Functions f(x) of the probability density of the thickness distribution in block 2: 1) Rayleigh distribution; 2) normal distribution; and 3) binomial distribution.

Fig. 4. Depth distribution of the specific absorbed dose in block 2: 1) normal distribution; 2) binomial distribution; 3) Rayleigh distribution; ——) calculation according to the analytic law of the thickness distribution; ▪) calculation according to the thickness distribution indicated in Table 1.

The calculation for the solid medium was made taking into account the ionization losses, the losses of protons by nuclear interactions, range straggling, and multiple Coulomb scattering. The data of Fig. 1 clearly illustrate the basic difference in the development of the depth distribution of the dose inside solid media and randomly inhomogeneous media. It follows from the analysis of these results that in the case of a randomly inhomogeneous medium, one can ignore range straggling and multiple Coulomb scattering *vis a vis* the dispersion of the distribution of the material in the equipment when the depth distribution of the absorbed dose is calculated.

The proposed method of calculating proton spectra and the corresponding functional relationships in blocks of equipment were verified in the Institute of High-Energy Physics on the linear I-100 proton accelerator (E_0 = 100 ± 0.5 MeV). The calculated values of the corresponding activation integrals were obtained with Eqs. (5) and (6). The blocks of equipment were in the experiment scanned in the proton beam for modeling a plane multidirectional source. Activation detectors made from 100-μm-thick LiF and Al were mounted in the depth of a block along the proton beam path. Ten detectors were mounted at each fixed depth of the block on a plane perpendicular to the beam. After the exposure, the activity of the products from the reactions $^{7}_{3}Li(p, n)^{7}Be$ (threshold ∿2 MeV), $^{19}_{9}F(p, pn)^{18}_{9}F$ (threshold ∿10 MeV), and $^{27}_{13}Al(p, 3pn)^{24}_{11}Na$ (threshold ∿30 MeV) was measured.

The confidence interval shown in Fig. 2 corresponds to the dispersion of the distribution function of the thickness of the material at a fixed depth in the blocks and reflects the possible error of the functional relationship under inspection at a specific point inside a block. This interval is much greater than the error made in the determination of the activity of an individual detector and also exceeds the average values of the activity in the particular depth.

It is interesting to determine firstly the influence which the analytic representation of the thickness distribution of the material has upon the proton dose (distribution used to smooth the results of the gamma thickness measurements) and secondly the requirements to the accuracy of determining the parameters of the analytic representation and their dependence upon the geometric dimensions; it is also of interest to determine the errors which arise in the calculation of the proton dose and which are associated with the replacement of all materials composing the equiment by an aluminum equivalent.

The test calculations were made for the incidence of a beam of protons with the energy E_0 = 100 MeV on a typical block with the average density $5 \cdot 10^2$ kg/m³. The experimental thickness distributions of the material in the block were smoothed by normal or binomial

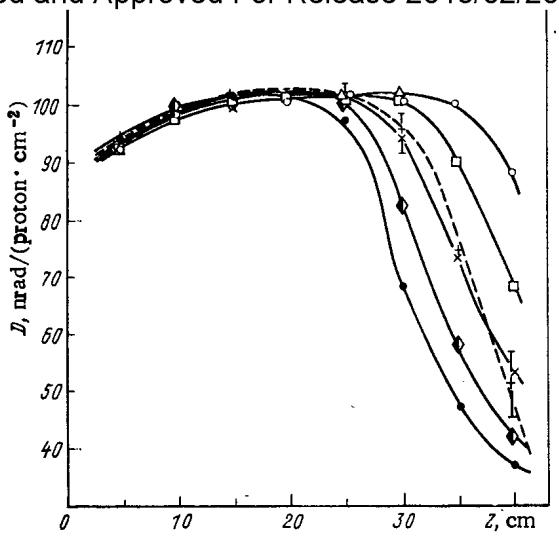

Fig. 5

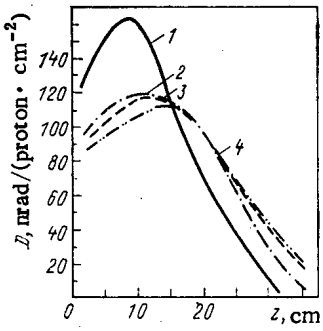

Fig. 6

Fig. 5. Depth distribution of the specific absorbed dose for various values of the parameters of the distribution function: $\gamma = az$ (○ □ × ◇ ● refers to a = 0.25, 0.293, 0.325, 0.36, and 0.39, respectively; b = 0.139); ---) $\sigma^2 = bz$ (b = 0.0815, 0.139, 0.163, or 0.202 (the curves merge within the error limits indicated); a = 0.325).

Fig. 6. Depth distribution of the specific absorbed dose for various materials of a block with the density $\rho = 0.53 \cdot 10^3$ kg/m^3; 1) tissue; 2) Al; 3) composition of materials with W_{eff} = 17.7; 4) Fe.

TABLE 1. Parameters of the Distribution Laws of the Material Thickness in a Typical Equipment Block

Normal distribution	Rayleigh distribution	Binomial distribution
$f(x,z) = \frac{1}{\sigma_z \sqrt{2\pi}} \times \exp\left[-\frac{(x-\bar{x}_z)^2}{2\sigma_z^2}\right]$; $\bar{x} = \bar{\rho} z$; $\sigma_z^2 = 1{,}844\bar{x}$; $x_{min} = 0{,}1\, z/1{,}9$; $x_{max} = z + 7$	$f(x,z) = \frac{(x-\gamma_z}{\eta_z^2} \times \exp\left[-\frac{(x-\gamma_z)^2}{2\eta_z^2}\right]$; $\gamma_z = \bar{x} - 1{,}91\,\sigma_z$; $\eta_z = 1{,}52\,\sigma_z$	$f(x,z) = C_N^n V^n (1-V)^{N-n}$; $n = x/D$; $N = z/D$; $V = 0{,}37$; $D = 2{,}92$

distributions and also by the Rayleigh distribution (see Table 1 and Fig. 3). The Rayleigh law renders the most satisfactory distribuiton.

Figure 4 illustrates the dependencies of the specific absorbed dose of primary protons in the depth of the equipment block in which the distribution of the material is described by the distribution functions listed in Table 1. The binomial distribution describes with great errors "tails" of the distributions; the maximum of the depth dependence of the dose differs from the maxima of the other distributions by about 20% and is shifted toward smaller depths in the block. In the case of the normal distribution, the proton dose attenuation resembles the Rayleigh distribution though the normal distribution only inaccurately describes the experimental distribution of the thickness in the range of small values. This range is characterized by a slight spread of the initial proton energy and by irrelevant attenuation by nuclear interactions. Accordingly, the depth dependencies of the dose are practically the same at low thicknesses of the material for these distribution functions. The proton doses differ substantially at great depths in the block. Thus, for z = 40 cm, D = 9.8 nrad/(proton·cm^{-2}) in the case of the normal distribution (1 rad = 0.01 Gr), whereas

in the case of the Rayleigh distribution, $D = 5.6$ nrad/(proton·cm^{-2}). It follows from this analysis that for a particular energy the thickness range which in regard to the deformation of the primary proton energy is large and which has a high stopping power is most important in the representation of experimental distribution laws by analytic functions.

This conclusion can be qualitatively drawn from an analysis of Eq. (4). Different changes in proton energy correspond to the same change in x with respect to γ_z. For $x < \gamma_z$, the change in the proton energy is small and the dE/dx changes are accordingly small. For $x > \gamma_z$ the transition to large dE/dx values takes place and, hence, the thickness range $>\gamma_z$ has a greater influence upon the dose.

The analytic smoothing of the experimental distribution function of the thickness of the material in the equipment implies that the first initial and the second central moments of the anlaytic and experimental distributions coincide. It is therefore interesting to assess the influence of the errors made in the determination of the moments of the function upon the depth dependence of the specific absorbed proton dose. For the purpose of establishing this influence, we calculated the depth distribution of the dose in the equipment block in which the distribution function of the thickness was given by the Rayleigh function of Eq. (1). The average thickness value γ_z was varied by ±20% and the dispersion in the range ±50% with $\gamma_z = 0.2z$ being constant. The results of the calculations have shown (Fig. 5) that a 5% error of the γ_z value implies a dose error of 10-12% over the depth of a block. Similarly, a 50% error of the dispersion implies a dose error of 17-20%. Disregarding the secondary nucleons leads to an error in the calculation of the proton dose and we must therefore conclude that the error of the average thickness value of the material must be $\leqslant$5-10% and the dispersion of the distribution must be $\leqslant$20-30%.

Aluminum with the atomic number 13 was used in the preceding calculations as the material of the block. In order to determine the validity of using aluminum equivalents in calculations, we studied the influence of the isotope composition in the equipment block upon the depth dependence of the attenuation of the absorbed dose of primary protons. The following materials were considered: biological tissue (effective atomic number W_{eff} = 3.4); Al (W_{eff} = 13); Fe (W_{eff} = 26); and a block consisting of a mixture of C, F, Si, Al, Cu, and Fe (W_{eff} = 17.7). All calculations were made with the distribution function of Eq. (1) for the proton energies 100, 72, and 30 MeV. Practically the same depth distributions of the proton dose were obtained for all the versions with the exception of the biological tissue (see Fig. 6); a noticeable change in the case of biological tissue is observed because a large amount of hydrogen is present in the composition of the block. However, taking into account that a noticeable hydrogen concentration, as in tissue, must not be expected in the composition of equipment blocks mounted in spacecraft, we may conclude that the use of the aluminum equivalent in calculations of the absorbed proton dose must not lead to important errors.

LITERATURE CITED

1. J. Haffner, Nuclear Radiation and Shielding in Outer Space [Russian translation], Atomizdat, Moscow (1971).
2. V. V. Bodin et al., "Experimental results of the disribution of the material thicknesses in the equipment of spacecraft," in: Reports of the Second All-Union Scientific Conference on Shielding Installations of Nuclear Technology from Ionizing Radiation [in Russian], Moscow Inst. of Physics Research, Moscow (1978), pp. 103-104.
3. R. Alsmiller et al., Shielding of Manned Space Vehicles, Report ORNR-RSIC-35 (1972), p. 99.
4. A. V. Kolomenskii, V. G. Mitrikas, V. A. Sakovich, and V. M. Sakharov, "The effective attenuation coefficient of radiation in an inhomogeneous medium," At. Énerg., 44, No. 6, 517 (1978).

MEASUREMENT OF THE NEUTRON-INDUCED FISSION CROSS SECTION RATIOS OF ^{236}U AND ^{235}U FOR ENERGIES OF 4-11 MeV

A. A. Goverdovskii, A. K. Gordyushin,
B. D. Kuz'minov, A. I. Sergachev,
V. F. Mitrofanov, S. M. Solov'ev,
and T. E. Kuz'mina

UDC 539.173

The buildup of ^{236}U nuclei in a reactor core and subsequent radiative capture lead to the formation of ^{237}Np and ^{238}Pu, which are largely responsible for the activity of spent fuel, and to the breeding of ^{235}U nuclei in the (n, 2n) reaction. Therefore, a strict requirement of a 2% error is imposed on the most important characteristic of the isotopic balance – the fast-neutron fission cross section [1]. Since this requirement is not met by the presently available experimental values of σ_f^6, particularly for $E_n > 4$ MeV, they need to be extended.

The ^{236}U and ^{235}U fission cross section ratios were measured for neutral energies of 4.24-10.69 MeV by pulse synchronization [2] at the ÉGP-10M FÉI accelerator. The neutron source was the D (d, n) ^3He reaction in a gaseous deuterium target at a pressure of $(1\text{-}1.2)\cdot 10^5$ Pa. The energy range 4.24-5.6 MeV was spanned by varying the angle between the directions of motion of the deuterons and neutrons. For a total resolving time of 3-4 nsec (full width at half-maximum) the main and background events were separated by time of flight with a 0.7 m flight path. The fission fragment detector was a back-to-back ionization chamber filled with a mixture of argon and methane to a pressure of $1.4\cdot 10^5$ Pa. The chamber plates were 2 mm apart, and the field intensity was 2.5 kV/cm. The chamber housing was made of silver plated brass whose linear dimensions were calculated by Monte Carlo methods to minimize neutron scattering from structural materials. The targets containing the fissile isotopes were fastened to one another in the chamber by backings so that at a distance of 50-60 cm from it the difference of the neutron flux at the nearest and farthest targets did not exceed 0.2-0.3%. The targets were prepared by depositing uranium oxides from aqueous solutions on thin aluminum backings which were subsequently annealed. Their isotopic composition was determined by a mass-spectrometric method (Table 1), and the nonuniformity in thickness (10%) was measured with a miniature silicon semiconductor alpha detector by scanning along a radius of the active spot.

We found the ratio of the numbers of ^{236}U and ^{235}U nuclei in samples No. 1 and No. 2 respectively by normalizing the energy dependence of σ_f^6/σ_f^5 by the method of isotopic admixtures: pairs of targets 4/3, 5/3, and 6/3 were irradiated in turn in a flux of fast neutrons with energies of 7.34, 8.10, and 8.91 MeV, and by neutrons slowed down to 0.5-0.6 MeV by a layer of polyethylene 20 cm thick. The region of normalization was determined on the stable "plateau" as a function of σ_f^6/σ_f^5 above 7 MeV. Corrections were introduced into the results of the absolute measurements to take account of factors which distort them: the complete stopping of part of the fragments in the target (δ_1), the background of scattered neutrons (δ_2), the difference of the efficiencies of recording fragments by the chambers with ^{235}U and ^{236}U (δ_3), the nonuniformity of the neutron flux (δ_4), the uncorrelated neutron background in the laboratory and the instability of the electronic recording circuit (δ_5), the fission of impurity isotopes (δ_6). Only the energy dependent corrections δ_1, δ_2, δ_5, and δ_6 were introduced into the unnormalized values of the fission cross section ratios obtained with targets No. 1 and No. 2 for the same E_n. The ratios of the values of σ_f^6/σ_f^5 obtained for pure targets and targets with an isotopic mixture gave the following values of the normalization factor K_N: for energies of 7.34, 8.10, and 8.91 MeV respectively, 1.142 ± 0.008, 1.157 ± 0.008, and 1.138 ± 0.008.

The procedure for introducing corrections was discussed in detail in [3], and the use of the method of isotopic admixtures in [4]. Typical values of the corrections and the errors they introduce into the measured values are the following:

Translated from Atomnaya Énergiya, Vol. 59, No. 6, pp. 429-432, December, 1985. Original article submitted February 1, 1985.

 0038-531X/85/5906-1004$09.50

TABLE 1. Isotopic Composition of Targets Used

Content, %				Thickness of layer, mg/cm²
^{234}U	^{235}U	^{236}U	^{238}U	
0,0020±0,0005	99,992±0,001	0,0040±0,0005	0,0020±0,0005	0,41±0,04
0,0001	0,041±0,002	99,845±0,005	0,101±0,002	0,49±0,05
0,0020±0,0005	99,992±0,001	0,0040±0,0005	0,0020±0,0005	0,258±0,026
	3,002±0,009	96,87±0,10	0,13±0,02	0,198±0,020
	4,913±0,015	94,90±0,09	0,13±0,02	0,198±0,020
	6,943±0,003	92,929±0,003	0,127±0,002	0,198±0,020

TABLE 2

E_n, MeV	ΔE, keV	σ_f^6/σ_f^5	Δ stat., %	Δ tot., %
4,24	190	0,790	1,60	1,86
4,65	180	0,794	0,90	1,22
4,97	130	0,801	0,95	1,25
5,21	123	0,780	1,00	1,30
5,43	120	0,782	1,00	1,30
5,66	116	0,825	0,32	0,81
5,90	108	0,846	0,85	1,16
6,11	102	0,849	1,03	1,30
6,32	97	0,873	0,73	1,09
6,50	93	0,860	0,70	1,03
6,68	89	0,866	0,83	1,14
6,86	86	0,914	0,79	1,09
7,02	83	0,908	0,72	1,04
7,19	80	0,926	1,05	1,29
7,34	78	0,921	0,66	1,00
7,51	76	0,923	0,95	1,21
7,66	74	0,893	0,99	1,25
7,81	72	0,892	1,06	1,29
7,96	70	0,884	0,93	1,28
8,10	68	0,893	0,89	1,20
8,25	67	0,873	1,07	1,31
8,39	65	0,871	0,74	1,05
8,52	64	0,874	0,75	1,06
8,64	63	0,875	0,73	1,05
8,78	62	0,886	0,79	1,08
8,91	61	0,874	0,78	1,11
9,03	60	0,875	0,99	1,30
9,18	59	0,880	0,75	1,05
9,33	58	0,871	0,72	1,05
9,44	57	0,887	0,76	1,10
9,56	56	0,875	0,64	1,02
9,67	55	0,872	0,72	1,07
9,82	54	0,872	0,66	1,05
9,94	53	0,897	1,07	1,46
10,06	53	0,899	0,87	1,21
10,20	52	0,893	1,05	1,32
10,44	51	0,847	0,96	1,36
10,56	50	0,861	0,82	1,45
10,69	50	0,874	1,26	1,66

correction	value	error
δ_1	0.2—0.3	—
δ_2	0.25	—
δ_3	0.3—0.4	0.6—0.8
δ_4	1.0—1.7	0.2
δ_5	1.0	0.15
δ_6	0.15	—

The correction δ_1 is small in spite of the appreciable thickness of the targets (0.2-0.5 mg/cm²). This is related to the use of the method of isotopic admixtures for determining the absolute energy dependence of σ_f^6/σ_f^5. In other cases under these same conditions δ_1 can reach several percent.

The possible inhomogeneity of the isotopic mixture can lead to an uneven average depth of deposition of the ^{235}U and ^{236}U nuclei, which affects δ_1. The inhomogeneity was determined by a method similar to that used earlier in [5]. The result was negative (the mixtures were homogeneous).

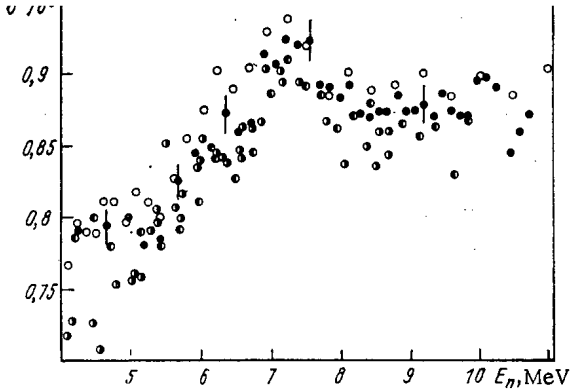

Fig. 1. Measured values of neutron-induced fission cross section ratios of ^{236}U and ^{235}U: •) our work; ○) [6]; ◐) [7]; ◑) [8].

In processing the results of the measurements particular attention was paid to the separation of the sources of systematic and random errors and their estimate. The statistical error was estimated from the spread of values of the ratios of the ^{236}U and ^{235}U fragment counting rates, taking account of corrections at various levels of discrimination in the corresponding recording channels. It amounted to 0.6-1.2%. The error of the fragment counting efficiency $\Delta\varepsilon$ was found by extrapolating the pulse-height spectrum to a zero level of discrimination. It reached 0.5-0.8% depending on the filling of the ionization chamber and the thickness of the sample. The error $\Delta\varepsilon$ is statistical, since it is determined by the statistics of the spectrum set in the transition part between fragments and alpha particles. At the same time the extrapolation is based on a model approach whose uncertainty is difficult to estimate, and hence a decrease of the error $\Delta\varepsilon$ does not follow from the observed constancy of the efficiency over the whole range of E_n. For this reason the ratio of the counting efficiencies and its error were determined separately for each point, and $\Delta\varepsilon$ entered the total error of the measurements quadratically. The situation is similar for the error $\Delta\varepsilon$ in measurements on moderated neutrons. The error of the normalization of the energy dependence of σ_f^6/σ_f^5 at reference points was 0.51%, and was determined from the spread of the normalization factor.

The error of the separation of spurious events related to all the components of the neutron background, including the part of them determined in measurements with an evacuated target, was 0.1-0.6%, and was random (the statistics of the set of corresponding parts of time-of-flight spectrum). The remaining errors – corrections, dead time of the recording channel, the instability of the timing etc. – are negligible (Table 2). It is clear from Fig. 1 that the spread of the experimental points reaches 6-8%, which is considerably larger than the listed errors of the mesurements. The character of the spread of the data was investigated in their statistical analysis, and consisted of two parts:

the determination of the correlations of the energy dependences in the range 4-9 MeV (the range spanned). A calculation of the corresponding correlation matrix showed a linear functional dependence of the experimental data, i.e. the collection of points of various experimenters can be displaced along both the energy axis and the axis of ordinates;

an estimate of the relative displacement of the sets of data along the σ_f^6/σ_f^5 and E_n axes.

For the first case averaging σ_f^6/σ_f^5 over the energy range 5.5-8.5 MeV gave the following values: 1, our work; 1.021, Behrens and Carlson [6]; 0.978, Meadows [7]; 0.974, Konde [8] (normalized to our data). The displacement on the energy scale was determined by analogy with [9]. To do this the cross section ratio was converted to the fission cross section by using the standard data on σ_f^5 [10], and the data of each author were described by a smooth curve in the region of rise to the second plateau

$$\sigma_f^6 = \sigma_f^1 + \sigma_{n,\,n'} \int_0^{E_n} \rho(\varepsilon)\, P(E_n - \varepsilon)\, d\varepsilon, \qquad (1)$$

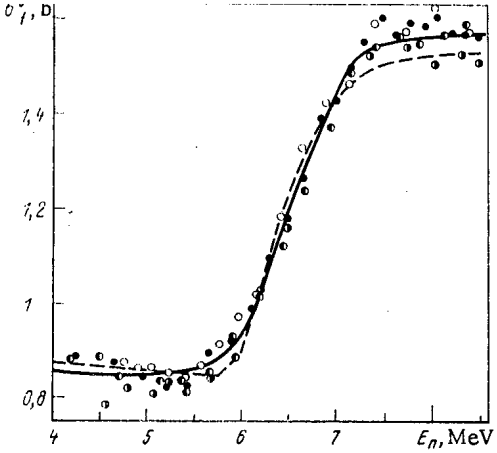

Fig. 2. Results of describing experimental data by a smooth curve.

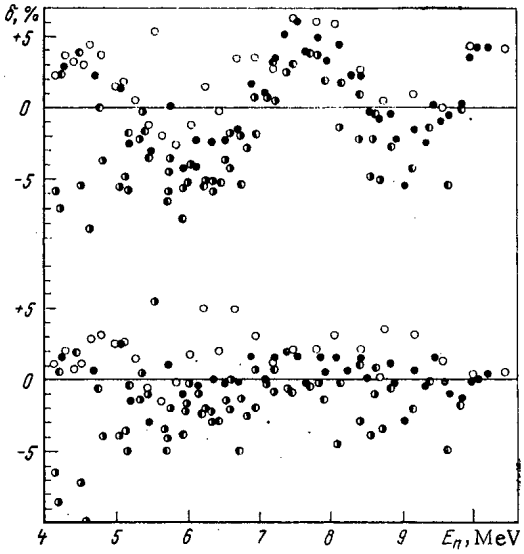

Fig. 3. Deviations of experimental data from ENDF/B V and from our estimate.

where σ_f^1 is the value of the cross section on the first plateau, $\sigma_{n,n'}$ is the cross section for the inelastic scattering of neutrons, $\rho(\varepsilon)$ is the neutron emission spectrum, and P $(E_n - \varepsilon)$ is the probability of fission of a nucleus after the emission of a neutron of energy ε. The parameter T_f, the height of the fission barrier entering P $(E_n - \varepsilon)$, characterizes the energy spread, and is $\sim$0.1 MeV. It was observed that by varying the parameters a curve of the form of Eq. (1) could describe the whole set of data, which serves as a basis for estimating the cross section for the fission of ^{236}U by neutrons of energy >5 MeV. Four sets of the paremters T (the nuclear temperature) and T_f were averaged with weights inversely proportional to the square of the rms deviations of the experimental values from the corresponding curves. The solid curve of Fig. 2 shows our estimated curve with parameters T and T_f varying over a wide interval, and the dashed curve with parameters closest to the most realistic values [11].

The lower part of Fig. 3 shows the deviations of σ_f^6/σ_f^5 from our estimate, and the upper part the deviations from ENDF/B V. The error of the estimate values is naturally determined by starting from the spread of the parameters of the approximation, which leads to 2-3%.

Our analysis shows that the energy dependence of σ_f^6/σ_f^5 is known reliably at the present time. The absolute values calculated from the cross section ratios have a 5-8% spread, which obviously is determined by the systematic errors of the various studies and

the realization of the procedure of isotopic weighting within the framework of the method of isotopic admixtures. On the whole it can be concluded that the existing set of data ensures an error of the estimate of σ_f^6 for $E_n > 4$ MeV at the 5% level (taking acocunt of the error of the standard σ_f^5).

The authors thank N. V. Kornilov for valuable discussions of the measurement procedure.

LITERATURE CITED

1. WRENDA 83/84. World request list for nuclear data. Nuclear data section. Vienna: IAEA (1983).
2. A. A. Goverdovskii, A. K. Gordyushin, B. D. Kuz'minov, et al., "Measurement of the fission cross sections of heavy nuclei by the method of pulse synchronization," in: Neutron Physics, Part 4 [in Russian], TsNIIatominform, Moscow (1984), p. 115.
3. A. A. Goverdovsky, A. K. Gordjushin, B. D. Kuzminov, et al., "The ^{236}U and ^{238}U to ^{235}U fission cross section ratios in the neutron energy range 5-11 MeV," in: Proc. Int. Spec. Meeting on Transactinium Isotopes Nuclear Data, Uppsala (1984).
4. A. A. Goverdovskii, A. K. Gordyushin, B. D. Kuz'minov, et al., "Measurement of the fission cross section ratios of ^{236}U and ^{235}U by the method of isotopic admixtures," Problems of Atomic Science and Engineering, Ser. Nuclear Constnats 3 (57) [in Russian], (1984), pp. 13-15.
5. A. A. Goverdovskii, A. K. Gordyushin, B. D. Kuz'minov, et al., "Measurement of the ratio of the neutron-induced fission cross sections of ^{237}Np and ^{235}U in the energy range 4-11 MeV," At. Énerg., 58, 137-139 (1985).
6. J. Behrens and G. Carlson, "Measurements of the neutron-induced cross sections of ^{234}U, ^{236}U, and ^{238}U to ^{235}U from 0.1 to 30 MeV," Nucl. Sci. Eng., 63, 250-267 (1977).
7. J. Meadows, "Neutron-induced fission cross section ratios of ^{234}U, ^{236}U and ^{235}U," Nucl. Sci. Eng., 65, 171 (1978).
8. C. Nordborg et al., "Fission cross section ratios of ^{232}Th, ^{236}U, and ^{235}U," in: Proc. Int. Conf. on Nuclear Data, Vol. 1, Harwell (1979), p. 910.
9. H. Knitter and C. Budtz-Jørgensen, "Barrier heights of plutonium isotopes from (n, n'f)," in: Proc. Int. Conf. on Nuclear Data for Science and Technology, Vol. 1, Antwerpen, Sept. 6-10 (1982), pp. 744-747.
10. ENDF/B V Third Ed. BNL (1979), ^{235}U (MAT 1395).
11. S. Bjørnholm and J. Lynn, "The double-humped fission barrier," Rev. Mod. Phys., 52, 725 (1980).

FIELDS OF IONIZING RADIATIONS ON THE TOKAMAK-10 FUSION UNIT

V. S. Zaveryaev, G. I. Britvich,
V. I. Lebedev, V. S. Lukanin,
F. Spurny, I. Potochkova,
and I. Kharvat

UDC 621.039.68

Tokamaks at the present time occupy a leading position in research on controlled thermonuclear fusion with magnetic confinement. The characteristics of the fields of ionizing radiations are of great interest in the use of such units since the design to be adopted and the composition of the equipment required for monitoring the irradiation of the personnel depend upon the fields. Besides that, research on the ionizing radiations can provide useful information for plasma diagnostics.

Our work relates to research on the T-10 unit as a source of radiation and provides an evaluation of the efficiency of the radiation shielding. The experimental results were obtained during several operational cycles of the T-10 by the co-workers of the Institute of High-Energy Physics (1977) and the Institute of Radiation Dosimetry of the Academy of Sciences of the Czechoslovakian SSR (1981-1983) together with the co-workers of the I. V. Kurchatov Institute of Atomic Energy.

Translated from Atomnaya Énergiya, Vol. 59, No. 6, pp. 432-436, December, 1985. Original article submitted February 1, 1985.

 0038-531X/85/5906-1008$09.50

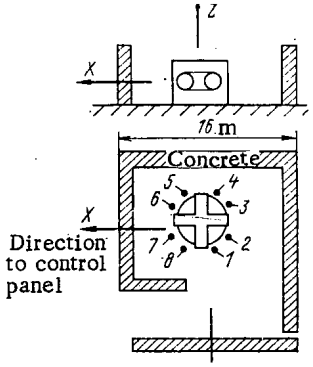

Fig. 1. Overall view of the T-10 unit: 1-8) points; X, Y, and Z) directions in which the detectors were moved.

Short Description of the T-10 Unit and of the Conditions Studied. The T-10 unit is a cruciform transformer the secondary "winding" of which consists of deuterium filling a toroidal vacuum chamber [1, 2]. The large radius of the torus is 150 cm, its small radius 39 cm. The inner chamber is inserted into an external stainless-steel chamber with a radius of 50 cm. A 5-cm-thick toroidal copper shield is placed between the chambers. The outer chamber is surrounded by the sturdy coils of the longitudinal magnetic field (Fig. 1). In order to reduce the interaction of the plasma with the walls, tungsten diaphragms (1977 and 1981) and graphite diaphragms (1982-1983) were employed. The unit is surrounded by a shadow-type radiation shield of heavy concrete (density 3.6 g/cm^3) with a thickness of 1 m and a height of 5 m.

A discharge pulse has a length of 1 sec; the plasma current is 200-400 kA. At a sufficiently high temperature (0.6-0.8 keV) and density ($(5\text{-}8)\cdot10^{13}$ cm^{-3}) of the ions in the plasma, the thermonuclear d + d reaction takes place and emission of neutrons with an intensity of 10^{10} sec^{-1} is observed during $\sim$0.6 sec. The total neutron yield amounted to $(1\text{-}8)\cdot10^9$. Such discharges are termed thermonuclear discharges.

In certain cases part of the plasma electrons were transferred into the continuous acceleration mode and reached an energy of several dozen megaelectron-volts. Being incident on a diaphragm, these electrons generated bremsstrahlung and photoneutron emission on a high intensity level. The neutron yield reached $(1\text{-}10)\cdot10^{12}$. Such discharges are termed acceleration-type discharges [3]. In 1977 a series of similar discharges was especially studied.

In the 1981-1983 experiments, usually the radiation characteristics averaged over several series of discharges were determined: in the 1981 experiments, acceleration-type discharges often appeared; in the 1982 experiments, acceleration-type discharges were observed only in the second half of the series of measurements; in 1983, the edge of the plasma touched on secondary steel objects in the second half of the series of measurements and therefore a considerable number of unstable and acceleration-type discharges developed.

We describe in the present work the dosimetric characteristics of individual discharges or average values for a series of T-10 discharge pulses. The unit makes it possible to obtain 30-40 discharges in a shift.

Measurement Methods. The bremsstrahlung was recorded with a Geiger–Müller counter having an extremely low relative neutron sensitivity for work in composite neutron-x-ray fields [4, 5]; various ionization chambers and thermoluminescence detectors (TLD) in the form of 0.85-mm-thick LiF and ^{7}LiF tablets with a diameter of 4.5 mm were used for the same purpose.

The neutron radiation was measured with: thermal-neutron detectors (In foil, BF_3 counters) surrounded by a moderator for recording neutrons with an energy <20 MeV; polystyrene scintillators with a diameter of 50 mm and a height of 50 mm in which neutrons and gamma quanta (reaction threshold 20 MeV) generate the β^+ emitting ^{11}C isotope (half-

life 20.478 min); after irradiation during one discharge, the detectors were placed into a radiometer unit for measuring the number of decay events; and dielectric polyester track detectors with emitters of the fission fragments of ^{232}Th, ^{235}U, and ^{209}Bi. The detectors were calibrated with standard AmBe and ^{252}Cf neutron sources in the Institute of Radiation Dosimetry of the Academy of Sciences of the Czechoslovakian SSR.

Spherical moderators with a diameter of 5.08, 7.62, 12.7, 20.32, and 30.48 cm were used for the spectrometry of the neutrons; ester track detectors in contact with ^{235}U or a proportional ^{3}He counter were disposed at the centers of the spheres. The spectrometer with the two detectors was calibrated with neutron sources; the capabilities of the spectrometer were tested in fields and beams of polyenergetic and monoenergetic neutrons [7, 8]. The characteristics obtained for the spectra from the data of the spectrometer with spherical moderators depend also upon the computation program. We used in our work the SPEC program (for calculating spectra in the form of linear combinations of given model spectra [9]) and the SAND program (for calculating a spectrum by correcting the *a priori* information in successive iterations [10]). The composite radiation was measured with nuclear emulsions and x-ray film. The dose rate of the gamma radiation emitted from the construction materials of the unit in the time interval between discharges was measured with a portable DRGZ-04 radiometer.

In order to verify the reproducibility of the results of the measurements from pulse to pulse, two types of detectors were used as monitors: a polyethylene sphere with In foil to be activated (1977) and a ^{3}He counter surrounded by a cylindrical paraffin moderator (1981-1983). In the latter case the readings of the monitor could be wrong owing to the overload of the counter by the high radiation intensity.

The x-ray emission from the discharge was monitored through the readings of a scintillation counter with an NaI(Tl) crystal.

General Characteristics of the Ionizing Radiation in the T-10 Unit. Charged particles which are present in a plasma or generated in it can leave the inner chamber of the Tokamak. Therefore, the T-10 unit is a source of only neutron radiation and bremsstrahlung and the low-energy component of the latter is absorbed by a thick copper shield. Measurements have shown that the level, the composition, and the spatial distribution of the radiation fields depend upon the material and the position of the diaphragm, the pressure of the operating gas, the energy concentrated in the discharge and its stability, interruptions of the current, impurities in the plasma, etc. Averaged dosimetric values are stated in the present work.

In thermonuclear discharges the neutrons are generated in the d + d reaction and have a medium energy of 2.5 MeV. The generation of the bremsstrahlung is not associated with the thermonuclear reaction in the plasma but depends upon the number and the energy of the electrons leaving the diaphragm. Therefore the flux of the neutrons is correlated with the flux of the gamma quanta. The greatest exposure dose near the T-10 chamber amounted to $2.3 \cdot 10^{-3}$ mGr and the equivalent neutron dose did not exceed $2 \cdot 10^{-3}$ mSv. Outside the unit (behind the radiation shield) the irradiation dose was on the level of the natural radiation background.

In the acceleration-type discharges, the bremsstrahlung causes a photoneutron flux by the (γ, n)-reaction. In such discharges, the radiation level on the external surface of the T-10 increased by 3-4 orders of magnitude and reached 0.3 Gr in individual pulses (gamma radiation) or 0.03 Sv (fast neutrons). In the case of acceleration-type discharges, the radiation dose, the energy of the radiations, and their composition were unstable and even when the monitoring was brought into account, the differences of the dosimetric details amounted to 200% from one discharge to another.

Neutrons and gamma quanta with an energy in excess of 20 MeV were generated in almost all discharges with an abnormally high radiation level. The maximum radiation energy did not exceed 60-70 MeV since the number of tracks in the dielectric track detectors (DTD) with a ^{209}Bi emitter was zero. This result is consistent with the estimate of the limit energy (35 MeV) of the electrons retained in the T-10 unit [11].

A comparison of the signals of the TLD detectors working with LiF with those of ^{7}LiF has shown that only an insignificant contribution to the dose results from the thermal neutrons to which LiF is 100 times more sensitive than ^{7}LiF. This observation is further confirmed by the data obtained with a dielectric track detector in contact with ^{235}U (with and without a cadmium shield).

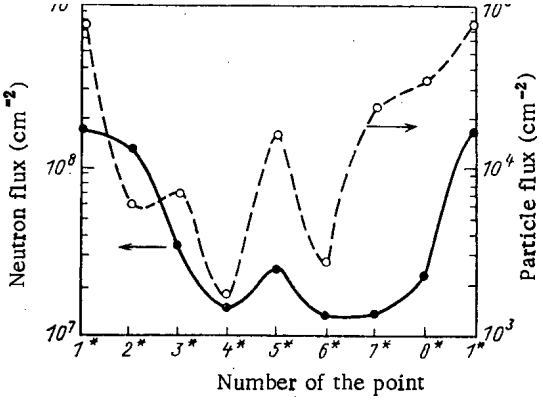

Fig. 2. Distribution of the neutron flux (E_n < 20 MeV) and of the particle flux (E > 20 MeV) along the T-10 chamber in acceleration-type discharges with a tungsten diaphragm. Points 1*-8* are situated on the plane of the vacuum chamber between the coils of the longitudinal field and are opposite to points 1-8 (see Fig. 1).

The photonuclear reactions which take place at the diaphragm under the influence of a beam of accelerated electrons produce unstable isotopes with various half-lives. Radioactivity measurements made immediately after an acceleration-type discharge have shown that the radioactivity is concentrated in the region of the diaphragm and that the dose rate of the radiation on the outer surface of the T-10 chamber proper reaches 20 μR/sec 3 min after a pulse (1 R = $2.58 \cdot 10^{-4}$ C/kg). When the decay of the activity is brought into account, the personnel near the chamber can receive the maximum admissible daily dose during 20-40 min.

Spatial Distribution of the Radiations Near the T-10 Chamber. A Geiger–Müller counter with energy compensation by lead and tin filters was used to study the spatial distribution of the bremsstrahlung in thermonuclear discharges [4]. The isotropy of the neutron radiation was determined with a ^{3}He counter in a sphere with a diameter of 12.7 cm. The detectors were mounted facing the gaps between the coils of the longitudinal field at a height of 0.4 m from the plane of the T-10 vacuum chamber at points 1-8 (see Fig. 1). Measurements have shown that the gamma radiation field is rather homogeneous (average dose $1.6 \cdot 10^{-2}$ mGy per discharge) though a noticeable signal increase is observed in the region of the diaphragm.

A comparison of the signals of the Geiger–Müller counter with and without filters has shown that the contribution of photons with an energy below 200 keV to the dose does not lead to a measurement error in excess of ±20%. This is a logical value when the radiation is shielded with the construction materials of the unit.

There were only a few thermonuclear discharges in the time of these measurements and our data suffice only to demonstrate qualitatively that the neutron emission in such discharges is homogeneous.

Investigations of the acceleration-type discharges provide more information on the radiation fields near the unit. By contrast to the thermonuclear discharges, a strong inhomogeneity of the neutron emission is observed in this case along the T-10 chamber (see Fig. 2) and sharp peaks appear in the region of the diaphragm (points 1* and 5*). The fluctuations are less pronounced for neutrons with E_n > 20 MeV. This means that the diaphragms are of great importance for the development of the radiation.

When the tungsten diaphragm was replaced by a graphite diaphragm, the level of the gamma radiation was reduced and the flux of the fast neutrons (E_n > 1 MeV) decreased by a factor of 100 (see Table 1). The rather large raidation dose observed in 1983 can be explained by a steel rod which was at the edge of the plasma string and acted as a diaphragm. Nevertheless, the radiation level was still much lower than in the 1981 experiments in which the tungsten diaphragm was employed.

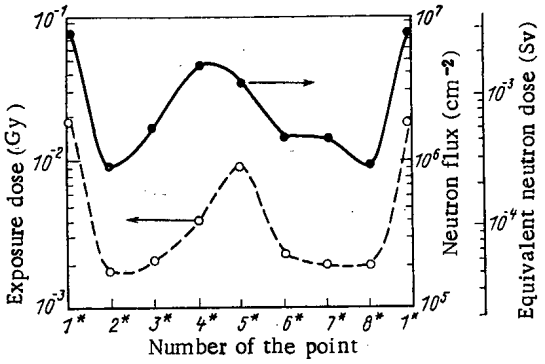

Fig. 3

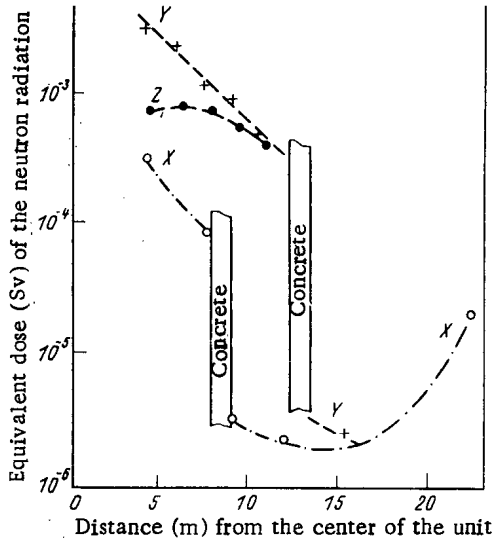

Fig. 4

Fig. 3. Distributions of the neutron flux (E_n > 1 MeV), of the equivalent dose (dielectric track detector in contact with ^{232}Th), and of the exposure dose of the gamma radiation (TLD detectors) along the T-10 chamber; averaging over 402 discharge pulses (1983).

Fig. 4. Equivalent dose at a considerable distance from the T-10 unit in acceleration-type discharges with a tungsten diaphragm: +, ○, ●) measurements; X, Y, Z) according to Fig. 1.

TABLE 1. Radiation Levels at Point 7* (see Fig. 2). Acceleration-Type and Unstable Discharges

Parameter	Detector	1981	1982	1983
Exposure dose (mGr per discharge)	TLD	4,5	$4{,}6\cdot10^{-2}$	2,0
Track density (cm^{-2} per discharge)	DTD with ^{232}Th	2,6	$1{,}6\cdot10^{-2}$	1,0
As above	DTD with ^{235}U	27	1,4	3,4

The change in the radiation from point 1* to point 5* (see Fig. 3) is less than indicated in Fig. 2. This is logical when an additional steel diaphragm is present at point 5*. Furthermore, there exists a direct correlation between the neutron flux and the exposure dose. The equivalent dose on the surface of the T-10 chamber is smaller than the exposure dose by a factor of 5-10.

The flux of neutrons with an energy <1 MeV is smaller than the flux of the fast neutrons by a factor of 100. Taking into account the data shown in Fig. 2, we can conclude that neutrons with an energy of 1-20 MeV render the greatest contribution to the dose.

Fields of the Ionizing Radiations Far from the T-10 Unit. The radiation conditions far from the T-10 unit (behind the radiation shield, at the work stations) were determined only in acceleration-type discharges. The neutron radiation is exponentially attenuated in the radial directions (Fig. 4). It follows from an analysis of the radial distribution of the radiation from the vacuum chamber to the radiation shield and behind the same in the direction of the hall with the control panel (X direction) that the attenuation coefficient of the T-10 shield is 20 instead of the expected value of 1000 for the direct beam. This means that scattered radiation dominates behind the shield which is without an upper cover. The same conclusion is obtained from the rather slow decrease of the equivalent dose in the vertical Z direction.

The average level of the scattered radiation behind the shield was $\sim 2\cdot10^{-5}$ Sv. The radiation level at the work stations did not exceed $6\cdot10^{-7}$ Sv per discharge.

Measurements have shown that sharp fluctuations occur in the composition of the neutron and gamma radiation. Inside the radiation shield, the dose ratio of gamma radiation to

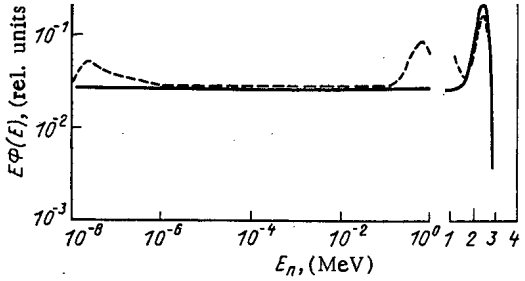

Fig. 5. Neutron spectrum in thermonuclear discharges: the spectrum was obtained with spherical moderators: ——) calculation with the SPEC program for the combination 1/E + G2.5; ----) calculation with the SAND program and the combination MAXW + 1/E + DTCU + G2.5.

neutron radiation dose is 10; behind the concrete shield in the hall proper and within the area in which the unit is directly visible, the ratio is 1-0.5; in the area of the controls and in the inner locations, the ratio is 0.5-0.1. Thus, a continuous dosimetric monitoring at the working stations is possible only through the dose equivalent of the neutron radiation.

Simultaneous measurements of the absorbed dose and the equivalent dose made it possible to estimate the quality of the neutron radiation in acceleration-type discharges; the quality index decreases with increasing distance from the unit (from 4.2 to 1.0) because the average neutron energy decreases by scattering.

Measurement of the Energy Spectrum of the Neutrons. The energy spectra of the neutrons were measured with the spherical moderators in thermonuclear discharges at some points near the T-10 unit. The spheres were changed from pulse to pulse and the detector signals were normalized with the aid of a monitor to eliminate the influence of the nonidentical form of the discharges. The ^{3}He detector signal was recorded for 0.8 sec 0.1 sec after the beginning of the current flow in the plasma. In order to eliminate nonthermonuclear discharges, the time dependencies of the "hard" x-ray radiation and the neutron radiation were monitored.

The signals of the ^{3}He detector were processed in two steps. At first the SPEC program was used to determine the spectra as linear combinations of modelling spectra: a Maxwellian spectrum (MAXW) with an average energy $\bar{E}$ = 0.025 eV; a Fermi spectrum (1/E spectrum); a spectrum of the neutrons scattered at copper (DTCU); and a Gaussian spectrum (G2.5 spectrum) with $\bar{E}$ = 2.5 MeV. Then the spectrum obtained with the SPEC program was used as *a priori* information for the SAND iteration program. When various combinations of modeling spectra (necessarily a Gaussian spectrum) were used, the overall characteristics of the neutron field differed only slightly (see Fig. 5).

The total neutron yield [12] can be determined from absolute spectra and compared with the calibration of the ^{3}He monitor with the aid of a PuBe neutron source. The neutron yield is $(5.4 \pm 1.2)\cdot 10^5$ per pulse of the monitor (averaged over 7 points of measurements (instead of the calibration constant of $7.9\cdot 10^5$ neutrons per pulse. Taking into account all the assumptions made in both the calibration and the calculations (absorption and scattering of neutrons, differences of the spectra of thermonuclear neutrons and of the PuBe source, etc. were disregarded), one must acknowledge that the results are satisfactorily close. In absolute measurements using the dielectric track detectors, the constant $9.7\cdot 10^5$ neutrons per monitor pulse was obtained in thermonuclear reactions; this figure is also in satisfactory agreement with the ^{3}He monitor calibration made with the aid of a neutron source.

The fraction of fast neutrons was 20-30% in the majority of cases. This is inconsistent with the results obtained in the data processing of the dielectric track detectors which had been irradiated on the outer side of the T-10 chamber. The conclusion is that the fraction of fast neutrons is ∿90%. There exist probably two reasons for this discrepancy. Firstly, the measurements with the spherical moderators were made at a certain distance from the unit, i.e., at points at which the fraction of the scattered neutrons is

logically higher than directly on the outer surface of the chamber. Secondly, there exists a methodological reason because a 1/E-Fermi spectrum was assumed when the results of the measurements with the spheres were evaluated.

It was shown that the second stage of data processing with the aid of the SAND program reduces the mean relative deviation of the measured and calculated spectra. This means that the "two-step" calculation of the spectra should be employed. The average deviations did not exceed the error of the signal mesurements, i.e., the suggested combinations of modeling spectra are consistent with the true spectra.

Conclusions. Coinciding or close results were obtained when the various methods were used in investigations of the radiation fields.

The level of the radiation dose in thermonuclear discharges poses no risk for the personnel. In acceleration-type discharges, the dose increases by 3-4 orders of magnitude in the case of neutrons, as well as in the case of gamma quanta, and the dose in individual pulses may reach 0.3 Gy (30 rad) on the outer surface of the chamber proper.

In acceleration-type discharges, the spatial distribution of the dose is characterized by sharp peaks around the diaphragms. When a diaphragm made from a material with a small Z (graphite) is employed, the dose is reduced by a factor of 100 in comparison with the case of the tungsten diaphragm. After an acceleration-type discharge, the chamber of the unit poses a risk owing to the induced activity.

The composition of the ionizing radiation changes with increasing distance from the chamber: hard bremsstrahlung is most dangerous near the chamber, whereas the neutron radiation dominates at greater distances. The dependence of the neutron radiation decreases upon the distance is exponential.

Scattered neutrons generate most of the dose outside the limits of the unit. The radiation shield attenuates the radiation by a factor of 20 instead of 1000 because an upper cover is missing.

In acceleration-type discharges, the maximum radiation energy is 20-60 MeV. This is consistent with the condition of retaining fast electrons in the T-10 unit. In thermonuclear discharges, the fraction of the fast neutrons in the total flux near the unit amounts to at least a few dozen per cent.

In calibrating the neutron detectors mounted outside the unit, dielectric track detectors with an emitter undergoing fission and detectors in spherical moderators can be employed.

The authors thank the team of the T-10 unit for their great help in preparing and performing the mesurements.

LITERATURE CITED

1. A. B. Berlizov, N. L. Vasin, E. P. Gorbunov, et al., "First Measurements of the Plasma Parameters in the Tokamak-10 Unit," Pis'ma Zh. Eksp. Teor. Fiz., 23, 502 (1976).
2. A. B. Berlizov, G. A. Bobrovskii, A. A. Bagdasarov, et al., "Results of the first experiments in the Tokamak-10 unit," At. Énerg., 43, No. 2, 90 (1977).
3. V. S. Zaveryaev and S. Yu. Luk'yanov, "Neutron radiation in large Tokamaks," Zh. Eksp. Teor. Fiz., 73, 178 (1977).
4. E. Wagner and G. Hurst, Health Phys., 5, 20 (1961).
5. Neutron Dosimetry in Biology and Medicine, ICRU Report, No. 26, ICRU, Washington (1976).
6. F. Spurný and A. Křivăková, Jad. Energ., 26, 2 (1980).
7. M. Tichý and A. Křivaňová, Jad. Energ., 26, 135 (1980).
8. B. Dořschel and F. Spurný, Kérnenergie, 24, 63 (1981).
9. M. Tichý, M. Králik, A. Křivăková, and F. Spurný, Výzkumna zpráva ŭDZ ČSAV 37/78 [in Czechoslovakian], Prague (1978).
10. W. McElroy et al., Report AFWL-TR 67-41 (1969).
11. K. Wong, Nucl. Fusion, 22, 1528-1531 (1982).
12. N. G. Gusev, E. E. Kovalev, D. P. Osanov, and V. I. Popov, Shielding from the Radiation of Extended Sources [in Russian], Gosatomizdat, Moscow (1961).

DISTRIBUTION OF LEAD IN ROCKS BY THE METHOD OF FISSION-FRAGMENT RADIOGRAPHY

V. P. Perelygin, G. Ya. Starodub, and S. G. Stetsenko

UDC 539.172.17/8

The investigation of the spatial distribution of concentrations of ore elements in minerals and rocks has in recent years become important both theoretically and practically in connection with the determination of possible sources of matter in ore-formation and evaluation of the industrial exploitation of separate geological blocks [1]. In particular, the solution of the problem of the local redistribution of trace contaminants of radioactive elements with the use of the method of fission-fragment radiography enabled forecasting the ore content of sedimentary strata, system of volcanic (magma) channels, cavities, craters, etc., and zones of secondary metasomatic transformations [2]. The use of the method of radiography for elements which do not have natural radioactive isotopes is made possible by the creation of artificial radioactivity of these elements by means of irradiation [3]. To study the spatial distribution of lead we irradiated the samples with α particles and $^{3}_{2}$He [4, 5], which led to the formation of $^{210}_{84}$Po in the reactions

$$^{208}_{82}\mathrm{Pb}(^{4}_{2}\mathrm{He},\ 2n)^{210}_{84}\mathrm{Po} \xrightarrow{\alpha}; \quad (1)$$

$$^{208}_{82}\mathrm{Pb}(^{3}_{2}\mathrm{He},\ n)^{210}_{84}\mathrm{Po} \xrightarrow{\alpha}, \quad (2)$$

whose cross sections >1 b (1b = 10^{-28} m^2) at an energy of $^{3}_{2}$He, $^{4}_{2}$He ∿ 30 MeV. This reaction cross section enables achieving a sensitivity in the determination of the lead content of $\geqslant 10^{-4}$%, but because of the long half-life of $^{210}_{84}$Po (138 days) this requires either intense irradiation over many days or the emitted α particles must be recorded for several months.

In [6, 7] the reaction of the formation of α-active isotopes in the following reactions with heavy ions was investigated:

$$^{208}_{82}\mathrm{Pb}(^{12}_{6}\mathrm{C},\ 4n)^{216}_{88}\mathrm{Ra} \xrightarrow{\alpha} {}^{212}_{86}\mathrm{Rn} \xrightarrow{\alpha} {}^{210}_{84}\mathrm{Po} \xrightarrow{\alpha}; \quad (3)$$

$$^{208}_{82}\mathrm{Pb}(^{12}_{6}\mathrm{C},\ 6n)^{214}_{88}\mathrm{Ra} \xrightarrow{\alpha} {}^{210}_{86}\mathrm{Rn} \xrightarrow{\alpha} {}^{206}_{84}\mathrm{Po} \xrightarrow{\alpha}. \quad (4)$$

The α particle detector consisted of cellulose nitrate, applied to the sample after irradiation. The energy of α particles from $^{210}_{84}$Po is ∿5.3 MeV (1), (2), ∿6.2 MeV (3) from $^{212}_{86}$Rn, and ∿6 MeV (4) from $^{210}_{86}$Rn. This is higher than the detection threshold of cellulose nitrate (∿3 MeV) [3], so that an absorber must be placed between the sample and the detector in order to reduce the energy of the α particles, which degrades the resolution of the method. The attainable sensitivity level is equal to $\geqslant 10^{-4}$%, and the attainable resolution is ≥20 μm. These are inadequate for the solution of a number of geological problems. The sensitivity for the determination of the content and the accuracy of the spatial distribuiton of lead can be increased by using for the analysis the fission reaction of lead induced by accelerated heavy ions. The fission cross section is much higher than the formation cross section of α-active nuclides and for optimally chosen energy and mass of heavy ions exceeds 2 b [8].

The mass distribution of the fragments from fissioning of lead by oxygen ions, evidently, has a maximum near A = 110 and Z = 45. In addition, α-active products are formed in the reaction

$$^{208}_{82}\mathrm{Pb}(^{16}_{8}\mathrm{O},\ 2n) \xrightarrow{\alpha} {}^{222}_{90}\mathrm{Th} \xrightarrow{\alpha} {}^{218}_{88}\mathrm{Ra} \xrightarrow{\alpha} {}^{214}_{86}\mathrm{Rn} \xrightarrow{\alpha} {}^{210}_{84}\mathrm{Po} \xrightarrow{\alpha}. \quad (5)$$

The difficulty of using the fission effect lies in the fact that the fission fragments must be detected simultaneously with the irradiation of the sample because of the short lifetime of the compound nuclei formed. This difficulty can be overcome by using the follow-

Translated from Atomnaya Énergiya, Vol. 59, No. 6, pp. 437-439, December, 1985. Original article submitted July 30, 1984; revision submitted December 17, 1984.

0038-531X/85/5906-1015$09.50

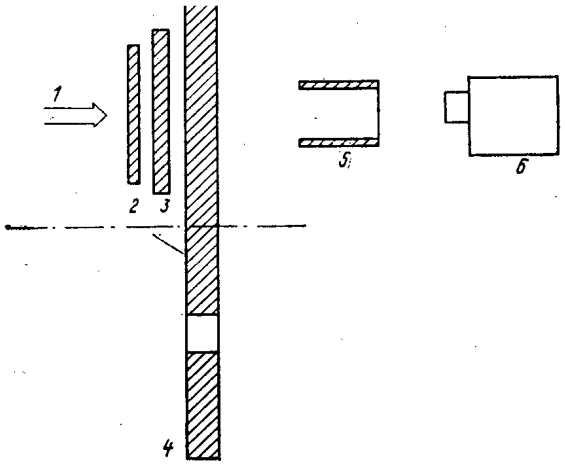

Fig. 1. Scheme used for irradiating the sample: 1) ion beam, 2) track detector; 3) sample; 4) rotating metallic disk; 5) Faraday cylinder with tantalum foil; 6) television camera.

ing irradiation scheme (Fig. 1): a thin (~10 μm) dielectric detector with a detection threshold chosen so that the ions of the primary beam are not detected is applied flush against the sample. The detector can consist of either natural or artificial mica, which has the required radiation resistance and a high detection threshold, and it is easy to obtain from it thin layers with the required area. To eliminate the characteristic background formed by the fission-fragment tracks, the mica layers are annealed prior to irradiation [3].

The object of investigation consisted of bituminous dolomites, in which the redistribution of the carbonate material is accompanied by mobilization of the ore impurity and growth of gallenite crystals. We did not observe in the chemical study of the samples in association with the lead, gold, mercury, bismuth, and thorium platinoids, whose fission fragments for the irradiation conditions used could distort the picture of the lead distribution. The content of uranium in these rocks is $\leqslant 10^{-60}$%. Thus the contribution of uranium fission fragments to the radiographic picture is more than two times smaller than the contribution of lead.

Oxygen ions with an energy of 9.3-MeV per nucleon were chosen for the irradiation. The mica was 10-15 μm thick, which decreased insignificantly (<0.7 MeV per nucleon) the energy of the ions. We fastened the samples with the detectors onto a heat-removing rotating metallic disk (see Fig. 1). The disk at a location free of the samples had an opening, through which the ions emerged into a Faraday cylinder those back wall consisted of tantalum foil. The thickness of the foil exceeded the mean-free path length of the ions. This cylinder enabled monitoring the ion current, and the geometry of the ion beam could be monitored according to the emission of the tantalum foil, observed with the help of a television camera. After irradiation we disassembled the disk with the samples, removed the mica detector for analysis, and placed a detector on the activated sample in order to record the α particles for purposes of obtaining an α radiographs.

We irradiated the samples with the mica detectors in two modes: with a narrow (3 mm) beam of heavy ions with an ion current of 5 μA on the target and an integrated particle flux of 10^{15} cm^{-2}, interacting with a 0.6-cm^2 preparation, and a wide (25 mm) beam with an integrated flux of $9\cdot10^{13}$-$1\cdot10^{14}$ cm^{-2} (the area of the preparation was equal to 3.1 cm^2). The first mode ensured high sensitivity on a narrow strip of the section, and the second ensured that a large surface area of the preparation would be covered, but with a lowered sensitivity. Then, in the first mode, we subjected the α particle detector (CR-39 plastic) to α radiographic exposure for six days, etching in a 40% solution of NaOH for 1 h 40 min at 60°C; in the second mode the α particle detector consisted of the usual cellulose nitrate (exposure for 1 day, etching in the same solution for 50 min at 50°C). Since in the mica, in addition to fission fragments, tracks from recoil nuclei and compound nuclei formed in the interaction of $^{18}_{6}O$ ions with different nuclei in the sample and the mica, were recorded, we annealed the muscovite detector in both modes after irradiation in order to eliminate

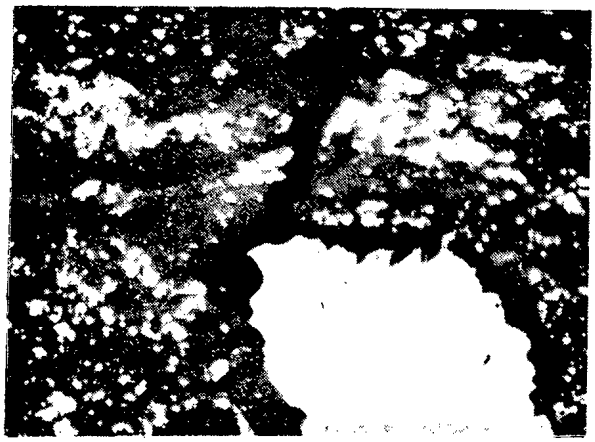

Fig. 2. Section in reflected light: the large white spot is gallenite; the dispersed strongly reflecting inclusions are lead, arsenic, and iron sulfides, the gray field consists of calcium and magnesium carbonates.

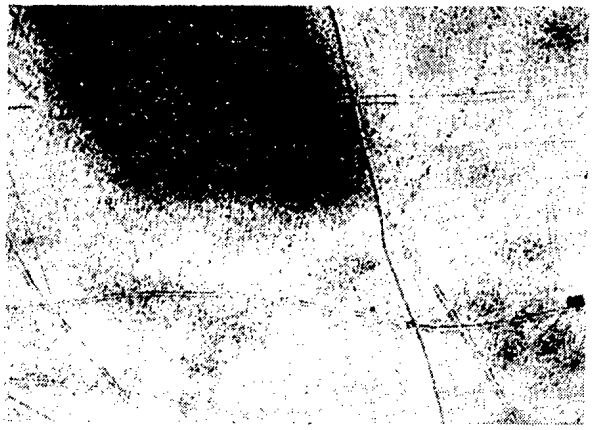

Fig. 3. Tracks of fission fragments from lead on a muscovite detector in transmitted light (particle flux 10^{14} cm^{-2}).

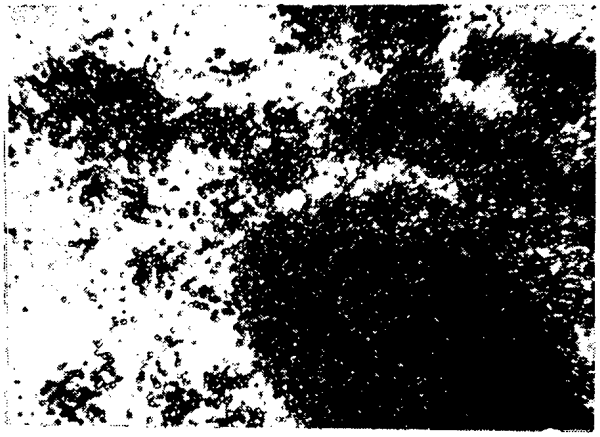

Fig. 4. Tracks of α particles in CR-39 in transmitted light (particle flux 10^{15} cm^{-2}).

TABLE 1. Number of Tracks per Counting Cell* with an Integrated Irradiation Flux of 10^{15} Particles Per 1 cm^2 of the Target (magnification by a factor of 320)

Object of study	No. of α tracks (CR-39)	No. of tracks of fission fragments in muscovite
Pb foil†	14,60	100‡
Dried drop of 1 M solution of $Pb(NO_3)_2$‡	3,37	42,50
Barite $BaSO_4$	2,88	22,63
Enclosing bituminous dolomite		
$CaMg_6O(CO_3)_2$	0,15	1,19
Calcite streaks $CaCO_3$	0,07	0,51

*A counting cell is the elementary area in which the tracks in the detector are counted (with a magnification of 320) – a square with an edge-length of 13.5 μm.
†For foil the lead content is 100%; for a drop the lead content is 38% (calculation for a layer 25 μm thick).
‡Not counted for the given integral particle flux.

tracks from recoil nuclei and the compound nuclei at 450°C (5 h) and etched it in a 40% solution of HF (2 h at room temperature). The characteristic background of the CR-39 plastic is very low (<0.01 tracks per 1 cm^2).

A large (∿700 μm wide) gallenite grain, surrounded by thin calcite streaks with dispersed lead, arsenic, and iron sulfides, is observed in the section in reflected light (Fig. 2). The fragment and α radiographs (Figs. 3 and 4) show that the ungrouped dispersed sulfides comprise about one-half of the strongly reflecting ore inclusions. The remaining submicron grains are arsenopyrite and pyrite. The large gallenite separation is surrounded by 100-μm border of supramolecular, as yet unformed mineral forms, and lead inclusions, whose inflow from the enclosing carbonate material enables the growth of the observed sulfide crystals.

Comparison of a mineralogical photograph (see Fig. 2) and radiographs, obtained based on different physical principles (see Figs. 3 and 4), enables drawing the following conclusions. First, the pattern of the lead distribution according to the α tracks is distinguished by wider contours than the area over which the ore concentrations fixed by the fission fragments are distributed, i.e., α radiography gives a more smeared picture. The dimensions of a grain of lead barite according to the data from fragment radiography are equal to 108 × 67 μm, while according to the α-radiography data the dimensions are 148 × 102 μm.

This is explained by the fact that for energies of α particles, recorded from $^{210}_{84}Po$, $^{212}_{86}Rn$, $^{210}_{86}Rn$, equal to 5.3-6.2 MeV, the mean-free path of the α particles in the sample studied and the detector is equal to 20-50 μm, and α particles emerging at different angles from a layer 15-20 μm thick are recorded in the detector.

Fission fragments have energies of <2 MeV per nucleon and a mean-free path in the sample and in mica of <12 μm (on the average 7 μm). They are recorded on emergence from a layer with thickness of ⩽5 μm. The difference in the thickness of the layers of matter and, especially, in the mean-free path lengths of α particles and fission fragments in the detectors enables refining the contours of ore localizations in fission-fragment radiography.

Second, one and the same mineral grains in fragment radiography are characterized by a much higher number of tracks than in α radiography (see Table 1), indicating that the fission method has a higher sensitivity.

Comparison of the results of the calculation of the number of tracks for one and the same area shows that the density of fragments for one and the same object is 7.5 to 10

times higher than the density of α particles. In reality, however, this difference is even higher, since the α particles are emitting by a significantly larger volume of the preparation than the fission fragments. It can be asserted that in order to study the surface distribution of lead in the sample the sensitivity of the fragment method is more than ten times higher than the sensitivity of α radiography and constitutes $\sim 10^{-5}$%. The sensitivity can be increased still further by exploiting the possibility of carrying out multiple irradiations of the same sample with the same detector in order to accumulate track information, and by using heavier ions than oxygen ions for the irradiation.

LITERATURE CITED

1. G. B. Naumov, N. P. Ermolaev, Z. M. Motorina, et al., "Geochemical role and place of preparatory processes in models of epigenetic ore formation," in: Genetic Models of Endogenic Ore Formations [in Russian], Vol. 1, Nauka, Novosibirsk (1983), pp. 34-42.
2. Problems in Radiogeology [in Russian], Nauka, Moscow (1983).
3. R. Fleischer, P. Price, and R. Walker, Nuclear Tracks in Solids (Principles and Application), University of California Press, Berkeley (1975).
4. B. Hamilton, Nature, 231, No. 5304, 1023-1029 (1971).
5. W. Wipawin, B. Thomos, and H. Khan, Int. J. Radiat. Phys. Chem., 6, No. 3, 203-210 (1974).
6. G. N. Flerov, I. G. Berzina, N. B. Berman, and I. V. Mel'nikov, "Determination of the spatial distribution of lead from α tracks," At. Énerg., 37, No. 6, 499-500 (1974).
7. G. N. Flerov and I. G. Berzina, Radiography of Minerals, Rocks, and Ores [in Russian], Atomizdat, Moscow (1979), pp. 204-208, 223.
8. E. Hide, I. Perlman, and G. Seaborg, Methods for Synthesizing Heavy Nuclei [Russian translation], Atomizdat, Moscow (1968), p. 133.

CALCULATION OF CREEP CONTOURS OF TEXTURED ZIRCONIUM ALLOYS ALONG POLAR FIGURES

S. B. Goryachev, A. V. Shalenkov, and P. F. Prasolov

UDC 669.296:539.3

The tensile yield stress of a single crystal, in the case of strain along one slip system, is not difficult to calculate, if the critical shear stress in this system and the orientation of the crystal are known [1]. In a polycrystal the orientation of the crystalline lattice changes from grain to grain, and to find its yield stress the yield stresses of separate grains must be averaged over orientations. The complexity of the problem is further increased by the fact that in the presence of combined elastoplastic deformation the grains interact with one another and this gives rise to a nonuniformity of the deformation of each grain over its volume and to several strain systems in it simultaneously. In strongly textured polycrystals, however, the orientations of the grains are close, so that their interaction should be weak. Thus the yield stress of strongly textured polycrystals can be calculated by using Sack's theory [1], in which this interaction is ignored.

In the calculation of the creep contour of textured Zircalloy-2 alloy in a biaxial stress state along polar figures [2], following Sack's theory we assumed that each grain is deformed independently of other grains and only one strain system – the primary strain system, i.e., the system which in a given stress state is manifested first when the load is increased because of its favorable orientation – operates in each grain.

At room temperature the system $\{10\bar{1}0\}\langle 1\bar{2}10\rangle$ (prismatic slip) is the main slip system in single crystals of zirconium and its alloys.

Aside from slipping, twinning in the $\{10\bar{1}2\}$ plane in the $\langle\bar{1}011\rangle$ direction (accompanying stretching along the $\langle 0001\rangle$ axis) and twinning in the planes $\{11\bar{2}2\}$ $\langle\bar{1}\bar{1}23\rangle$ (accompanying compression along the $\langle 0001\rangle$ axis) are observed [3, 4].

Translated from Atomnaya Énergiya, Vol. 59, No. 6, pp. 439-440, December, 1985. Original article submitted December 10, 1984.

0038-531X/85/5906-1019$09.50

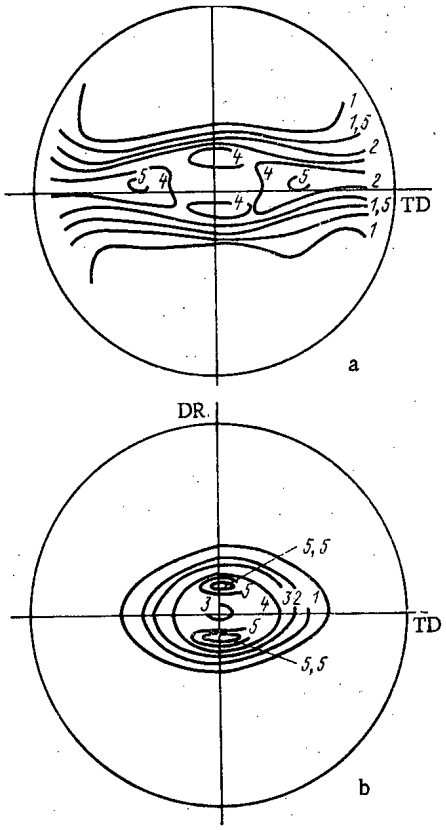

Fig. 1. Basic polar figures of Zircalloy-2 JA (a) and KA (b): DR) direction of rolling; TD) transverse direction.

We carried out the calculation of the creep on a computer by the Monte Carlo method. Using a random number generator we selected along the polar figure ⟨0001⟩ (Fig. 1a) [2] the orientation of the direction ⟨0001⟩ of a separate grain relative to the stress axes. Because of the absence of a polar figure we chose the orientation of the $\langle 11\bar{2}0\rangle$ direction in this grain arbitrarily, i.e., we assumed that the $\langle 11\bar{2}0\rangle$ directions are oriented randomly in space.

We determined the primary strain system for the given stress state and took the strain under which the reduced tangential stress in the primary system reaches a critical value as the yield stress. We then selected the orientation of another grain, etc. For the yield stress of the polycrystal we used the average value of the yield stresses of separate grains. The accuracy of the calculation of average values is ±4% with a confidence probability of 0.95.

Because the values of the critical shear stress τ_0 (in the system $\{10\bar{1}0\}\langle 1\bar{2}10\rangle$), and τ_1 (in the system $\{10\bar{1}2\}\langle\bar{1}011\rangle$), and τ_2 (in the system $\{11\bar{2}2\}\langle 11\bar{2}3\rangle$) are unknown for Zircalloy-2 single crystals, we selected them from the experimental data in [2] so as to obtain the best agreement with three points on the creep contour, corresponding to uniaxial stretching along the direction of rolling, biaxial all-around stretching, and compression (Fig. 2a). We used the values found (τ_0 = 208 MPa, τ_1 = 302 MPa, τ_2 = 364 MPa) to calculate the entire creep contour. Good agreement was obtained with the experimental points which we did not use for selecting the stresses. We then used the values obtained for the critical shear stresses to calculate the creep contour of Zircalloy-2 with a different polar figure (see Fig. 1b) [2] and obtained data which were in agreement with the experimental data (see Fig. 2b). Since we used in the calculation experimental values of the yeild stresses of the polycrystal, the good agreement with experiment could also be linked with the fact that in this calculation we took into account the intercrystalline interaction in an implicit form.

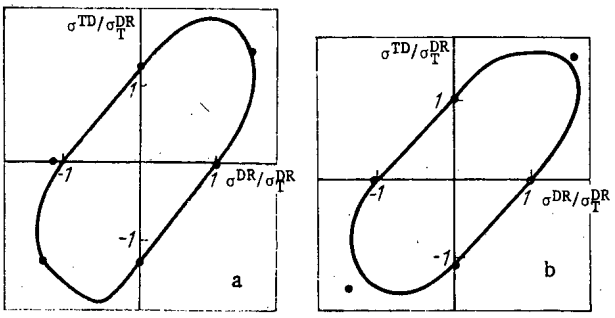

Fig. 2. Flow contours of Zircalloy-2 JA (a) and KA (b): •) experiment; ——) results of calculation; σ_T yield stress under stretching along the direction of rolling; σ^{DR} stress in the direction of rolling; σ^{TD} stress in the transverse direction.

Thus the results presented above show that the simplest theory of deformation of polycrystals – Sack's theory – can be used to calculate the creep contour of strongly textured polycrystals.

LITERATURE CITED

1. R. W. Honeycombe, Plastic Deformation of Metals, St. Martin (1968).
2. R. Ballinger and R. Pelloux, "The effect of anisotropy on the mechanical behavior of Zircalloy-2," J. Nucl. Mater., 97, 231-253 (1981).
3. E. Tenckhoff, "Operable deformation systems and mechanical behavior of textured Zircalloy tubing," in: Zirconium in Nuclear Applications, ASTM STP-551 (1974), pp. 179-200.
4. A. Akhtar, "Basal slip in zirconium," Acta Metal., 21, 1-11 (1973).

THREE-DIMENSIONAL CALCULATIONS OF A SUBCRITICAL HETEROGENEOUS REACTOR WITH A NEUTRON SOURCE

V. M. Malofeev

UDC 621.039.512.2

Iterative algorithms for multidimensional calculations of critical and subcritical reactors are similar to a large extent. As a rule, calculation programs for a critical reactor may be easily applied, as a rule, to the calculation of subcritical systems with a source. However, if the subcritical reactor is in a near-critical state the system of equations which describes it is almost degenerate, which leads to considerable increase in machine time when using traditional iterative algorithms. In the present work, a method of three-dimensional calculation is outlined for a subcritical heterogeneous reactor or pile with a neutron source, allowing near-critical systems to be effectively calculated. It is assumed that the system is described by the three-dimensional equations of the theory of a heterogeneous reactor. The method is based on difference transformations of heterogeneous equations and the expansion of the axial component of the neutron flux in Fourier series in terms of sines, as realized in the TREC program [1] intended for three-dimensional calculations of critical reactors.

A subcritical reactor of height H with cylindrical fuel channels of inhomogeneous structure over the height is considered; at the reactor surfaces, of radius ρ, the following boundary conditions are specified (notation as in [1])

$$\rho\,\partial N(z)/\partial\rho = \Lambda(z)\,N(z) - S(z), \tag{1}$$

Translated from Atomnaya Énergiya, Vol. 59, No. 6, pp. 440-442, December, 1985. Original article submitted February 28, 1985

0038-531X/85/5906-1021$09.50

 neutron groups and K is the number of channels); $\Lambda(z)$ and $S(z)$ are the matrix and vector formed from the effective group matrices and vectors of the external sources specified for channels of each type. It is assumed that in the moderator the group neutron fluxes satisfy the system of equations

$$-\Delta N^g(r, z)+\xi_g N^g(r, z)=\xi_{g-1}N^{g-1}(r, z); \quad g=1, \ldots, G;$$
$$\xi_g=1/\tau_g \quad (g<G); \quad \xi_G=1/L^2, \tag{2}$$

and the neutron flux is zero at the external boundary of the reactor.

After expansion of the axial component of the flux in Fourier series in terms of sines

$$N^g(r, z)=\sum_{m=1}^{M} N_m^g(r)\sin \alpha m z; \quad \alpha=\pi/H$$

and difference transformation of the linear algebraic system corresponding to the boundary problem in Eqs. (1) and (2), the equation for a reactor with a source may be written in the form

$$PN=Q(\gamma N+q). \tag{3}$$

Here is the Fourier-coefficient vector for fluxes at the channel surfaces; P and Q are spatially local two-dimensional difference operators; γ and q are the matrix and vector associated with the Fourier components of matrix Λ and vector S by simple linear relations.

Teh relation between the axial harmonics in Eq. (3) is solely through the matrix γ. If the matrix Λ does not depend on z, the matrix γ is diagonal with respect to the harmonics, and Eq. (3) breaks down to a system of M independent equations, each of which includes only one harmonic. Hence, three-dimensional calculation of a pile which is homogeneous over the height and has an arbitrarily located source reduces to a series of completely independent two-dimensional calculations with subsequent summing of the results in calculating $N(z)$. The number of such calculations is determined by the nonuniformity of the axial neutron-flux distributions.

The two-term Chebyshev method is used to solve Eq. (3) [2]

$$N^{k+1}=(1-\omega_{k+1})N^k+\omega_{k+1}(TN^k+f);$$
$$T=P^{-1}Q\gamma; \quad f=P^{-1}Qq; \quad N^k \to N, \tag{4}$$

where k is the number of the iteration; ω_k is the iteration parameter; TN^k is calculated using a separate algorithm of internal iterations. The parameters ω_k are usually selected from the condition of uniform suppression of the error in all eigenfunctions of operator T. In this case, as the reactor approaches the critical state, the number of iterations required to reach the specified accuracy in calculating N increases as $(1-\lambda_1)^{-1/2}$, where λ_1 is the maximum eigenvalue of operator T, equal to unity in the critical state. In addition, a sufficiently accurate estimate of λ_1 is required for optimal choice of ω_k, and this necessitates preliminary solution of the critical problem.

By analogy with the method of solving the eigenvalue problem proposed in [3], consider the following procedure for selecting the parameters ω_k, which is effective for a weakly subcritical system when

$$1-\lambda_1 \ll 1-\lambda_2, \tag{5}$$

where λ_2 is the second largest eigenvalue of the operator T. Assume that the eigenvalue spectrum of operator T is in a region consisting of the segment $[\lambda_{min}, \lambda_2]$ (λ_{min} is the minimum eigenvalue) and an isolated point λ_1 whose position is unknown. The parameters ω_k are determined in two stages. In the first stage, the parameters ω_k are determined from the condition of uniform suppression of the errors in the eigenfunctions with eigenvalues $\lambda \in [\lambda_{min}, \lambda_2]$:

$$\omega_k=2/[(b+a)+(b-a)\cos \pi\theta_k];$$
$$a=1-\lambda_2; \quad b=1-\lambda_{min},$$

where $\{\theta_k\}$ is a numerical sequence distributed over [0, 1]. Simultaneously, the first eigenvalue is calculated from the formula

$$\lambda_1^k = \frac{1}{\omega_{k-1}} + \frac{1}{\omega_k}\frac{\delta^k}{\delta^{k-1}}; \quad \delta^k = l(N^k - N^{k-1}), \tag{6}$$

where $l(N)$ is a linear functional. The calculation at this stage continues until λ_1^k takes a stable value, indicating that the basic part of the error in the solution is concentrated in the first eigenfunction. Suppose that the first stage ends when $k = k_0$.

The second stage consists of several iterations, the aim of which is to suppress the error in the first eigenfunction and subsequently "equalize" it for the remaining eigenfunctions. Let

$$\omega_{k_0} = 1/a_0; \quad a_0 = 1 - \lambda_1^{k_0}.$$

If the system of eigenfunctions of operator T is complete, then

$$|\varepsilon^{k_0+k_1}| \leqslant \max_{\lambda} |P_{k_1}(\lambda)| \, |\varepsilon^{k_0}|; \quad \varepsilon^k = N^k - N;$$

$$P_{k_1}(\lambda) = \left(1 - \frac{\lambda}{a_0}\right) \prod_{k=k_0+2}^{k_0+k_1} (1 - \omega_k \lambda).$$

The parameters ω_k ($k = k_0 + 2, \ldots, k_0 + k_1$) are defined so that the maximum value of $P_{k_1}(\lambda)$ with respect to $\lambda \in [a, b]$ reaches a minimum. This problem is solved analytically at $k_1 = 2$

$$\omega_{k_0+2} = \begin{cases} \dfrac{2b - 3a_0 + 2\sqrt{2}(b - a_0)}{4b^2 - 4a_0 b - a_0^2}, & c \geqslant 0 \\ \dfrac{a + b - 2a_0}{a^2 + b^2 - a_0(a+b)}, & c < 0, \end{cases}$$

where $c = b - a - \sqrt{2}(a - a_0)$.

If after the second stage the specified accuracy of the solution is not attained, the iterative process returns to the first stage, and so on. The better the observance of Eq. (5), the higher the efficiency of the procedure in comparison with the traditional method of choosing the iteration parameters. In calculating a deeply subcritical system, Eq. (5) does not hold, and λ_1^k calculated from Eq. (6) may not take stable values. In this case, sufficiently fast convergence of the iterations is usually achieved with the application only of the first stage. Note that a fairly rough estimate may be used for λ_2, for example, $\lambda_2 = 0$.

The method here outlined has been realized in the TRECS program; intended for three-dimensional calculations of subcritical heterogeneous systems with local or extended neutron sources. Calculations by the TRECS program show that, for weakly subcritical systems (λ_1 0.9), this procedure allows the number of iterations to be reduced more than threefold in comparison with the traditional method of selecting the iteration parameters.

LITERATURE CITED

1. B. P. Kochurov and V. M. Malofeev, "Three-dimensional calculations of a heterogeneous reactor," At. Énerg., 48, No. 6, 387-388 (1980).
2. G. I. Marchuk and V. I. Lebedev, Numerical Methods in the Theory of Neutron Transfer [in Russian], Atomizdat, Moscow (1981).
3. V. I. Lebedev, "Iterative method with Chebyshev Parameters for determining the greatest eigenvalue and corresponding eigenfunction," Zh. Vychisl. Mat. Mat. Fiz., 17, No. 1, 100 (1977).

INFLUENCE OF THE FINITE MODERATOR DIMENSIONS UPON THE CHARACTERISTICS OF A PULSED SOURCE OF SLOW NEUTRONS

N. I. Alekseev, A. V. Drobinin, and Yu. M. Tsipenyuk

UDC 539.103

In addition to nuclear reactors, various accelerators of charged particles and, in the near future, probably also fusion units working with lasers are increasingly used as sources of neutrons. In such pulsed sources, fast neutrons (E = 1-2 MeV) are usually moderated in a hydrogen-containing material and slowed down to thermal energies to use the neutrons in research on the physics of the condensed state or in nuclear physics research.

In experiments in which flight times are measured, the neutrons interact with the material of the sample located beyond the neutron source. The density φ of the flux of neutrons incident on the sample is proportional to the visible part of the irradiated surface and the density of the neutron flux from it. Thus, the finite thickness of the moderator in the direction of the sample or a channel in an infinite moderator necessarily imply a reduction of the neutron flux density. In a thick moderator (thickness much greater than the length ℓ_m of the moderator), the undisturbed flux density of the slow neutrons exceeds in the maximum of the spatial distribution the maximum flux density on the surface of a thin ($\sim\ell_m$) moderator by a factor of 6.

The goal of the present work is to investigate the influence of a channel with an infinite moderating medium and with finite moderator dimensions upon the characteristics of the neutron source. The experiments were made with a pulsed neutron source based on the microtron of the Institute of Physics Problems of the Academy of Sciences of the USSR [1]. A lead cylinder with a diameter of 80 mm and a length of 60 mm served as the neutron converter. The cylinder was surrounded by polyethylene moderators of different geometries (Fig. 1). The neutron spectrum was measured with ^{3}He counters via the flight time; the pulse length at various neutron energies was determined from the width of half the maximum height of the peak of elastic scattering at a pyrographite single crystal in the range of large angles in which geometrical broadening can be disregarded. Neutron flux densities averaged over time and zones were calculated in cylindrical geometry with the Monte Carlo method usign the MMKFK program [2] with a 21-group system of constants; the pulse parameters were determined with the method of [3]. It was assumed in the calculations that the conversion neutrons are uniformly distributed over the target volume and that their spectrum is close to the spectrum of the fission neutrons and that the flux density of the neutrons incident on the sample is proportional to the flux density on the irradiated surface and its area. It turned out that the experimental data are appropriately described by the calculated data in these approximations.

First of all the contribution of the various moderator portions to the neutron flux density was determined. The dependence of the flux density of the slow neutrons upon the parameter D of the irradiated surface was studied by coating this surface with cadmium. The neutron converter was placed at a distance δ = 4 cm from the irradiated surface. This corresponds approximately to the maximum of the flux density of the neutrons incident on the sample in dependence upon the thickness of the plane moderator [4] (Fig. 2).

The following details should be noted: The neutron flux density on the sample as a function of the diameter of the irradiated surface decreases rather slowly in the case of a source of type A + B and amounts to about 50% at D $\approx 3\ell_m$ but reaches 90% at D $\approx 6\ell_m$; a reduction of the thickness to 7 cm of the moderator portion which is located in the direction opposite to the beam (zone B missing) hardly influences the flux density of the neutrons which are incident on the sample (the reduction amounts to a few percent); at D = 15 cm, the flux density is increased by only 17% when the lateral parts of zone A are present; the extraction of the neutrons from an "infinite" moderator through a channel with a

Translated from Atomnaya Énergiya, Vol. 59, No. 6, pp. 442-443, December, 1985. Original article submitted March 13, 1985.

 0038-531X/85/5906-1024$09.50

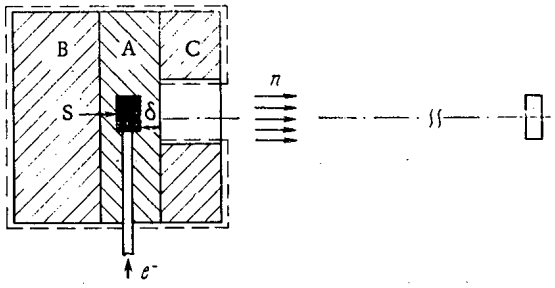

Fig. 1. Geometry of the experiment: A, B, and C) moderator layers; S) source.

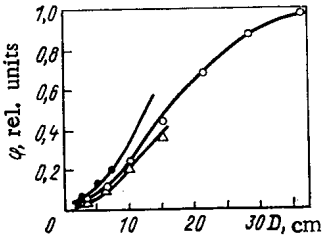

Fig. 2

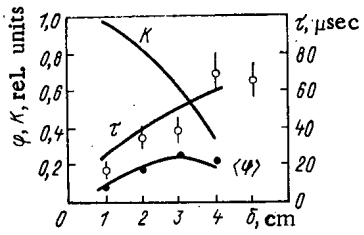

Fig. 3

Fig. 2. Dependence of the average neutron flux density on the sample upon the diameter of the irradiated surface: ○) moderators A and B; •) moderators A + B + C; Δ) moderator A; ——) calculation; ----) sections of the cadmium-coated surface (the calculated values were normalized to the experimental values at the point D = 30 cm).

Fig. 3. Dependence of the pulse length of the slow neutrons, the pulse quality, and the neutron flux density upon the thickness of the moderating layer in the scheme A + B + C with a superficially cadmium-coated converter (——) calculation; • and ○) experimental results).

cadmium-coated lateral surface (zone C present) at D < 20 cm implies an increase in the flux density by 30-50%; and when the channel diameter is increased, zone C becomes irrelevant.

Apart from the flux of neutrons incident on the sample, the length τ of the neutron path and, consequently, the pulse quality $K = \varphi/\tau^2$ are important in flight-time measurements. In the case of a two-dimensional moderator, these quantities have been studied in detail at an earlier date [4] but only in the case of weakly absorbing targets and thin moderators. In our work these characteristics were studied in the moderator geometry A + B + C with a channel diameter of 5 cm (Fig. 3). The dependence of these characteristics upon the thickness δ of the moderator layer between the cadmium-coated neutron converter (simulation of a strongly absorbing target) and the irradiated surface was considered. The calculations rendered the effective pulse length $\tau = [\int_0^{1/\nu} \varphi(t)\,dt]/\varphi_{peak}$ of the neutrons, where φ_{peak} denotes the peak value of the neutron flux density; and ν denotes the pulse frequency or, in the experiment, the width $\tau_{1/2}$ of the pulse on half its maximum height. The τ value is greater than $\tau_{1/2}$ by 10-20% (depending upon the neutron energy) [4], and therefore the results obtained in calculations and experiments are in rather good agreement with the error limits. In the scheme A + B + C, as well as in the two-dimensional moderator geometry, the neutron pulse length can be adjusted by changing the thickness of the moderating layer as suggested by the authors of [5] (see Fig. 3).

The quality of the pulse reaches its maximum at D $\approx$ 15 cm in all the geometries (A, A + B, and A + B + C). On the other hand, when δ decreases, the pulse quality increases

 a reduction of the neutron pulse length.

Our results allow a more efficient use of a moderating system in real experiments. The good correspondence between experimental data and calculations makes it possible to calculate also other source versions.

The authors thank A. S. Kochenov, I. P. Sadikov, and V. S. Stolypin for useful discussions.

LITERATURE CITED

1. A. N. Bazhan, B. S. Zakirov, L. M. Zykin, et al., "A pulsed neutron source on the basis of a 30-MeV microtron," in: Neutron Physics [in Russian], Part 4, Central Scientific-Research Institute of Atomic Information, Moscow (1980), pp. 76-80.
2. L. V. Maiorov, The MMKFK Program Set Developed by A. D. Frank-Kamentskii for Calibrating Reactors with the Monte-Carlo Methods, Problems of Atomic Science and Technology, Series Physics and Technology of Nuclear Reactors [in Russian], No. 8 (21), pp. 7-20 (1981).
3. N. I. Alekseev, "Neutron sources on the basis of a booster," At. Énerg., 58, No. 1, 64 (1985).
4. S. N. Ishmaev, I. P. Sadikov, and A. A. Chernyshov, Selection and Optimization of a Moderator for a Pulsed Source of Slow Neutrons [in Russian], Preprint of the Inst. of Atomic Energy-2019, Moscow (1970).
5. N. I. Alekseev, A. S. Kochenov, and V. S. Stolypin, "A pulsed source of slow neutrons," Inventor's Certificate No. 915,640, Byull. Izobr., No. 7, 314 (1983).

LIQUID REFERENCE SOURCES OF GAMMA RADIATION

B. Ya. Shcherbakov

UDC 539.122.164

Only two types of gamma radiation sources are at the present time released for determinations of the efficiency of gamma spectrometers: spectrometric gamma radiation reference sources and radioactive reference solutions with various gamma emitting nuclides [1]. Since in calibration work the geometrical shape, the dimensions, and the activities of the reference sources and the samples to be measured must be identical, spectrometric gamma radiation reference sources are employed in measurements of samples with a small volume and with a sufficiently high activity of the nuclide; radioactive reference solutions are employed in measurements of voluminous samples with a low activity of the nuclide.

In the analysis of samples with a low activity of the nuclide, one can proceed in two ways: either use a large-volume sample [2] or reduce the sample volume required for measuring the activity of the nuclide by a preliminary concentrating. The possibilities of the first method are limited (particularly at low energies of the gamma raidation of the nuclide) because the detector efficiency decreases with increasing sample volume as a consequence of the increasing distance between the detector and the peripheral sample sections and because of the absorption of the gamma radiation by the sample material. Therefore, and owing to the development of concentrating techniques without uncontrollable losses of the nuclide under inspection [3], the second method is being preferred. The liquid sample obtained after concentrating is poured into a relatively small vessel, e.g., into a jar with a diameter of 50 mm and a volume of 100 cm^3 (TU 6-19-110-78) made from high-pressure polyethylene (All-Union State Standard 16337-77, brand 15803-020). When measurements are made with a gamma spectrometer, such a sample and the reference source are alternatingly placed directly on the lid of the detector. In this case the activity of the nuclide of interest in the sample is $A_X = A_0(S_X/S_0)$, where A_0 denotes the activity of the same nuclide in the reference source having the same shape and dimensions as the sample; and S_X and S_0 denote the areas of the total absorption peak of the gamma quantum energy of the nuclide under consideration

Translated from Atomnaya Énergiya, Vol. 59, No. 6, pp. 443-444, December, 1985. Original article submitted April 3, 1985.

 0038-531X/85/5906-1026$09.50

determined with the gamma spectrometer in measurements of the sample and the reference source, respectively, under identical conditions and in identical time intervals. Since reference sources of sufficiently large volume are not yet available, working sources must be prepared from radioactive reference solutions. The activity of the working source is $A_0 = am$, where a denotes the specific activity (Bq/g) of the particular nuclide as indicated in the specification data of the radioactive reference solution; and m denotes the mass (g) of the radioactive reference solution used for preparing the working source. Thus, the relative error of the total activity of the nuclide in the working source is $\delta_{A_0} = \sqrt{\delta_a^2 + \delta_m^2}$, where δ_a and δ_m denote the relaitve errors made in the determination of the specific activity a and the mass m of the radioactive reference solution, respectively. In the class-one specification data of a radioactive reference solution, the a value is given with a relative error of ±3% on the 0.95 confidence level; the mass of the solution in the tube is indicated with a relative error of 10%, e.g., m =5.0 ± 0.5 g. Thus, when the tube is opened and used as a working source of gamma radiation, the relative error of the total activity of the nuclide in the source will exceed ±10%. Therefore, for preparing a working solution, the tube of the reference solution is weighed on an analytic balance with an error such that the relative error of the total activity of the nuclide in the resulting source does not exceed at most ±4%. But since the total activity of the nuclide in the tube is usually $\sim 5 \cdot 10^5$ Bq and since for calibrating a gamma spectrometer in measurements of, say, samples of the environment close to the detector, working sources with a nuclide activity of $1 \cdot 10^3$ Bq are required in the case of scintillation detectors or of $1 \cdot 10^4$ Bq in the case of germanium detectors, only a small fraction of the contents of the tube of a radioactive reference solution is used for preparing a working source. Furthermore, since an opened tube cannot be hermetically sealed again, the unused radioactive reference solution must be poured into a vessel made of a material with a well-known absorption. As early as a few hours after opening the tube, neither the portion used for preparing the working source nor the remaining unused part of the radioactive reference solution can be used for reference sources or for working sources as uncontrollable losses of the nuclide can take place by, say, sorption or evaporation. Thus, a carefully prepared radioactive reference solution is used in an uneconomic fashion and is discarded after a single use.

Therefore one should prepare radioactive reference solutions and liquid spectrometric gamma radiation sources with a total nuclide activity of 10^3-10^5 Bq on the basis of radioactive reference solutions of nuclides of a longer half-life; these solutions should be certified with a relative error of at most ±4% on the 0.95 confidence level. It suffices for this purpose to pour into a tube a certain quantity of the radioactive reference solution measured off with high accuracy. Since the relative error δ_a of the specific activity in sources of class one is ±3%, the error δ_m in the determination of the mass of the radioactive reference solution must not exceed ±0.5%. Polyethylene vessels with a lower nuclide-sorption capacity than glass [4] should be employed for the tubes of such sources. Different total activities of the nuclides in such sources are required, e.g., $1 \cdot 10^3$, $5 \cdot 10^3$, $1 \cdot 10^4$, $5 \cdot 10^4$ Bq, etc. The volume of the radioactive solution in such sources may also differ in dependence upon the gamma radiation energy of the nuclide and the requirements of the user, e.g., 10, 25, 50 cm^3, etc.

Such hermetically sealed sources are advantageous over radioactive reference solutions because these sources can be repeatedly employed as reference sources during an extended period of time. The consumption of the radioactive reference solution is reduced and it is not necessary to open the tubes for preparing working sources nor to discard radioactive reference solutions in radioactive waste so that not only savings are obtained but also the contamination of the environment is reduced.

LITERATURE CITED

1. Reference Sources, Sources of Alpha, Beta, and Gamma Radiation, Plutonium-Beryllium Sources of Fast Neutrons, and Radioactive Sample Solutions (Catalog) [in Russian], V/O Izotop, Moscow (1982).
2. É. G. Tertyshnik and A. T. Korsakov, "Determination of the detector efficiency in the gamma spectrometry of large-volume samples," At. Énerg., 58, No. 1, 44 (1985).
3. Yu. A. Zolotov and N. M. Kuz'min, Concentrating of Microelements [in Russian], Khimiya, Moscow (1982).
4. W. Grummit and G. Lahaie, "Problem of monitoring radioactive effluents," in: Monitoring of Radioactive Effluents from Nuclear Facilities (Proc. Symp. Protoroz., 1977), IAEA-SM-217/2, IAEA, Vienna (1978), pp. 9-18.

A SPECIALIZED MASS-SPECTROMETER UNIT FOR ANALYZING AGGRESSIVE GAS MIXTURES

N. N. Bobrov-Egorov, V. N. Ignatov, and G. I. Kir'yanov

UDC 543.51.026

We have made investigations* and have developed the specialized UMT-5 mass spectrometer unit designated for research on processes of fluorine conversion of irradiated fuel from atomic power stations. The unit works as an automatic continuous monitor with a frequency of ten analyses per hour. The characteristics of the unit were calibrated and periodically checked with the aid of six control samples of gas mixtures of different compositions.

Figure 1 illustrates the general form of the UMT-5 unit which consists of an analytic system, and also a control system and an information processing system.

The analytic system comprises a 180° mass analyzer, a vacuum-pumping unit, and a sample-feeder unit. The mass analyzer comprises a dispersing magnet, an ion source, and a block of collectors. The magnetic field induction is 0.8 T, the radius of the mean trajectory 60 mm. Since the ion source is in the magnetic field area, an additional magnetic field has been provided at the output for compensating for the effect of mass discrimination. The block of collectors makes it possible to record simultaneously six components of a gas to be analyzed. The positions of the collectors are adjusted without disturbing the vacuum in the mass analyzer.

The sample-feeder unit comprises an automatically adjustable four-valve flow regulator, a tank for purifying discharged gas from chemically toxic materials, and a tank with a standard gas sample for calibrating the instrument.

A preliminary evacuation of the mass analyzer is obtained with zeolite sorption pumps. Mercury-vapor diffusion pumps are employed for obtaining high vacuum. The operating pressure

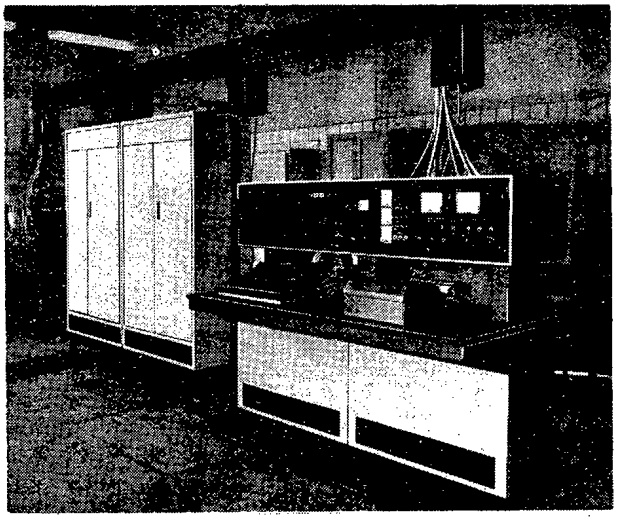

Fig. 1. Overall view of the UMT-5 system.

*N. N. Bobrov-Egorov, V. N. Ignatov, G. I. Kir'yanov, and I. V. Kolodeshnikov, "Results of experimental research on a mass-spectrometer unit in the analysis of aggressive gases," in: All-Union Scientific-Technological Conference "Development of Specialized Mass Spectrometer Units" [in Russian], Moscow, All-Union Scientific-Research Institute of RT, Moscow (1983), p. 182.

Translated from Atomnaya Énergiya, Vol. 59, No. 6, pp. 444-445, December, 1985. Original article submitted June 21, 1985.

 0038-531X/85/5906-1028$09.50

TABLE 1. Results of Concentration Changes in a Five-Component Gas Mixture

Component	Analysis 1		Analysis 2		Analysis 3	
	c_p	c_a	c_p	c_a	c_p	c_a
UF_6	20±3	19,9±0,7	6,7±0,2	6,4±0,4	26,7±1,6	26,4±0,4
Ar	10±1	9,8±0,5	20±3,3	21±1,5	3,4±0,2	3,4±0,2
F_2	20±1	19,1±1,0	20±1,3	19,5±0,5	3,3±0,1	3,6±0,2
O_2	30±2	30,4±1,3	30±3,5	29,9±0,4	33,3±3,4	33,6±0,2
N_2	20±3	20,8±1,0	23,3±3,3	22,7±1,2	33,3±3,4	33,0±0,3

Remark: C_p) concentration of the mixtures prepared; C_a) concentration measured in the analysis.

TABLE 2. Concentrations (%) of UF_6 and Measurement Error

Concentration	1st sample	2nd sample	3rd sample
C_p	50±2	10±0,3	1,0±0,1
C_a	49,0±0,8	9,6±0,2	1,0±0,1

in the chamber of the mass analyzer is 10^{-4}-10^{-5} Pa. Electrometer dc amplifiers with the following characteristics have been developed for recording the ion currents: input current up to $2\cdot10^{-4}$ A; noise level ±150 μV; and zero drift ±150 μV in 8 h.

An "Élektronika DZ-28" microcomputer is employed for the automatic control and for monitoring the operation or for evaluating the data and accumulating the results. The recording and controlling system provides the following operations: reception and processing of the information according to a particular algorithm; outputting of the results in digital form on a digital printer; issuing controlling commands to excuting members; and receiving information on the operation of the unit from monitoring points. If the microcomputer fails, information on the composition of the gas mixture can be obtained from the service block.

Experimental work in which the characteristics of the two systems were determined for the analysis of aggressive gases was performed on the UMT-5 system and the system for preparing control samples (system produced by the I. V. Kurchatov Institute of Atomic Energy).

In order to provide for reproducibility of the results of an analysis, the unit was passivated with fluorine and other fluorine-containing gases.

The system was calibrated with standard samples for the purpose of determining the coefficients of the relative sensitivity for components of a gas mixture. The coefficients of the relative sensitivity were determined with binary gas mixtures in which the basic gas was argon. The formula

$$K_i = I_{Ar}/I_i\,(C_i/C_{Ar})$$

was employed, where I_{Ar} and I_i denote the ion currents of argon and of the i-th component, respectively; and C_{Ar} and C_i denote the concentrations of Argon in the standard sample and of the i-th component, respectively. The following coefficients of the relaitve sensitivity were obtained for Ar, UF_6, F_6, N_2, and O_2 from the calibration: 1, 11.0, 3.76, 1.74, and 1.85, respectively.

The relative sensitivity coefficients were used to analyze various gas mixtures; the concentration of the components was determined with the formula

$$C_i = K_i I_i / \left(\sum_{i=1}^{6} K_i I_i\right) 100\%.$$

The results of the analyses are listed in Table 1 which shows that the error of the gas mixtures prepared is greater than the error of the analysis.

The reproducibility of the results can be assessed from data obtained during several days in an analysis of the volume fraction (%) of UF_6: 25.8 (initial value), 25.3 (after 1 day), 26.0 (after 2 days), and 25.4 (after 5 days). It follows from the data that a

daily calibration of the instrument is not necessary. The instrument is made with fluorine before an analysis and at the beginning of a shift. The mean-square deviation of the results is 2.5%.

Investigations in which the concentration-dependent sensitivity (minimum concentration at which the error does not exceed a given limit) was determined have shown (Table 2) that when the UF_6 concentration is reduced from 50% to 1%, the error of the analysis does not increase and is within the error limtis in the preparation of the gas mixtures.

The dynamic range of the amplifiers must be increased for determining UF_6 concentrations of less than 1%. Thus, in the case of components in which the coefficients of the relative sensitivity are small, the concentration sensitivity was 0.1% (see the cited paper) and reched 1% in the case of UF_6 (relative concentration-dependent sensitivity = 11).

The specialized UMT-5 mass-spectrometer unit therefore allows determinations of the volume concentration of the components in gas mixtures of HF, H_2, O_2, F_2, Ar, and UF_6 in the range of 0.1-100% with a relative erorr of less than 10% on the 0.95 confidence level. The unit can be operated in manual operation as well as in continuous automatic monitoring.

EQUIVALENT X-RAY DOSES IN A HETEROGENEOUS HUMAN PHANTOM

V. I. Ivanov, L. A. Lebedev,
V. P. Sidorin, R. V. Stavitskii,
and V. V. Khvostov

UDC 621.039.553.5

The main contribution to the population dose from man-made ionizing-radiation sources comes from x-ray diagnosis. At low doses, the unfavorable consequences are evidently stochastic, insofar as they can be identified at the population level. The threshold-free linear hypothesis on the action of ionizing radiation enables one to take the effective equivalent dose as a measure of the damage:

$$H_E = \sum_{j=1}^{n} H_j w_j,$$

where Hj is the equivalent dose in organ or tissue j, while wj is a weighting factor characterizing the ratio of the stochastic risk on irradiating that organ or tissue to the total risk in uniform irradiation of the whole body [1].

To determine the effective equivalent dose, one has to know the distribution of the equivalent doses in the body. However, such information is lacking from published sources [2-4], and only particular cases are considered, from which it is difficult to generalize.

Here we derive the characteristics of the x-ray field in the human body by means of a Monte Carlo program [5] and a mathematical model for an anthropomorphic heterogeneous phantom [6], which is based on data on body structure, and on organ sizes, shapes, and positions for an average human being of European type. Figure 1 gives the general form of the phantom. The head and trunk are represented by a truncated elliptical cone. The origin lies at the center of the trunk cylinder.

We used 34 second-order surfaces forming 35 geometrical zones to describe a phantom with 22 internal organs and tissues; each zone corresponds to a certain composition: air, lung tissue, muscle, or bone. The data on the elemental compositions were taken from [7].

We calculated the x-ray flux density, the energy flux density, and the equivalent dose using 60 point detectors distributed within the phantom, while the equivalent dose to an organ was determined by averaging the doses over the volume of it. An exception was represented by the equivalent dose for the active bone marrow H_{abm} in Sv:

$$H_{abm} = \sum_i H_i^{abm} \cdot m_i / \sum_i m_i,$$

Translated from Atomnaya Énergiya, Vol. 59, No. 6, pp. 446-447, December, 1985. Original article submitted July 3, 1985.

 0038-531X/85/5906-1030$09.50

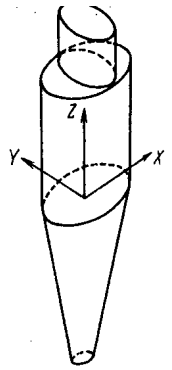

Fig. 1. General form of anthropomorphic heterogeneous phantom (human internal organs not shown).

TABLE 1. Dependence of the Specific Equivalent Dose δj in fSv·cm^2 on Photon Energy for Various Human Organs

E, keV	Thyroid	Gonads	Mammary gland	Lungs	Stomach	Spleen	Liver	Lower section of large intestine	Upper section of large intestine	Active bone marrow	Bone surfaces
10	0,00072	0,070	0,065	0,45	4,5	31,0	0,14	0,045	2,1	0,51	2,1
20	0,0014	0,14	0,13	0,90	9,1	63,0	0,28	0,091	4,3	1,0	4,3
30	0,0079	0,22	0,41	1,4	16,0	91,0	0,52	0,29	6,2	1,6	6,0
40	0,022	0,33	1,0	2,1	28,0	110,0	0,96	0,70	7,5	2,5	7,1
50	0,036	0,44	1,5	2,7	38,0	130,0	1,4	1,0	8,7	3,4	8,1
60	0,049	0,55	2,1	3,3	47,0	140,0	2,0	1,3	10,0	4,2	9,3
70	0,062	0,65	2,6	3,9	54,0	150,0	2,7	1,5	11,0	5,1	10,0
80	0,074	0,76	3,1	4,4	60,0	160,0	3,5	1,7	12,0	6,0	11,0
90	0,085	0,87	3,5	4,9	64,0	170,0	4,3	1,8	13,0	6,8	13,0
100	0,095	0,98	3,9	5,4	67,0	170,0	5,3	1,8	15,0	7,7	14,0
110	0,10	1,0	4,3	5,9	68,0	180,0	6,3	1,8	16,0	8,5	15,0
120	0,11	1,2	4,7	6,4	69,0	170,0	7,4	1,7	17,0	9,4	17,0

Note: The source is at the point with coordinates (8 cm, 50 cm, 35 cm), with the photon beam intersecting the plane y = −10 cm to give a square with a side of 20 cm.

where H_i^{abm} is the equivalent dose in part i of the active bone marrow in Sv and m_i is the mass of part i in kg.

The data on the active bone marrow distribution were taken from [8]. In calculating the equivalent dose in the active bone marrow, we corrected for the dose buildup at the bone–bone marrow boundary.

The calculations gave the specific equivalent doses in organs and tissues for a monoenergetic photon radiation source with energy in the range from 10 to 120 keV for various irradiation geometries (Table 1). The statistical error was 2-5% for organs falling in the irradiation field or 20-50% for organs outside it, in accordance with their positions in the phantom.

The results are universal and can be used in calculating equivalent doses to human organs for x radiation with any spectrum. Then

$$H_j = \Phi \int_0^{E_{max}} n(E)\,\delta_j(E)\,dE,$$

where Φ is the photon fluence at the surface in 1/cm^2; n(E), normalized photon energy distribution as incident on the phantom in 1/keV; $\delta j(E)$, specific equivalent dose in organ j for photons of energy from E to E + dE in Sv·cm^2; and E_{max}, maximum photon energy in the spectrum in keV.

1. Radiation Protection: ICRP Recommendations, Publication No. 26 [Russian translation], Atomizdat, Moscow (1978).
2. I. Gray, M. Ragozzino, M. Van Lysel, et al., "Normalized organ doses for various diagnostic radiologic procedures," Am. J. Roentgenology, 137, No. 3, 463 (1981).
3. B. Archer, R. Whitmore, L. North, et al., "Bone marrow dose in radiography," Radiology, 133, No. 1, 211 (1979).
4. M. Rosenstein, Organ Doses in Diagnostic Radiology, FDA 76-8030 (1976).
5. É. B. Brodkin and T. V. Germogenova, Solving a Transport Equation by Random Sampling [in Russian], Preprint IPM, Moscow (1973).
6. W. Snyder, M. Ford, G. Warner, et al., "Estimation of absorbed fraction for monoenergetic photon sources uniformly distributed in various organs of a heterogeneous phantom," J. Nucl. Med., 10, Suppl. 3, 51 (1969).
7. Man: Biomedical Data, ICRP Recommendations, Publication No. 23 [Russian translation], Meditsina, Moscow (1977).
8. R. Ellis, "The distribution of active bone marrow in adults," Phys. Med. Biol., 5, No. 2, 255 (1964).

INDEX

SOVIET ATOMIC ENERGY

Volumes 58-59, 1985

SOVIET ATOMIC ENERGY

Volumes 58-59, 1985

(A translation of Atomnaya Énergiya)

F

G

I

K

L

M

N

O

P

R

S

T

U

AUTHOR INDEX

SOVIET ATOMIC ENERGY

Volumes 58-59, 1985

(A translation of Atomnaya Énergiya)

Volume 58, Number 1 January, 1985

Volume 58, Number 2 February, 1985

Volume 58, Number 3 March, 1985

Volume 58, Number 4 April, 1985

Volume 58, Number 5 May, 1985

Volume 58, Number 6 June, 1985

Volume 59, Number 1 July, 1985

ARTICLES

Volume 59, Number 2 August, 1985

Volume 59, Number 3 September, 1985

Volume 59, Number 4 October, 1985

Volume 59, Number 5 November, 1985

ARTICLES

Volume 59, Number 6 December, 1985

MEASUREMENT TECHNIQUES
Izmeritel'naya Tekhnika
Vol. 27, 1984 (12 issues) $520

MECHANICS OF COMPOSITE MATERIALS
Mekhanika Kompozitnykh Materialov
Vol. 20, 1984 (6 issues) $430

METAL SCIENCE AND HEAT TREATMENT
Metallovedenie i Termicheskaya Obrabotka Metallov
Vol. 26, 1984 (12 issues) $540

METALLURGIST
Metallurg
Vol. 28, 1984 (12 issues) $555

PROBLEMS OF INFORMATION TRANSMISSION
Problemy Peredachi Informatsii
Vol. 20, 1984 (4 issues) $420

PROGRAMMING AND COMPUTER SOFTWARE
Programmirovanie
Vol. 10, 1984 (6 issues) $175

PROTECTION OF METALS
Zashchita Metallov
Vol. 20, 1984 (6 issues) $480

RADIOPHYSICS AND QUANTUM ELECTRONICS
Izvestiya Vysshikh Uchebnykh Zavedenii, Radiofizika
Vol. 27, 1984 (12 issues) $520

REFRACTORIES
Ogneupory
Vol. 25, 1984 (12 issues) $480

SIBERIAN MATHEMATICAL JOURNAL
Sibirskii Matematicheskii Zhurnal
Vol. 25, 1984 (6 issues) $625

SOIL MECHANICS AND FOUNDATION ENGINEERING
Osnovaniya, Fundamenty i Mekhanika Gruntov
Vol. 21, 1984 (6 issues) $500

SOLAR SYSTEM RESEARCH
Astronomicheskii Vestnik
Vol. 18, 1984 (6 issues) $365

SOVIET APPLIED MECHANICS
Prikladnaya Mekhanika
Vol. 20, 1984 (12 issues) $520

SOVIET ATOMIC ENERGY
Atomnaya Énergiya
Vols. 56-57, 1984 (12 issues) $560

SOVIET JOURNAL OF GLASS PHYSICS AND CHEMISTRY
Fizika i Khimiya Stekla
Vol. 10, 1984 (6 issues) $235

SOVIET JOURNAL OF NONDESTRUCTIVE TESTING
Defektoskopiya
Vol. 20, 1984 (12 issues) $615

SOVIET MATERIALS SCIENCE
Fiziko-khimicheskaya Mekhanika Materialov
Vol. 20, 1984 (6 issues) $445

SOVIET MICROELECTRONICS
Mikroélektronika
Vol. 13, 1984 (6 issues) $255

SOVIET MINING SCIENCE
Fiziko-tekhnicheskie Problemy Razrabotki Poleznykh Iskopaemykh
Vol. 20, 1984 (6 issues) $540

SOVIET PHYSICS JOURNAL
Izvestiya Vysshikh Uchebnykh Zavedenii, Fizika
Vol. 27, 1984 (12 issues) $520

SOVIET POWDER METALLURGY AND METAL CERAMICS
Poroshkovaya Metallurgiya
Vol. 23, 1984 (12 issues) $555

STRENGTH OF MATERIALS
Problemy Prochnosti
Vol. 16, 1984 (12 issues) $625

THEORETICAL AND MATHEMATICAL PHYSICS
Teoreticheskaya i Matematicheskaya Fizika
Vol. 58-61, 1984 (12 issues) $500

UKRAINIAN MATHEMATICAL JOURNAL
Ukrainskii Matematicheskii Zhurnal
Vol. 36, 1984 (6 issues) $500

Send for Your Free Examination Copy

Plenum Publishing Corporation, 233 Spring St., New York, N.Y. 10013
In United Kingdom: 88/90 Middlesex St., London E1 7EZ, England
Prices slightly higher outside the U.S. Prices subject to change without notice.

RUSSIAN JOURNALS IN THE PHYSICAL AND MATHEMATICAL SCIENCES

AVAILABLE IN ENGLISH TRANSLATION

ALGEBRA AND LOGIC
Algebra i Logika
Vol. 23, 1984 (6 issues) $360

ASTROPHYSICS
Astrofizika
Vol. 20, 1984 (4 issues) $420

AUTOMATION AND REMOTE CONTROL
Avtomatika i Telemekhanika
Vol. 45, 1984 (24 issues) $625

COMBUSTION, EXPLOSION, AND SHOCK WAVES
Fizika Goreniya i Vzryva
Vol. 20, 1984 (6 issues) $445

COSMIC RESEARCH
Kosmicheskie Issledovaniya
Vol. 22, 1984 (6 issues) $545

CYBERNETICS
Kibernetika
Vol. 20, 1984 (6 issues) $445

DIFFERENTIAL EQUATIONS
Differentsial'nye Uravneniya
Vol. 20, 1984 (12 issues) $505

DOKLADY BIOPHYSICS
Doklady Akademii Nauk SSSR
Vols. 274-279, 1984 (2 issues) $145

FLUID DYNAMICS
Izvestiya Akademii Nauk SSSR, Mekhanika Zhidkosti i Gaza
Vol. 19, 1984 (6 issues) $500

FUNCTIONAL ANALYSIS AND ITS APPLICATIONS
Funktsional'nyi Analiz i Ego Prilozheniya
Vol. 18, 1984 (4 issues) $410

GLASS AND CERAMICS
Steklo i Keramika
Vol. 41, 1984 (6 issues) $590

HIGH TEMPERATURE
Teplofizika Vysokikh Temperatur
Vol. 22, 1984 (6 issues) $520

HYDROTECHNICAL CONSTRUCTION
Gidrotekhnicheskoe Stroitel'stvo
Vol. 18, 1984 (12 issues) $385

INDUSTRIAL LABORATORY
Zavodskaya Laboratoriya
Vol. 50, 1984 (12 issues) $520

INSTRUMENTS AND EXPERIMENTAL TECHNIQUES
Pribory i Tekhnika Eksperimenta
Vol. 27, 1984 (12 issues) $590

JOURNAL OF APPLIED MECHANICS AND TECHNICAL PHYSICS
Zhurnal Prikladnoi Mekhaniki i Tekhnicheskoi Fiziki
Vol. 25, 1984 (6 issues) $540

JOURNAL OF APPLIED SPECTROSCOPY
Zhurnal Prikladnoi Spektroskopii
Vols. 40-41, 1984 (12 issues) $540

JOURNAL OF ENGINEERING PHYSICS
Inzhenerno-fizicheskii Zhurnal
Vols. 46-47, 1984 (12 issues) $540

JOURNAL OF SOVIET LASER RESEARCH
A translation of articles based on the best Soviet research in the field of lasers
Vol. 5, 1984 (6 issues) $180

JOURNAL OF SOVIET MATHEMATICS
A translation of Itogi Nauki i Tekhniki and *Zapiski Nauchnykh Seminarov Leningradskogo Otdeleniya Matematicheskogo Instituta im. V. A. Steklova AN SSSR*
Vols. 24-27, 1984 (24 issues) $1035

LITHOLOGY AND MINERAL RESOURCES
Litologiya i Poleznye Iskopaemye
Vol. 19, 1984 (6 issues) $540

LITHUANIAN MATHEMATICAL JOURNAL
Litovskii Matematicheskii Sbornik
Vol. 24, 1984 (4 issues) $255

MAGNETOHYDRODYNAMICS
Magnitnaya Gidrodinamika
Vol. 20, 1984 (4 issues) $415

MATHEMATICAL NOTES
Matematicheskie Zametki
Vols. 35-36, 1984 (12 issues) $520

continued on inside back cover